Mapping of the differential exchange & dynamics of type IVa pilus machine components:

Implications for function

Dissertation
zur Erlangung des Doktorgrades
der Naturwissenschaften (Dr. rer. nat.)

dem Fachbereich der Biologie
der Philipps-Universität vorgelegt von

Memduha Muratoğlu

aus Wiesbaden

Marburg an der Lahn 2023

Die vorliegende Dissertation wurde von Oktober 2019 bis Oktober 2023 am, Max-Planck-Institut für terrestrische Mikrobiologie unter Leitung von Prof. Dr. Lotte Søgaard-Andersen angefertigt.

Vom Fachbereich Biologie der Philipps-Universität Marburg (Hochschulkennziffer 1180) als Dissertation angenommen am 27.10.2023

Erstgutachter(in): Prof. Dr. Lotte Søgaard-Andersen

Zweitgutachter(in): Prof. Dr. Martin Thanbichler

Weitere Mitglieder der Prüfungskommission:

Prof. Dr. Victor Sourjik

Prof. Dr. Lennart Randau

Tag der Disputation: 13.03.2024

Havaya bakarsam hava alırım
Toprağa bakarsam dua alırım
Topraktan ayrılsam nerde kalırım
Benim sâdık yârim kara topraktır

(Âşık Veysel)

Canım anneme

Contents

Part I

1 Abstract

Large multiprotein complexes perform various biological processes. In the past decade, *in vivo* fluorescence labeling of proteins and advanced microscopy techniques have revealed that many protein complexes, previously assumed to be static, contain components that dynamically exchange subunits with cellular pools. The type IVa pilus machine (T4aPM) drives the extension/adhesion/retraction cycles of T4aP and is the prototype of a large family of prokaryotic cell envelope-spanning macromolecular complexes involved in motility, DNA-uptake, secretion, and adhesion. Here, we used the T4aPM in *Myxococcus xanthus* as a model to investigate whether proteins of this nano-machine dynamically exchange and if exchange is coupled to the activity of the T4aPM. We performed Fluorescence Recovery After Photobleaching (FRAP) experiments on live cells, in which selected fluorescently-tagged proteins of the T4aPM were synthesized at close to native levels. We demonstrate different dynamics for individual components of the T4aPM. The PilQ secretin and its associated periplasmic protein TsaP, that jointly form the outer membrane (OM) pore, as well as the inner membrane (IM) proteins PilP and PilO, and likely also the IM protein PilN, that jointly form the alignment complex connecting the outer OM pore to the IM platform protein PilC, were stably incorporated into the T4aPM. By contrast, the three cytoplasmic proteins PilM, PilB and PilT were dynamically incorporated into the T4aPM and displayed different exchange kinetics. In the case of PilM, the exchange rate was dependent on the functional state of the T4aPM and were reduced by binding of the extension and retraction ATPases, PilB and PilT, to the base of the T4aPM. Remarkably, using an active variant of the PilM that was stably incorporated into the T4aPM, we demonstrate that PilM exchange is not essential for T4aPM function. The ATPases PilB and PilT underwent rapid exchange; however, PilB exchange was much faster than PilT exchange, supporting that the rate of T4aP formation is limited by slow PilT unbinding from the T4aPM. The different exchange kinetics of PilM, PilB and PilT support that they exchange independently of each other. Moreover, our data support that the dynamic exchange of PilB and PilT reflect neither the incorporation of the hundreds of individual PilA building block of the T4aP per second into the extending pilus nor their removal during retractions, and that the PilA subunits are delivered and removed to the T4aPM independently of any T4aPM component. We conclude that the trans-envelope structural elements of the T4aPM are stable structures once assembled, that the only dynamically incorporated proteins are the cytoplasmic PilM, PilB and PilT, with PilM exchange not being important for T4aPM function, while PilB and PilT exchange reflects

the binding and unbinding of these proteins to the T4aPM to power T4aP extension and retraction, respectively.

The second part of this study focus on SgmO, a regulator of exopolysaccharide synthesis. Detailed genetic analyses confirmed that SgmO is important for exopolysaccharide synthesis, T4aP-dependent motility, and development. Moreover, Δ*sgmO* cells had reduced T4aP levels.

Zusammenfassung

Große Multiprotein-Komplexe führen unterschiedliche biologische Prozesse aus. In den letzten zehn Jahren haben *in-vivo*-Fluoreszenzmarkierung von Proteinen und hochentwickelte Mikroskopie Techniken gezeigt, dass viele Protein-Komplexe, die zuvor als statisch angesehen wurden, Komponenten enthalten, die sich dynamisch mit zellulären Proteinen austauschen. Die Typ-IVa-Pilus-Maschine (T4aPM) treibt die Verlängerungs-/Haftungs-/Rückzugszyklen von T4aP an und ist ein Prototyp einer großen Familie prokaryotischer, die Zellhülle durchspannender makromolekularer Komplexe, die an Bewegung, DNA-Aufnahme, Sekretion und Haftung beteiligt sind. Hier haben wir die T4aPM in *Myxococcus xanthus* als Modell verwendet, um zu untersuchen, ob Proteine dieser Nanomaschine dynamisch ausgetauscht werden und ob der Austausch mit der Aktivität der T4aPM gekoppelt ist. Wir führten *Fluoreszenz-Recovery-after-Photobleaching* (FRAP)-Experimente an lebenden Zellen durch, in welchen ausgewählte fluoreszenzmarkierte Proteine der T4aPM auf einem nahezu nativen Level synthetisiert wurden. Wir zeigen unterschiedliche Dynamiken für individuelle Komponenten der T4aPM. Das PilQ-Secretin und das assoziierte periplasmatische Protein TsaP, die gemeinsam die äußere Membranpore bilden, sowie die innere Membran (IM) Proteine PilP und PilO und wahrscheinlich auch das IM-Protein PilN, die gemeinsam den *Alignment*-komplex bilden, welcher die äußere Membran Pore mit dem IM-Plattformprotein PilC verbindet, wurden stabil in die T4aPM eingebaut. Im Gegensatz dazu wurden die drei zytoplasmatischen Proteine PilM, PilB und PilT dynamisch in die T4aPM eingebaut und zeigten unterschiedliche Austauschkinetiken. Im Fall von PilM war die Austauschrate abhängig vom funktionellen Zustand der T4aPM und wurde durch die Bindung der Verlängerungs- und Rückzugs-ATPasen PilB und PilT an der Basis der T4aPM reduziert. Bemerkenswert ist, dass wir mithilfe einer aktiven Variante von PilM, die fest in die T4aPM eingebaut war, zeigen, dass der Austausch von PilM für die Funktion der T4aPM nicht entscheidend ist. Die ATPasen PilB und PilT unterlagen einem schnellen Austausch; jedoch war der Austausch von PilB wesentlich schneller als der von PilT, was darauf hinweist, dass die Geschwindigkeit der T4aP-Bildung durch das langsame Lösen von PilT von der T4aPM begrenzt ist. Die unterschiedlichen Austauschkinetiken von PilM, PilB und PilT unterstützen die These, dass sie unabhängig voneinander ausgetauscht werden. Darüber hinaus stützen unsere Daten die Annahme, dass der dynamische Austausch von PilB und PilT weder die Aufnahme der Hunderte von einzelnen PilA-Bausteinen pro Sekunde in den wachsenden Pilus noch deren Entfernung während des

Rückzugs widerspiegelt, und dass die PilA-Untereinheiten unabhängig von jeder T4aPM-Komponente zur T4aPM transportiert und entfernt werden. Wir schließen daraus, dass die Zellhülle durchspannenden strukturellen Elemente der T4aPM stabile Strukturen sind, sobald sie zusammengebaut sind, und dass die einzigen dynamisch eingebauten Proteine die zytoplasmatischen PilM, PilB und PilT sind, wobei der Austausch von PilM für die Funktion der T4aPM nicht wichtig ist, während der Austausch von PilB und PilT das An- und Abbinden dieser Proteine an die T4aPM zur Verlängerung bzw. zum Rückzug der T4aP reflektiert.

Der zweite Teil dieser Studie konzentriert sich auf SgmO, einen Regulator der Exopolysaccharidsynthese. Detaillierte genetische Analysen bestätigten, dass SgmO wichtig für die Exopolysaccharidsynthese, die T4aP-abhängige Beweglichkeit und die Entwicklung ist. Außerdem hatten Δ*sgmO*-Zellen reduzierte T4aP-Spiegel.

2 Abbreviations

aa	amino acid
ATP	Adenosine triphosphate
bp	base pairs
c-di-GMP	bis-(3'-5')-cyclic dimeric guanosine monophosphate
Com	competence
CTT	casitone Tris medium
DNA	deoxyribonucleic acid
DMSO	dimethyl sulfoxide
EPS	exopolysaccharides
FRAP	fluorescence recovery after photobleaching
GAP	GTPase activating protein
GEF	Guanine nucleotide exchange factor
GTP/GDP	guanine tri-/diphosphate
h	hours
IM	IM
IPTG	Isopropyl β-D-1 thiogalaktopyranoside
kDa	kilo Dalton
LPS	lipopolysaccharides
MCP	methyl-accepting chemotaxis protein
min	minutes
MOPS	3-(N-morpholino) propane sulfonic acid
Msh	mannose sensitive hemaglutinin
OD	optical density
OM	OM
pN	piconewton
PG	peptidoglycan
s	seconds
SDS-PAGE	sodium dodecyl sulfate-polyacrylamide gel electrophoresis
sfGFP	super-folded green fluorescent protein
$t_{1/2}$	recovery halftime
tad	Tight adherence
T2SS	type 2 secretion system
T3SS	type 3 secretion system
T4SS	type 4 secretion system
T4P(M)	Type 4 pilus (machine)
WT	wildtype

Part I

3 Introduction

Antony van Leeuwenhoek described in 1676 in a letter to the Royal Society the observations he had made through his microscope in a rainwater sample. "*When these animacula or living Atoms did move, they put forth two little horns, continually moving themselves; the body was roundish, sharpning a little towards the end, where they had a tayl, near four times the length of the whole body, of the thickness (by my Microscope) of a Spiders-web;"* (Leeuwenhoek). He first observed moving bacteria, and movement became a defining feature of life. Since then, different bacterial motility systems have been identified, their importance in ensuring bacterial survival in various environments have been documented, and the nano-machines that power the translocation of cells analyzed (Thomas *et al.*, 2006, Wadhwa & Berg, 2022).

3.1 Bacterial motility – an overview

Bacterial cells can swim in liquid using rotating flagella (Silverman & Simon, 1974, Larsen *et al.*, 1974, Berg, 1974) and translocate across surfaces using extending/retracting type IVa pili (T4aP) (O'Toole & Kolter, 1998, Wu & Kaiser, 1995) or gliding motility (Hodgkin & Kaiser, 1979, Miyata & Hamaguchi, 2016, Wadhwa & Berg, 2022).

Flagella are rotating filaments, and the direction of rotation of one or multiple flagella determine the direction of movement of the cell (Silverman & Simon, 1974, Larsen *et al.*, 1974, Berg, 1974, Wadhwa & Berg, 2022). The nano-machine that drives flagellar rotation is trans-envelope and highly conserved. Interestingly, a core part of this machine shares homology with another macromolecular trans-envelope complex; the injectisome. The core of both complexes consists of a type III-secretion system (T3SS) (Diepold & Armitage, 2015). The injectisome is a bacterial syringe like structure (Hu *et al.*, 2018, Park *et al.*, 2018), which is used to secrete effector proteins across the bacterial cell envelope into eukaryotic cells (Galan & Collmer, 1999, Galan & Wolf-Watz, 2006, Cornelis, 2006).

T4aP are long, thin filaments that undergo cycles of extension, adhesion to a surface, and retraction. A force of up to 150 pN per T4aP is generated during the retraction of T4aP, which pulls the cell forward (Clausen *et al.*, 2009a, Maier *et al.*, 2002). The nano-machine driving the extension/adhesion and retraction cycles consists of several ring-like structures and spans the cell envelope from the cytoplasm to the cell surface (Leighton *et al.*, 2015,

Craig *et al.*, 2019, Chang *et al.*, 2016, Gold *et al.*, 2015, Karuppiah *et al.*, 2013, Georgiadou *et al.*, 2012). Interestingly, the nano-machine powering T4aP function is highly conserved (Craig *et al.*, 2019) and shares similarities with the type II-secretion system (T2SS), which also consists of several interconnected rings, spans the cell envelope and is used to translocate a wide range of proteins from the periplasm across the OM (Peabody *et al.*, 2003, Craig *et al.*, 2019). It was suggested that the T2SS has evolved later in evolution from T4PM (Denise *et al.*, 2019).

While the nano-machines driving flagella- T4aP- formation and function are widespread and conserved, (Wadhwa & Berg, 2022, Pelicic, 2008, Craig *et al.*, 2019), the nano-machines for gliding motility are much less conserved (Craig *et al.*, 2019). Gliding motility is defined as movement across a surface along the cell length, independent of flagella or pili (Burchard, 1981, Kearns, 2010). Different gliding motility systems have been identified, each with a narrow taxonomic distribution, including ~50 nm long leg-like structures in *Mycoplasma mobile* (Miyata & Hamaguchi, 2016), focal adhesion complexes in *M. xanthus* (Mignot & Nöllmann, 2017), and the type IX secretion/gliding motility system in *Bacteroidetes* spp (McBride & Nakane, 2015).

3.2 Protein exchange in the flagellar motor and the T3SS

In Gram-negative bacteria, membrane-spanning multiprotein complexes including the flagellar nano-machine, the injectisome, the T2SS and the T4aPM consist of multiple ring-like structures that are anchored in the inner and OM (Ayers *et al.*, 2010, Chang *et al.*, 2016, Chernyatina & Low, 2019, Paul *et al.*, 2011, Yamaguchi *et al.*, 2021). In the past, techniques such as X-ray crystallography and electron microscopy have solved the overall structure and/or architecture of these nano-machines in minute detail. However, these techniques are based on static imaging and thus convey the impression that these large multi-protein complexes consist of static units. More recently, live-cell imaging techniques based on fluorescent labeling of proteins and FRAP (Fluorescence recovery after photobleaching), FLIP (Fluorescence loss in Photobleaching) and single molecule microscopy have unraveled, that components of multiprotein complexes are either stably incorporated into a protein complex or dynamically exchange over time. As described below, this work has been spearheaded in the flagellar nano-machine and the T3SS, while the dynamic exchange of components of the T4aPM and the T2SS is largely unexplored. Using a combination of TIRF (total internal reflection fluorescence) microscopy, FLIP and

FRAP, it was found that the stator protein MotB of the flagellar motor constantly exchanges with an IM pool and one MotB protein only dwells in the motor for ~30 sec (Figure 1) (Leake *et al.*, 2006). Similarly, a single FliM protein, which forms the cytoplasmic ring of the bacterial flagellar motor, has a motor dwell time of ~40 sec (Delalez *et al.*, 2010). Moreover, its dynamic exchange depends on the binding of the chemotaxis signaling protein CheY (Figure 1). Based on these findings, it was suggested that FliM exchange is important for directional switching of the flagellum (Delalez *et al.*, 2010). The rotor protein FliN was found to exchange with very similar dynamics to FliM, and FliM/N sub-complexes are suggested to exchange, and play a role in fine-tuning cytoplasmic ring function by varying subunit stoichiometry (Figure 1) (Fukuoka *et al.*, 2010). FlhA is a part of the flagellar export apparatus and was also described to exchange subunits in a range of minutes (Figure 1) (Li & Sourjik, 2011). FliI the ATPase of the bacterial export apparatus was shown to exchange subunits within a minute (Bai *et al.*, 2014). However, in these two cases, the benefit of the protein exchange, if any, is currently not clear. By contrast, FliG and FliF, which are part of the motor switch ring (MS-ring), were both reported to not exchange subunits and, thus are stably incorporated (Figure 1) (Li & Sourjik, 2011).

In case of the *Yersinia enterocolitica* T3SS, FRAP microscopy of the OM secretin YscC demonstrated that it is stably incorporated into this complex and does not undergo exchange (Diepold *et al.*, 2015). YscV, which is a homolog of the dynamically exchanging FlhA of the flagellar motor, is also stably incorporated (Diepold *et al.*, 2015). By contrast, the cytoplasmic ring forming YscQ protein exchanges subunits over a timescale of minutes, similar to FliM/N (Figure 1) (Diepold *et al.*, 2015). Interestingly, YscQ exchange is faster under secreting conditions than under non-secreting conditions and even faster in the presence of a catalytically inactive T3SS ATPase variant of YscN. It was discussed that the YscQ exchange in the cytosolic ring of the injectisome might be linked to effector export, however YscQ exchange would be to slow to be directly linked to the export of effectors (Diepold *et al.*, 2015). As several components of the injectisome, e.g. YscQ, YscL, YscN and YscK assemble to form sub-complexes, it has been suggested that sub-complexes might exchange as units (Diepold *et al.*, 2017, Tusk *et al.*, 2018).

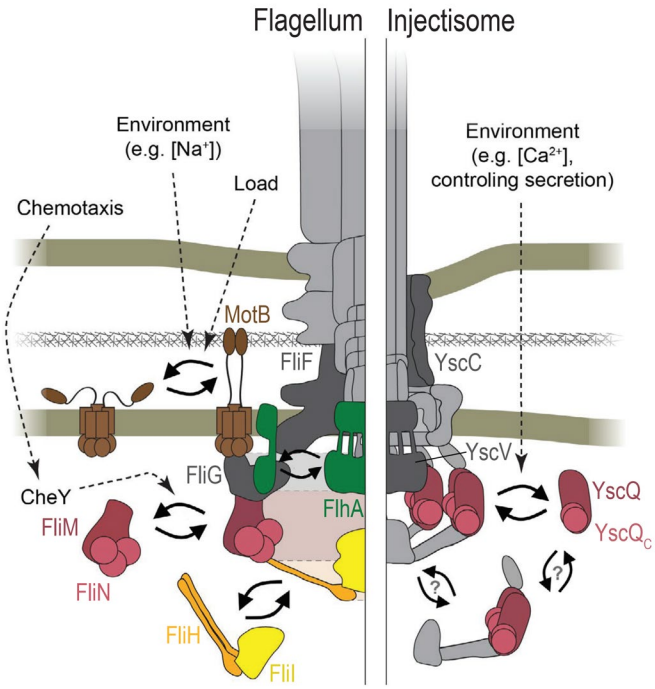

Figure 1 Summary of protein exchange in the multiprotein complexes of the bacterial flagellum and the injectisome. Schematic overview of the flagellum (left) and the injectisome (right). Protein exchange is marked by colors and arrows, and proteins found to not exchange are shown in dark grey. Components not studied for protein exchange are shown in light grey. Arrows with question marks show suggested protein exchange without direct evidence. Dashed arrows indicate external factors influencing the protein exchange. Adapted from (Milne-Davies *et al.*, 2021).

3.2.1 The T4aPM - a representative of a large family of macromolecular machines

The T4aPM belongs to the type IV filament (TFF) superfamily, diverse and widespread group of macromolecular machines. The TFF superfamily includes type IVa pili, type IVb pili, type IVc pili (Tad pili), Msh pili, competence pili, the type II secretion system and archaeal flagella (Beeby, 2019, Denise *et al.*, 2019). Thus, the TFF members are involved in bacterial motility, surface adherence, biofilm formation, protein secretion and DNA-uptake (Denise *et al.*, 2019). T4P are thin, filamentous cell appendages, several microns in length and ~6-9 nm in width (Craig & Li, 2008, Pelicic, 2008). They consist of polymers of thousands of copies of a major pilin, fewer minor pilins and in some cases the PilY1 adhesins (Giltner *et al.*, 2010, Treuner-Lange *et al.*, 2020). T4P are categorized into T4aP, T4bP and T4cP, based on differences in the leader peptides and the size of the mature major pilin (Giltner *et al.*, 2012, Chlebek *et al.*, 2021, Pelicic, 2023). Despite their functional differences, the TFF members share homologous proteins that allow the extrusion on the cell surface of pili, or pseudopili in the periplasm in case of the T2SS. Four core proteins

are represented in all of TFF systems, the major pilin, the pre-pilin peptidase that cleaves the signal peptide off to generate mature pilins, an inner IM platform protein, and an extension ATPase (Figure 2) (Denise *et al.*, 2019). In Gram-negative bacteria, the TFF systems all contain an OM secretin. All other components are less conserved (Figure 2). Here, I focus on T4aP and the T4aPM in Gram-negative bacteria.

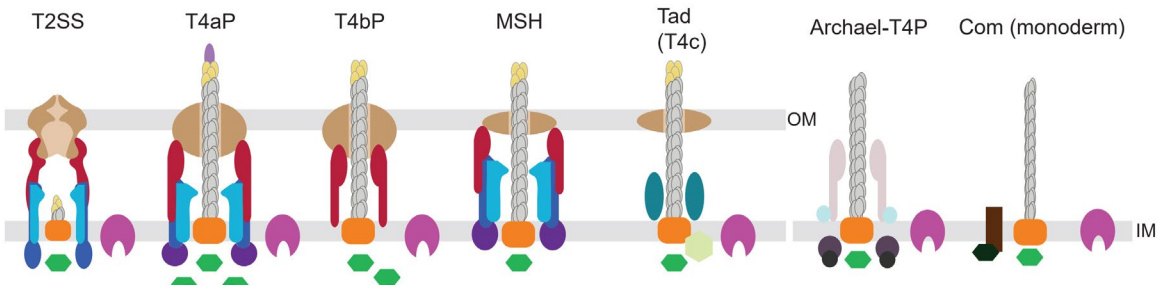

Figure 2 Representatives of the TFF superfamily. Schematic overview of TFF nano-machines as the T2SS, T4aP, Tad- MSH-,T4bP, Archaeal T4P as well as Com pili in Gram-positive bacteria. Homologous components are shown in the same colors. The OM secretin is depicted in brown, secretin-associated proteins are shown in red and assembly proteins in blue shades and magenta. ATPases are shown as green hexagons. The IM platform proteins are shown in orange, major pilins in grey, minor pilins in yellow and pre-pilin peptidases in pink. Modified from (Denise *et al.*, 2019).

3.2.2 The type IVa pilus machine (T4aPM)

The T4aPM constitutes the conduit across the cell envelope for the T4aP, and power the dynamic pilus extension and retraction. Systematic genetic analyses identified genes encoding T4aP biogenesis proteins in several organisms. Overall the structure of the T4aPM can be divided into an OM pore formed by the secretin PilQ and the secretin surrounding TsaP, an IM platform made by PilC, a periplasmic alignment complex that connects these two structural elements formed by PilP, PilN, PilO and PilM, a priming complex, and the ATPases for T4aP extension and retraction (Figure 3) (Giltner *et al.*, 2010, Treuner-Lange *et al.*, 2020). The T4aPM allows pilus extension and retraction by adding pilin subunits to the pilus or removing subunits from the pilus fiber with rates of ~1000 subunits per second (Merz *et al.*, 2000, Clausen *et al.*, 2009a, Skerker & Berg, 2001),

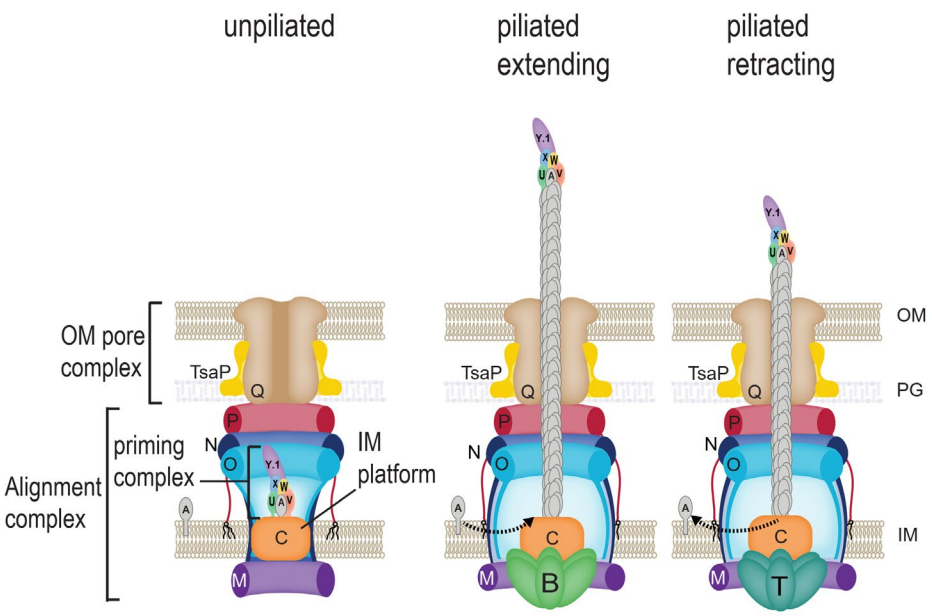

Figure 3 Overview of the T4aPM. Schematic model of three versions of the T4aPM. The T4aPM spans the cell envelope. PilQ, TsaP form a OM pore complex PilN, PilO, PilP, PilM form an alignment complex and PilC forms the inner membrane platform and localize in the piliated extending (left), retracting (middle), and unpiliated (right) T4aPM. PilA and the minor pilins localize in the IM and form together with PilY1 a priming complex in the unpiliated machine. PilA polymers form the pilus fiber with the minor pilins and PilY1 at the tip. The two cytoplasmic ATPases, PilB and PilT, power the extension and retraction of the pilus fiber.

3.2.2.1 The major pilin

The major pilin PilA as well as minor pilins (see below) are synthesized as pre-pilins and contain an N-terminal class III signal peptide (Szabo *et al.*, 2007, Giltner *et al.*, 2012). The PilA precursor is targeted to the Sec machinery by the signal recognition particle and then translocated across the IM (Arts *et al.*, 2007b, Francetic *et al.*, 2007). The pre-pilin remains in the IM due to its hydrophobic N-terminal α-helix, and is processed by the pre-pilin peptidase that cleaves off the signal peptide after the conserved Gly residue the membrane and methylates the conserved N-terminal Phe residue (Nunn & Lory, 1991, Strom *et al.*, 1993). The mature pilin is, thus, anchored in the IM with no remaining domain in the cytoplasm and its globular C-terminal domain in the periplasm (Lemkul & Bevan, 2011). The mature major pilin has a characteristic lollipop-like shape consisting of an N-terminal α1-helix, followed by a C-terminal β-strand rich globular domain (Figure 4) (Hartung *et al.*, 2011, Wang *et al.*, 2017). The hydrophobic N-terminal α1-helix has dual functions and not only anchors the protein in the IM but also mediates subunit-subunit interactions in the assembled pilus (Craig *et al.*, 2003).

Based on cryo-electron microscopy (cryoEM) and crystal structures, the T4aP structure has been elucidated. The T4aP filaments are helical polymers in which the α1-helices provide the major polymerization interface and build the core of the filament. The C-terminal globular domains build up the outer surface of the filament (Figure 4) (Craig *et al.*, 2003, Hartung *et al.*, 2011, Parge *et al.*, 1995, Craig & Li, 2008). Recently, the structure of the major pilin of *M. xanthus* was solved using cryoEM, and it was shown that its larger C-terminal domain, compared to other major pilins, causes more extensive inter-subunit contacts, causing higher bending and axial stiffness of the T4aP of *M. xanthus* (Treuner-Lange *et al.*, 2023).

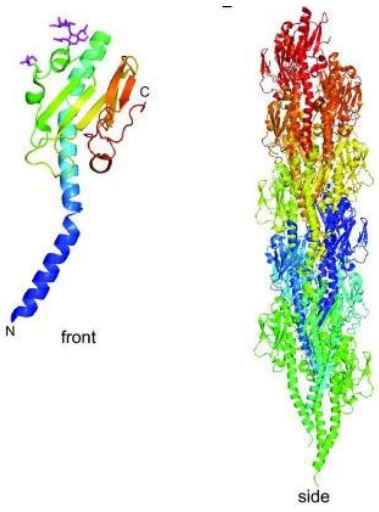

Figure 4 Common structural features of T4P and major pilin subunits, illustrated with an example of *Neisseria gonorrhoeae* T4aP (Berry & Pelicic, 2015).On the left side the structure of the full-length major pilin PilE from *N. gonorrhoeae*. The protein is rainbow colored from its N-terminus (blue) to its C-terminus (red)**.** On the right side, the assembled T4aP filament is shown. Each pilin subunit has a different color. Adapted from (Berry & Pelicic, 2015, Carreira *et al.*, 2022)

3.2.2.2 The secretin

Secretins are key elements in OM pore complexes of T2SS, T3SS and T4aPM as well as bacteriophage extrusion systems (Thomassin *et al.*, 2017, Majewski *et al.*, 2018, Hospenthal *et al.*, 2017, Marciano *et al.*, 2001, Opalka *et al.*, 2003). Secretins form channels with a diameter of 50-80 Å and allow passage of DNA, folded proteins and polymeric fibers.

Secretins are multimeric proteins that are assembled from 12-15 subunits (Figure 5) (Daefler *et al.*, 1997, Kowal *et al.*, 2013, Howard *et al.*, 2019, Hu *et al.*, 2018, Yan *et al.*, 2017, Chang *et al.*, 2016, McCallum *et al.*, 2021, D'Imprima *et al.*, 2017, Siewering *et al.*, 2014). Electron microscopy and sequence analyses of secretins from various systems and organisms revealed their overall structural similarities. Secretin protomers comprise two major subdomains, an N-terminal species-specific region and the C-terminal conserved pore-forming region (Majewski *et al.*, 2018, Daefler *et al.*, 1997, Berry *et al.*, 2012). In the assembled secretin, C- terminal the pore-forming domains of the protomers form a β-barrel. The C-terminal region comprises the secretin domain and the β-lip region (Weaver *et al.*, 2020, Worrall *et al.*, 2016). The N-terminal region can be divided into different subdomains. The N0 subdomain is followed by one or several repeat subdomains (N1-5) separated by flexible linkers. In some T4aP secretins, the N-terminal part can contain peptide glycan- (PG) binding AMIN-domains (Carter *et al.*, 2017). Recently, it was shown that in the absence of the N-terminal AMIN domains, PilQ-sfGFP does not assemble into multimers in *M. xanthus,* and it was suggested that the presence or absence of AMIN domains in secretins determines the T4aPM localization pattern in bacteria (Herfurth *et al.*, 2023).

In T4aP systems, the oligomerization and OM localization of the secretin depend on a pilotin. In *P. aeruginosa* and *M. xanthus*, PilQ localization to the OM depends on the pilotins PilF and TgI, respectively (Nudleman *et al.*, 2006, Koo *et al.*, 2008). PilF is thought to act as a co-chaperone with the Lol system to facilitate PilQ transit across the periplasm to the OM (Koo *et al.*, 2008, Hoang *et al.*, 2011). TgI of *M. xanthus* is essential for PilQ stability and its multimerization in the OM (Nudleman *et al.*, 2006, Rodriguez-Soto & Kaiser, 1997, Herfurth *et al.*, 2023a, Herfurth *et al.*, 2023). In *N. meningitidis,* lack of the PilW pilotin did not affect PilQ localization, and PilQ insertion to the OM is thought to be Bam dependent (Carbonnelle *et al.*, 2005, Voulhoux *et al.*, 2003, Silva *et al.*, 2020).

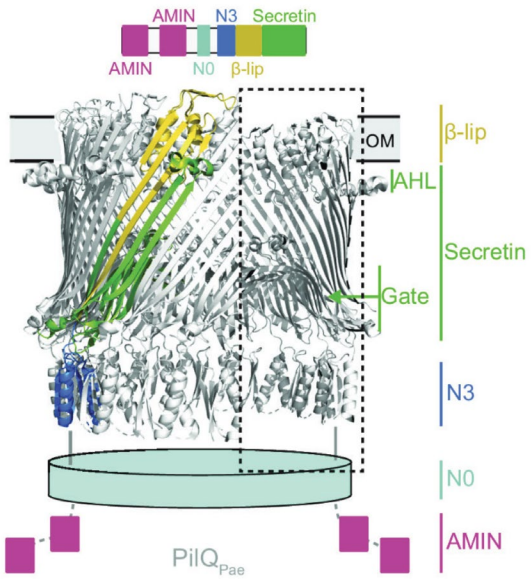

Figure 5 Cryo-EM structure of tetradecameric PilQ of *P. aeruginosa*. The upper panel shows the domain architecture of PilQ of *P. aeruginosa*. In the lower panel the Cryo-EM structure, in which the different domains of one PilQ protomer are indicated. The N3 (marine blue), secretin (green), and β-lip region (yellow) are shown. The N0 and two AMIN domains, which are not resolved in the structure, are shown as a cyan cylinder and pink boxes, respectively. The dashed box marks the part of the secretin in which the front part of the barrel structure has been removed to show the inside of the barrel with the gate. Adapted from (Herfurth *et al.*, 2023).

3.2.2.3 Peptidoglycan binding TsaP

TsaP is conserved among T4aP systems and has a PG-binding N-terminal LysM domain (Siewering *et al.*, 2014, Buist *et al.*, 2008). The C-terminal domain of TsaP was predicted to be similar to the C-terminal part of the flagellar FlgT protein, which has a β-roll structure with an extruding finger subdomain (Terashima *et al.*, 2013, Chang *et al.*, 2016, McCallum *et al.*, 2021). According to the current models, TsaP interacts with PilQ via its C-terminus, and its N-terminus anchors it to the PG (Chang *et al.*, 2016, McCallum *et al.*, 2021).

Cryo-electon tomography (cryoET) suggested 12 TsaP proteins to form a belt around the 12mer secretin in *M. xanthus*. However, in more recent studies, seven copies of TsaP were shown to form the belt around the 14-meric *P. aeruginosa* secretin (Figure 6) (Chang *et al.*, 2016, McCallum *et al.*, 2021). TsaP is thought to be important to anchor the secretin complex to the PQ and to help aligning PilQ with the IM complex (Chang *et al.*, 2016,

McCallum *et al.*, 2021, Siewering *et al.*, 2014) as lack of TsaP led to membrane protrusions filled with T4aP in *N. gonorrhoeae* (Siewering *et al.*, 2014).

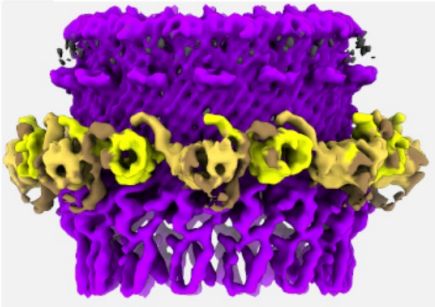

Figure 6 TsaP forming a heptameric ring around PilQ. Map summarizing the predicted heptamer structure of TsaP modeled into PilQ cryo-EM spike densities. PilQ is shown in magenta and TsaP in yellow. Adapted from (McCallum *et al.*, 2021).

3.2.2.4 The lipoprotein PilP

The lipoprotein PilP forms a ring-like structure in the periplasm and is anchored to the IM via its lipidated N-terminus (Figure 3). PilP directly interacts with PilQ, PilN, and PilO (Figure 3)(Balasingham *et al.*, 2007, Ayers *et al.*, 2009, Chang *et al.*, 2016, Tammam *et al.*, 2013). The N-terminus of PilP has a type II signal peptide. Structural characterization of PilP revealed that the N-terminal part of PilP is disordered, while the C-terminal part has a β-sandwich type fold, which is similar to the homology region (HR) of GspC in T2SS that interacts with the secretin (Figure 3 and Figure 7) (Tammam *et al.*, 2011, Golovanov *et al.*, 2006, Tammam *et al.*, 2013, Korotkov *et al.*, 2011). The HR of PilP directly interacts with the N0 domain of PilQ, while the N-terminal disordered region interacts with PilN and PilO (Tammam *et al.*, 2013). Thus, PilP builds the bridge, connecting the OM secretin with the other alignment complex components of the T4aPM namely PilN, PilO and PilM (Figure 3).

Figure 7 Overview of the PilP domain architecture. The N-terminus of PilP contains a signal sequence and a conserved lipidation site. This is followed by the N-terminal disordered region of PilP (pink) and the C-terminal β-sandwich type fold, which is similar to the homology region (HR) of GspC in T2SS (red). Based on an overview of the *M. xanthus* PilP adapted from (Tammam *et al.*, 2011).

3.2.2.5 The integral membrane proteins PilN and PilO

CryoET has demonstrated that the integral IM proteins PilN and PilO form a ring-like structure in the periplasm (Figure 3) (Chang *et al.*, 2016). Among PilN proteins in different species, the N-terminus is highly conserved, while PilO is more conserved at its C-terminus. The secondary structure of PilN and PilO is very similar, although the sequence identity of these two proteins is low (Sampaleanu *et al.*, 2009, Georgiadou *et al.*, 2012). Both proteins have a short cytoplasmic N-terminus, followed by a transmembrane domain, a coiled-coil (cc) domain, and C-terminal a globulardomain with a ferredoxin-like fold (Figure 8). PilO alone forms homodimers *in vitro,* but when mixed with PilN, heterodimers were formed preferably (Sampaleanu *et al.*, 2009). Disulfide bond crosslinking assays have also demonstrated that PilN and PilO can form heterodimers *in vivo* (Leighton *et al.*, 2016). It has been proposed that the cc domains of PilN and PilO serve as the primary interaction interfaces in the heterodimers. In contrast, the core regions might mediate homodimer formation. Because cross-linked PilN or PilO homodimers have minimal functional impact on *P. aeruginosa* motility, it was suggested that heterodimers are the physiologically relevant state of PilN and PilO (Leighton *et al.*, 2016). Furthermore, PilN and PilO were shown in Bacterial Adenylate Cyclase-Based Two-Hybrid (BACTH) interaction studies to interact with the major pilin. PilO interactions with the inner membrane platform protein PilC were also shown (Georgiadou *et al.*, 2012). Since only PilN and PilO heterodimers could interact with PilP (Tammam *et al.*, 2011) and the three proteins stabilize each other in *M. xanthus*, PilN and PilO likely form heteromers in the T4aPM (Friedrich *et al.*, 2014).

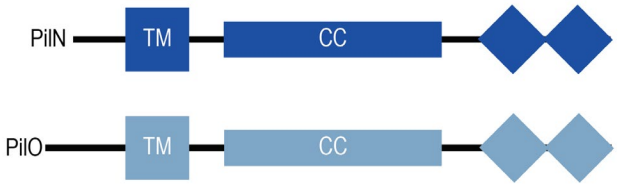

Figure 8 Overview of the PilN and PilO domain architecture. The domain organization of PilN and PilO. Both protein have a short cytoplasmic N-terminus. The C-terminal ferredoxin-like fold is shown as a pair of diamonds, the coiled-coil domains and the TM domain are indicated. Adapted from (Sampaleanu *et al.*, 2009).

3.2.2.6 Cytoplasmic ring forming PilM

PilM is a cytoplasmic component of the T4aPM possessing an actin-like fold. PilM interacts with the conserved N-terminus of PilN (Georgiadou *et al.*, 2012, Karuppiah & Derrick,

2011, McCallum *et al.*, 2016). PilM is structurally closely related to FtsA or MreB (Figure 9), which belong to the actin-like ATPases, and can polymerize upon ATP-binding (Carballido-Lopez, 2006, Karuppiah & Derrick, 2011). ATP binding of PilM has been demonstrated in different organisms (Karuppiah & Derrick, 2011, McCallum *et al.*, 2016, Bischof *et al.*, 2016). CryoET demonstrated that PilM forms an oligomeric ring at the base of the T4aPM (Figure 3) (Chang *et al.*, 2016). It has been proposed that upon ATP binding by PilM, conformational changes facilitate its interaction with the PilN N-terminus (McCallum *et al.*, 2016). PilM also interacts with the extension ATPase PilB (Bischof *et al.*, 2016, McCallum *et al.*, 2016), the retraction ATPase PilT (Georgiadou *et al.*, 2012), and the IM platform forming PilC (McCallum *et al.*, 2016). CryoET also demonstrated that the PilM ring in the cytoplasm undergoes conformational changes upon binding of PilB or PilT to the T4aPM as the diameter of the PilM ring in piliated machines is larger than in unpiliated machines (Figure 3) (Chang *et al.*, 2016).

Figure 9 Overview of the PilM domain architecture. Domain organization showing the MreB (light magenta) and FtsA (magenta) like regions of PilM and the sequence motifs of actin-like ATPases (dark magenta) based on a SMART analysis of *M. xanthus* PilM (Letunic *et al.*, 2021).

3.2.2.7 The IM platform protein PilC

The conserved platform protein PilC is a polytopic IM protein (Takhar *et al.*, 2013, Korotkov *et al.*, 2012). Different studies of PilC and homologs have suggested two or three trans-membrane segments, resulting in discrepancies concerning PilC topology, i.e. either the two globular domains are both in the cytoplasm (Thomas *et al.*, 1997, Arts *et al.*, 2007a), or one globular domain faces the cytoplasm and the other the periplasm (Blank & Donnenberg, 2001). The number of transmembrane helices is important for the topology and to identify which domains are facing the cytoplasm or periplasm constituting potential interaction sites for other proteins of the T4aPM. More recent studies suggest that the PilC N-terminus interacts with the cytoplasmic ATPase PilB and the C-terminus interacts with PilT (Takhar *et al.*, 2013), indicating that both domains are in the cytoplasm. CryoET

in *M. xanthus* demonstrated that PilC forms an IM structure that extends into the cytoplasm (Chang *et al.*, 2016).

Dimer as well as tetramer formation for PilC and PilC homologs were suggested in the past based on crystal structures, single particle EM and CryoET (Chang *et al.*, 2016, Karuppiah *et al.*, 2010, Abendroth *et al.*, 2009, Collins *et al.*, 2007). However, most recently, a model with trimers of the platform protein has been suggested based on high accuracy Alphafold predictions of the PilC homolog ComGB from *Streptococcus sanguinis* (Figure 10)(Pelicic, 2023). PilC interacts with the cytoplasmic ATPases PilB (Bischof *et al.*, 2016, Georgiadou *et al.*, 2012, McCallum *et al.*, 2016). BACTH assays in *P. aeruginosa* also suggested an interaction with PilA, PilM and PilO (McCallum *et al.*, 2016).

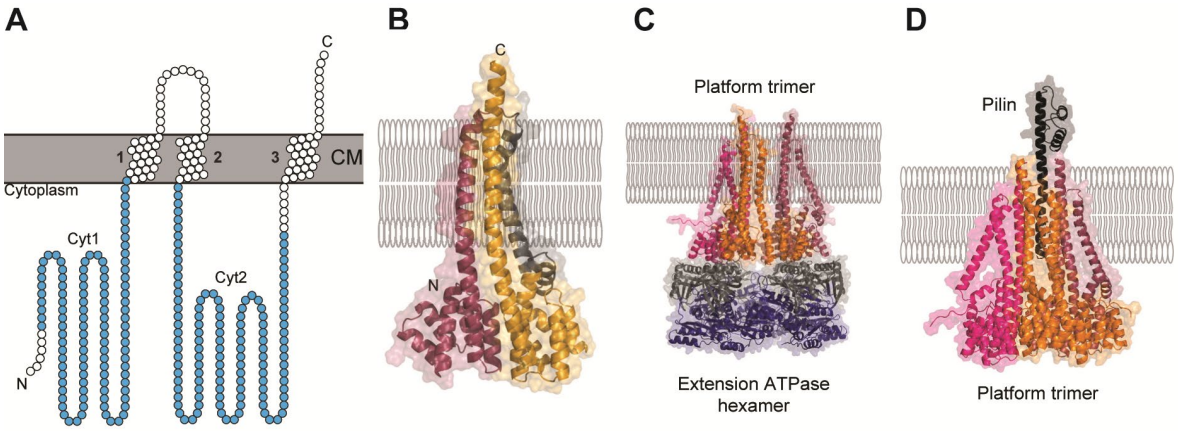

Figure 10 Bioinformatics analysis and Alphafold predictions of the platform protein ComGB from *S. sanguinis*. A. Topology of platform proteins with three TMs, defining two large cytoplasmic domains named Cyt1 and Cyt2. The IPR018076 motif of ComGB in Cyt1 and Cyt2 has been highlighted in blue. The protein TM topology was determined using DeepTMHMM. **B.** Alphafold prediction of the full-length platform protein ComGB from *S. sanguinis*. The two repeated domains are highlighted in color. **C.** Predicted complex of the extension ATPase and the suggested platform protein trimer. **D.** Predicted complex of the pilin and the ComGB trimer (Pelicic, 2023).

3.2.2.8 The ATPases PilB and PilT

Extension and retraction of the T4aP require energy. According to current models, the two ATPases PilB and PilT generate chemical energy by ATP hydrolysis. PilB and PilT belong to the superfamily of secretion ATPases (Planet *et al.*, 2001, Peabody *et al.*, 2003). Specifically, PilB is required to power T4aP extension (Turner *et al.*, 1993), while PilT powers T4aP retraction (Wolfgang *et al.*, 1998). Recently, bifunctional ATPases have been proposed to power Tad- and MshA pilus extension and retraction (Ellison *et al.*, 2019, Hughes *et al.*, 2022).

Secretion ATPase subunits to have a bilobed structure with a flexible hinge connecting the N-terminal and C-terminal domains. A cleft between the two domains is responsible for nucleotide binding by conserved Walker A and Walker B boxes and Asp and His box motifs in the C-terminal domain. PilB and PilT form hexameric rings (Yamagata & Tainer, 2007, Misic *et al.*, 2010), and ATP hydrolysis leads to conformational changes, resulting in movement of the N-terminal domains using the linker region as a hinge, while the C-terminal regions remain fixed (Figure 11B,C). Thus, the chemical energy from ATP hydrolysis is transformed to mechanical energy, which is thought to deliver the power for pilus extension or retraction. PilB possesses a longer N-terminus compared to PilT (Figure 11A). A new binding domain for the second messenger c-di-GMP was discovered in the N-terminus of MshE, the orthologue for the Msh pilus in *Vibrio cholerae* (Wang *et al.*, 2016b). And conservation of the c-di-GMP binding motif in N-termini of PilB ATPases were shown including PilB of *M. xanthus*, *Chloracidobacterium thermophilum*, and *T. thermophilus* (Dye & Yang, 2020). Direct c-di-GMP binding of PilB via its c-di-GMP binding motif of the MshEN domain at the N-terminus was demonstrated in PilB of *C. thermophilum* and recently also *M. xanthus* and binding of PilB to c-di-GMP was suggested to be important for T4aP-dependent motility and biofilm formation (Dye & Yang, 2020, Wang *et al.*, 2016b, Dye *et al.*, 2023).

PilB and PilT bind the cytoplasmic ring component PilM (McCallum *et al.*, 2016), and the IM platform protein (McCallum *et al.*, 2016, Bischof *et al.*, 2016, Georgiadou *et al.*, 2012). According to current models based on cryoET, a PilB hexamer interacts with every second PilM in the cytoplasmic ring via its N-terminal MshEN domain (Chang *et al.*, 2016). A retraction ATPase is not present in all known systems. However, systems lacking a retraction ATPase are suggested to spontaneously retract due to interruption of ATP or pilin subunit supply and are less efficient compared to ATP-driven retraction (Ng *et al.*, 2016, Ellison *et al.*, 2018, Ellison *et al.*, 2017, Craig *et al.*, 2019).

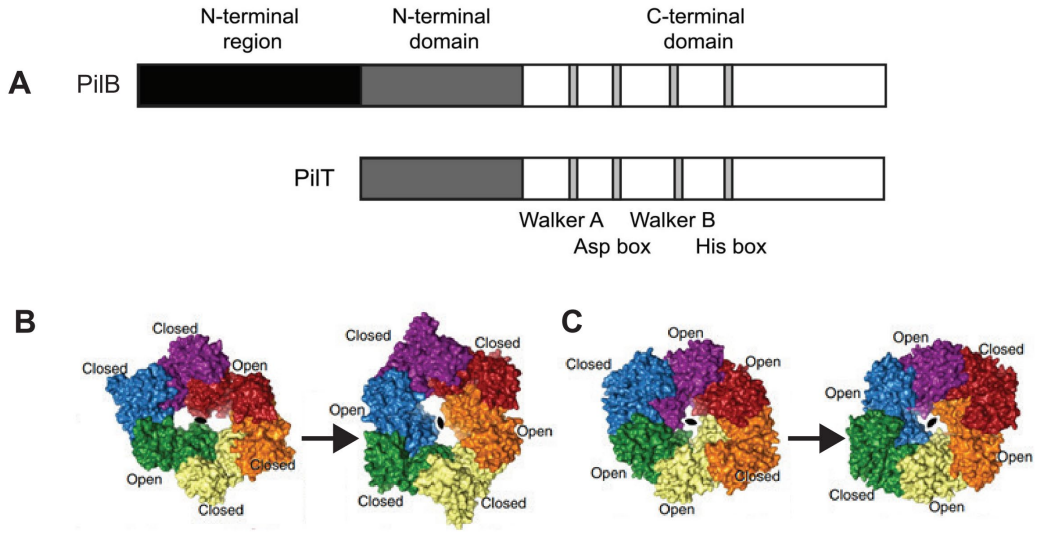

Figure 11 PilB and PilT domain organization, structures and conformational changes upon nucleotide exchange. **A.** Domain organization of PilB and PilT of *M. xanthus***.** PilB has an elongated N-terminus (black). The N-terminal domains are depicted as a grey box. The Walker A, Walker B and Asp and His box important for ATP binding are shown in grey. Adapted from (Jakovljevic *et al.*, 2008) **B**. The structure of *Geobacter metallireducens* PilB was solved in an ADP and non-hydrolyzable ATP analogon bound state. These structures showed that nucleotide exchange must lead to domain movements of hexameric PilB. While PilB was suggested to rotate clockwise, the domain movement of PilT was meant to be counterclockwise **C.** The model is based on the structure of *Aquifex aeolicus* PilT (Satyshur *et al.*, 2007) and was created by structural comparison of the interfaces of PilB. The bottom parts show a cross-section through PilB and PilT, respectively. According to the model, PilB hexamers consist of four closed and two open units, while PilT hexamers are comprised of four open and two closed units. Adapted from (McCallum *et al.*, 2017).

3.2.2.9 Minor pilins and PilY1

Compared to the major pilin, the minor pilins are present in a lower abundance in T4aP (Giltner *et al.*, 2010). In *M. xanthus* and *P. aeruginosa,* minor pilins are essential for T4aP extension (Chang *et al.*, 2016, Nguyen *et al.*, 2015) and important for T4aP formation in *Neisseria* (Nguyen *et al.*, 2015, Winther-Larsen *et al.*, 2005, Carbonnelle *et al.*, 2006). Similar to the major pilin, the minor pilins are synthesized with a type III signal peptide and the signal peptide is cleaved off by the pre-pilin peptidase PilD (Strom *et al.*, 1993). The mature minor pilins have an N-terminal, hydrophobic α-helix followed by a globular domain (Winther-Larsen *et al.*, 2005). Structurally, minor pilins are similar to major pilins with a lollipop-like shape with an N-terminal α-helix followed by a globular domain. Minor pilins are either anchored in the IM via the N-terminal α-helix, incorporated into the T4aPM to

form a priming complex together with PilY1, or forming a tip complex in the assembled pilus (Figure 3, 12) (Craig *et al.*, 2019, Wang *et al.*, 2017, Chang *et al.*, 2016, Treuner-Lange *et al.*, 2020). It has been suggested that minor pilins prime T4aP extension, counteract retraction and promote surface adhesion (Winther-Larsen *et al.*, 2005, Carbonnelle *et al.*, 2006). Furthermore, minor pilins are thought to act as a cork for terminating pilus retraction (Treuner-Lange *et al.*, 2020).

Minor pilins are often encoded in gene clusters with PilY1, which is important for T4aP formation in *P. aeruginosa*, *N. meningitidis*, *N. gonorrhoeae* and *M. xanthus* (Nguyen *et al.*, 2015, Heiniger *et al.*, 2010, Ryll *et al.*, 1997, Wolfgang *et al.*, 1998, Treuner-Lange *et al.*, 2020). PilY.1 has been demonstrated to be part of the priming complex made by the major pilin and minor pilins and has been located at the tip of the pilus fiber, likely essential for pilus adhesion (Figure 3,12) (Xue *et al.*, 2022, Treuner-Lange *et al.*, 2020).

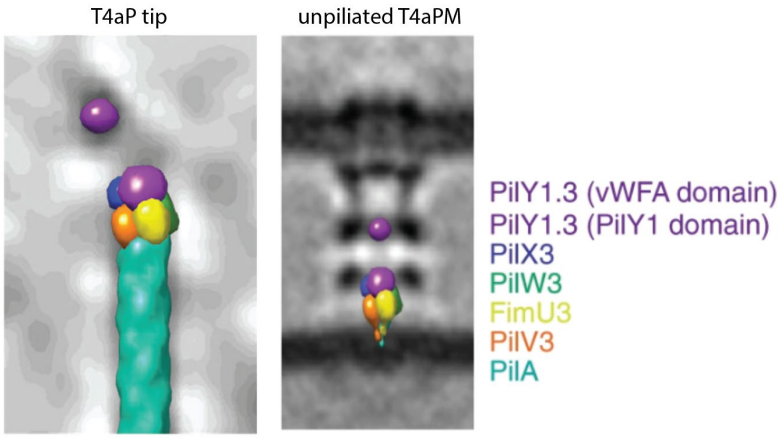

Figure 12 Model of the minor pilins and PilY.1 at the tip of the T4aP and in the unpiliated T4aPM. Hypothetical structural models of the minor pilins, PilA and PilY.1 at the tip of a T4aP (left) or in the priming complex in the unpiliated T4aPM (right). The models were placed into a cryoEM image of a kinked T4aP tip structure or the subtomogram averages of unpiliated T4aPM, respectively. Adapted from (Treuner-Lange *et al.*, 2020).

3.3 The molecular mechanism of T4aP assembly and disassembly

Overall the T4aPM can exists in three different states, non-piliated, in extension mode with PilB bound to the base, and a retraction mode with PilT bound at the base (Chang *et al.*, 2016, Treuner-Lange *et al.*, 2020). In all three structural states, the T4aPM span from the OM across the periplasm, IM to the cytoplasm and, furthermore, the PilQ secretin and TsaP are bound to the PG (Chang *et al.*, 2016). According to the current working model for how the machine works, PilB and PilT bind in a mutually exclusive manner to the

cytoplasmic base of the T4aPM. For T4aP extension, PilB binds to the base via interactions with PilC and PilM; upon ATP hydrolysis by PilB the PilC platform rotates resulting in PilA subunits being added to the base of the priming complex from a reservoir of in the IM. As PilA incorporation continues, the pilus grows from the base leaving the priming complex at the pilus tip. For pilus retraction, PilB unbinds and is replaced by PilT. PilT is suggested to rotate PilC in the opposite direction and thus facilitate removal of PilA subunits from the base of the pilus fiber and their reinsertion into the IM (Chang *et al.*, 2016).

In the model of the unpiliated machine (Figure 3) a cage like structure is formed by the coiled-coil regions of PilN and PilO, however, the space between the coiled-coil structures is not sufficiently wide to allow PilA to pass through. Therefore, it was suggested that once PilB binds to the T4aPM, the PilN-PilO coiled-coil structures spread apart, allowing PilA entry to the cage, thereby gaining access to the PilC platform (Chang *et al.*, 2016). According to this model, PilA subunits enter into the T4aPM laterally from the IM as long as PilB is hydrolyzing ATP. However, in an alternative model proposed for the T2SS, the major pseudo-pilin PilG directly interacts with the PilO homolog PulM in the IM. By binding to the PilM-PilN hybrid homolog PulL, PulM targets PulG and channels it to the site for the pseudo-pilus assembly. This model postulates PulG to be delivered to the T2SS in sub-complexes with PulM and, thus, PulM would dynamically associate with the T2SS (Figure 13) (Dazzoni *et al.*, 2023).

Little is known about the molecular exchange of subunits in the T4aPM. FRAP experiments performed on the cytosolic ATPase of the DNA-uptake machinery of *Bacillus subtilis*, which is required for pseudopilus assembly, the PilB homolog ComGA showed only 10% recovery within a timescale of few minutes. Therefore, it was suggested that the DNA-uptake machinery of competent *B. subtilis* cells is a stable complex (Kaufenstein *et al.*, 2011). By contrast, FRAP microscopy of a fluorescent fusion of the retraction ATPase PilT of the *M. xanthus* T4aPM showed fast recovery of the fluorescence intensity and, thus, fast protein exchange within two minutes (Bulyha *et al.*, 2009, Bulyha *et al.*, 2013).

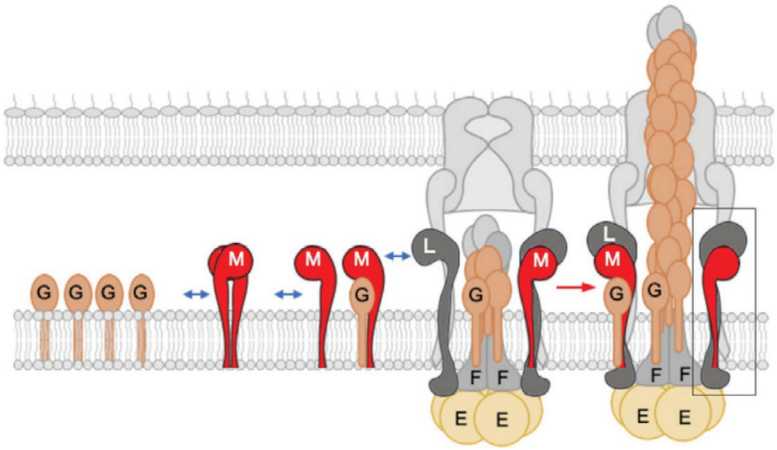

Figure 13 Model of PulG delivery to the T2SS by PulM. In this model, PulG interacts to PulM. PulM in turn binds to PulG in the T2SS and targets PulG to the PulL, PulF, PulE complex of the T2SS. Then PulG is released from PulM and added to the growing endopilus. Adapted from (Dazzoni *et al.*, 2023).

3.4 *M. xanthus*

M. xanthus is a Gram-negative member of the Myxococcales and belongs to the phylum Myxococcota (Waite *et al.*, 2020). It is an obligate aerobe soil bacterium. It encounters various environmental challenges and uses different processes to respond to them. Its life-cycle includes growth in spreading colonies, predation on other microorganisms and nutrient starvation-induced formation of spore-filled fruiting bodies (Figure 14) (Munoz-Dorado *et al.*, 2016).

During these phases of its lifecycle, *M. xanthus* uses and regulates two motility systems to translocate across surfaces: gliding motility and T4aP-dependent motility (Hodgkin & Kaiser, 1979). Gliding motility was previously known as adventurous motility and is used on hard surfaces, allowing single-cell movement. Single cells can leave the edge of the *M. xanthus* colony and explore their environment (Spormann, 1999), leaving a slime trail behind (Wolgemuth *et al.*, 2002). This trail is recognized by other *M. xanthus* cells, which start to follow these trails, leading to an organized expansion of the colony (Gloag *et al.*, 2015, Burchard, 1982). If nutrients are depleted, and in the presence of prey, *M. xanthus* cells can use T4aP-dependent motility to prey on other microorganisms, organizing themselves in wave structures known as rippling formation (Berleman *et al.*, 2006). The cells secrete exoenzymes via various systems e.g. a Tad-like apparatus (Kil) and an

atypical T3SS like apparatus, to lyse the prey and take up the released nutrients (Hart & Zahler, 1966, Seef *et al.*, 2021, Thiery *et al.*, 2022). If these nutrients are depleted, the starving cells start a developmental process using gliding motility and T4aP-dependent motility to form fruiting bodies. These structures are large multicellular aggregates, in which the rod-shaped cells differentiate into myxospores. In the presence of nutrients, the myxospores can germinate to start a new lifecycle (Dworkin, 1996, Sudo & Dworkin, 1969).

The rod-shaped *M. xanthus* cells translocate across surfaces in the direction of their long axis with defined leading and lagging cell poles. Cells reverse their direction of movement and polarity irregularly but with an average reversal frequency of one reversal in 8-10 min (Spormann & Kaiser, 1995), independently of the cell cycle.

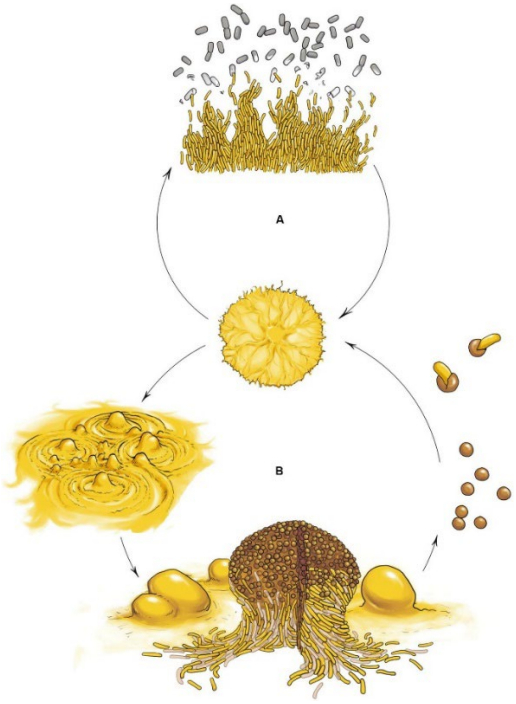

Figure 14 Multicellular cell cycle of *M. xanthus*. A. Vegetative growth of *M. xanthus* cells in the presence of nutrients. Cells grow, divide and move in a coordinated manner, forming swarms. Once cells make contact with other microorganisms, *M. xanthus* cells start to predate by penetrating the prey colony and lysing the cells. **B.** Upon starvation, the *M. xanthus* cells undergo a developmental program. Extracellular and physical contact signals initiate the formation of aggregates and fruiting body formation. These fruiting bodies are filled with myxospores. Myxospores germinate when nutrients are available again. Adapted from (Muñoz-Dorado *et al.*, 2016).

3.4.1 T4aP-dependent motility in *M. xanthus*

T4aPM assemble at both cell poles; however, T4aP are only assembled at the leading cell pole of *M. xanthus* cells (Figure 15). This polarity is brought about because the extension ATPase PilB predominantly localizes at the leading cell pole, while the retraction ATPase PilT predominantly localize at the lagging pole and only occasionally localizes to the leading pole (Bulyha *et al.*, 2009). During a cellular reversal, which is induced by the Frz chemosensory system (Kaimer *et al.*, 2012), the two ATPases disassemble from their poles and switch to the opposite poles (Bulyha *et al.*, 2009). Ultimately, piliated and unpiliated T4aPM are present at the leading pole, while only unpiliated T4aPM are at the lagging pole (Chang *et al.*, 2016, Friedrich *et al.*, 2014, Nudleman *et al.*, 2006, Siewering *et al.*, 2014). Systematic analysis of Pil mutants suggested that the T4aPM assembles in an outside-in manner, starting with the secretin in the OM (Friedrich *et al.*, 2014).

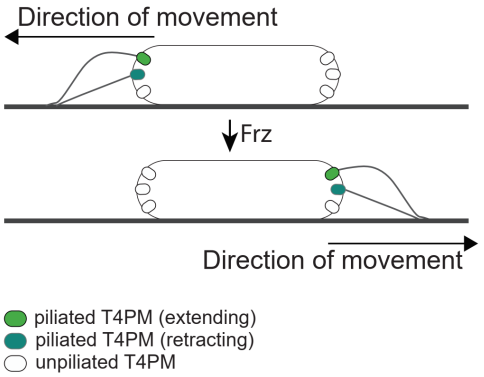

Figure 15 Localization of T4aP and T4aPM variants before and after reversals. PilQ, TsaP, PilM, PilN, PilO, PilP and PilC form a stationary complex and localize at both poles during and after Frz induced reversals. Three variants of the T4aPM can be found at the leading pole: piliated T4aPM that extend the pilus fiber, powered by PilB (light green), piliated T4aPM that retract the pilus fiber (dark green) and unpiliated T4aPM (white). While at the lagging pole only unpiliated T4aPM can be found.

3.4.2 Gliding motility in *M. xanthus*

Gliding motility allows single-cell movement and is often called adventurous motility (A-motility) (Spormann, 1999). The gliding motility machine in *M. xanthus* consists of three sub-complexes. The AglRQS proteins localize in the IM and use the proton-motive force to drive forward translocation of the cell (Sun *et al.*, 2011, Nan *et al.*, 2011). They interact with the 11 Glt proteins, which are known to be structural components of the gliding motility

machine and span the cell envelope (Jakobczak *et al.*, 2015, Luciano *et al.*, 2011). The third sub-complex is in the cytoplasm and consists of the Ras-like GTPase MglA, AglZ and the actin-like MreB (Treuner-Lange *et al.*, 2015).

Several proteins involved in gliding motility localize at the leading pole in moving cells, switch polarity during reversals, and colocalize in three to four complexes that are distributed along the cell length and fixed to the substratum (Jakobczak *et al.*, 2015, Luciano *et al.*, 2011, Treuner-Lange *et al.*, 2015). These complexes are known as focal adhesion complexes (FAC) and are the sites of force generation for gliding motility (Mignot *et al.*, 2007).

According to the current model, the AglRQS complex assembles at the leading cell pole, connects with the cytoplasmic and IM Glt proteins and is stimulated by the AglZ/MglA/MreB complex (Treuner-Lange *et al.*, 2015). The fully assembled machine adheres to the substratum, and then the AglRQS motor translocates the machine towards the lagging pole in a proton-motive force-dependent manner (Sun *et al.*, 2011, Schumacher & Sogaard-Andersen, 2017, Mignot *et al.*, 2007). While the cell is moving forward, the gliding motility machine is fixed to the substratum. Once the gliding motility machine reaches the lagging pole , it disassembles (Mignot *et al.*, 2007).

3.4.3 Regulation of motility in *M. xanthus*

M. xanthus cells translocate across surfaces along their long axis with defined leading and lagging cell poles (Zhang *et al.*, 2012a). Cells revert their direction of movement irregularly but with an average reversal frequency of one reversal in 8-10 min (Spormann & Kaiser, 1995). A reversal switches the direction of translocation and cell polarity. Two protein modules regulate the polarity of the two motility machines in *M. xanthus* (Figure 16)**.** The polarity module consists of at least six cytoplasmic proteins; the small Ras-like GTPase MglA, the MglB/RomY complex, which has GTPase activating complex (GAP) activity, the RomR-RomX complex, which has Guanine nucleotide exchange factor (GEF) activity, and the adaptor protein MglC (Figure 16 A,B) (Szadkowski *et al.*, 2022, Szadkowski *et al.*, 2019, Keilberg *et al.*, 2012b, Leonardy *et al.*, 2010b, Zhang *et al.*, 2010, Zhang *et al.*, 2012b, Carreira *et al.*, 2023). The polarity inversion module consists of the Frz chemosensory system (Figure 16D) (Blackhart & Zusman, 1985, Carreira *et al.*, 2022).

MglA can bind GTP and GDP and has a low intrinsic GTPase activity. MglA is active when bound to GTP, and it is essential for both motility systems. MglA-GTP directly interacts

with SgmX, which stimulates the polar localization of the PilB extension ATPase (Mercier *et al.*, 2020, Potapova *et al.*, 2020). For gliding motility, MglA-GTP directly interacts with actin-like protein MreB and polarly localized AglZ and is incorporated into the Agl-Glt machinery at the leading pole (Figure 16A) (Mercier *et al.*, 2020, Yang *et al.*, 2004, Treuner-Lange *et al.*, 2015, Mauriello *et al.*, 2010, Nan *et al.*, 2014).

MglA GTPase activity is stimulated by MglB (Leonardy *et al.*, 2010a, Zhang *et al.*, 2010, Zhang *et al.*, 2012b). MglA-GTP, which is the active form, localizes at the leading pole and the inactive form MglA-GDP is diffusely localized (Figure 16C) (Leonardy *et al.*, 2010a, Zhang *et al.*, 2010, Miertzschke *et al.*, 2011). MglB/RomY and RomR/RomX localize similarly to the cell poles, each with a large cluster at the lagging pole and a small cluster at the leading pole (Figure 16C) (Zhang *et al.*, 2010, Leonardy *et al.*, 2010a, Leonardy *et al.*, 2007, Szadkowski *et al.*, 2019, Szadkowski *et al.*, 2022). Nevertheless, GAP activity dominates at the lagging and GEF activity at the leading pole. Due to the spatial separation of the GAP and GEF activities, MglA-GTP specifically localizes to the leading pole (Figure16C) (Zhang *et al.*, 2012b, Keilberg *et al.*, 2012a, Zhang *et al.*, 2010). Recently RomR/MglC/MglB were found to form a complex, that helps to establish correct polarity of MglB/RomY and RomR/RomX (Carreira *et al.*, 2023).

The polarity inversion module consists of the Frz chemosensory system, which is homologous to the chemotaxis regulating systems in other bacteria (Porter *et al.*, 2011, Kaimer *et al.*, 2012, Mercier & Mignot, 2016). The core of this system consists of a methylated chemotaxis protein (MCP) homolog FrzCD, the CheW homolog FrzA, and the hybrid histidine protein kinase FrzE (Mauriello & Zusman, 2007, Bustamante *et al.*, 2004). All three components are essential for inducing reversals (Bustamante *et al.*, 2004). FrzE autophosphorylates on a conserved His residue. FrzE can transfer the phosphate to the two response regulators FrzZ and FrzX to induce the polarity inversion (Figure 16D) (Inclan *et al.*, 2007, Guzzo *et al.*, 2018, Inclán *et al.*, 2008, Kaimer & Zusman, 2013). Phosphorylated FrzZ localizes to the leading pole during and between reversals in an MglA-dependent manner (Kaimer & Zusman, 2016). By contrast, phosphorylated FrzX localizes to the lagging pole in an MglB-dependent manner (Guzzo *et al.*, 2018). By an unknown mechanism, phosphorylated FrzZ and FrzX at the two poles causes the inversion of the polarity of the six proteins of the polarity module (Guzzo *et al.*, 2018, Kaimer & Zusman, 2013, Carreira *et al.*, 2022, Carreira *et al.*, 2023). Thus, after a reversal MglA-GTP localizes to the new leading pole where it recruits its effector protein SgmX that

brings about polar localization of PilB at the leading pole. As a consequence, T4aP are assembled at the new leading pole after a reversal (Potapova *et al.*, 2020, Mercier *et al.*, 2020).

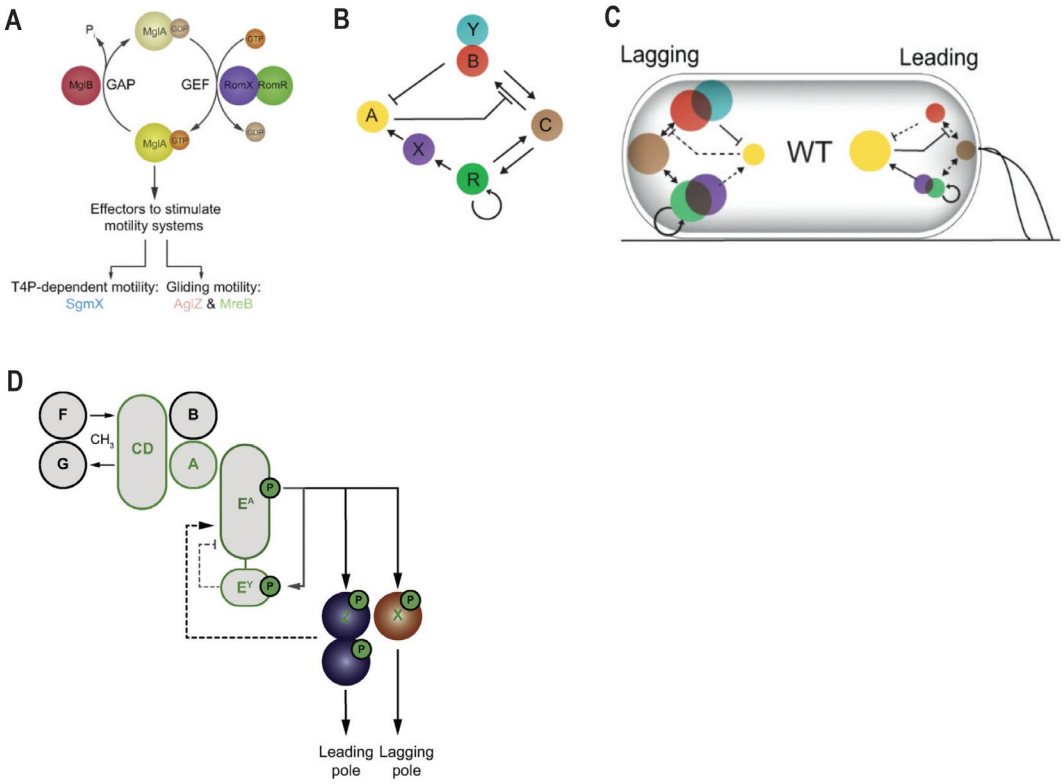

Figure 16 Regulation of cell polarity and motility in *M. xanthus*. A. MglA GTPase (yellow) cycle including effectors of MglA-GTP. The GAP MglB is shown in red and the GEF RomR-RomX is shown in purple and green. **B.** Regulatory protein interactions that establish and maintain front-rear polarity in *M. xanthus.* RomY is shown in cyan and MglC in light brown. **C.** Protein interactions between the polarity proteins at leading and lagging cell poles of *M. xanthus* cells. Arrows show locally strong interactions, dashed arrows show locally suppressed interactions. The arrow from RomR on itself indicates the positive feedback that reinforces its polar localization. **D.** Schematic overview of the Frz polarity inversion module. The methyl-accepting chemotaxis protein (MCP) FrzCD, the CheA-like histidine kinase FrzE with an N-terminal kinase domain (FrzEA) and a C-terminal receiver domain FrzEY, the CheW-like coupling proteins FrzA and FrzB, FrzF and FrzG with FrzCD methyltransferase and methylesterase activity, respectively, and the response regulators FrzZ and FrzX are shown. The suggested phosphotransfer from FrzEA at low signaling levels to FrzEY is shown in grey, and the experimentally verified phosphotransfer at higher signaling levels to FrzZ and FrzX is shown as black lines. The suggested feedback regulation of FrzEA by FrzEY~P is shown as dashed grey and by FrzZ~P as dashed black arrows. The core Frz proteins are indicated in green. Adapted from (Carreira *et al.*, 2023).

4 Scope of this study

In this study, we aim to gain insights into the structure and function of the T4aPM. To this end, we use FRAP microscopy to determine whether components of the T4aPM in *M. xanthus* are stably incorporated into the T4aPM or not.

5 Results

To investigate whether components of the T4aPM in *M. xanthus* are stably incorporated into the T4aPM or not, we used FRAP microscopy. To minimize the chances of artefacts, we tagged components of the T4aPM with a fluorescent protein and expressed the corresponding alleles from the native site. Subsequently, the fluorescent fusion proteins were analyzed for functionality, accumulation and localization.

For the FRAP experiments, we focused on experiments in a hyporeversing strain background because this allows us to distinguish clearly between events at the leading and lagging cell poles. Therefore, to avoid reversals, the chosen strain background carries an in-frame deletion of *frzE*, which encodes the FrzE kinase of the Frz system and is essential for reversals (Bustamante *et al.*, 2004). Moreover, in the chosen strain background, the gliding motility system was inactivated and, thus, cells could only move by means of T4aP-dependent motility. To this end, the chosen strain carries an in-frame deletion of *aglQ*, which is essential for gliding (Sun *et al.*, 2011). By performing the FRAP experiments under conditions where cells could move by T4aP-dependent motility, we ensured that the bleaching events did not interfere with cell viability and the the proper function of the T4aPM.

5.1 Functionality, accumulation and localization of PilQ-sfGFP

As previously described (Potapova *et al.*, 2020), the PilQ-sfGFP fusion protein encoded by the *pilQ-sfGFP* allele at the native site was fully functional in motility assays (Figure 17A). Immunoblot analyses demonstrated that PilQ-sfGFP accumulated at similar levels in all four strains and at a level similar to that of unlabeled PilQ suggesting that the fusion is indeed stable in the different strains (Figure 17B). Additionally, we confirmed by that in the Δ*frzE* strains, no FrzE accumulated (Figure 17B).

To determine whether the localization of PilQ-sfGFP was affected when FrzE and/or AglQ were lacking, PilQ-sfGFP was localized in exponentially growing cells using fluorescence microscopy. As previously shown (Potapova *et al.*, 2020), localization of PilQ-sfGFP in the wildtype (WT) strain was predominantly bipolar asymmetric, but it can also localize in a bipolar symmetric or a unipolar manner. Similar results were obtained in the absence of FrzE and/or AglQ (Figure 17C), demonstrating that neither of these two proteins affects PilQ localization.

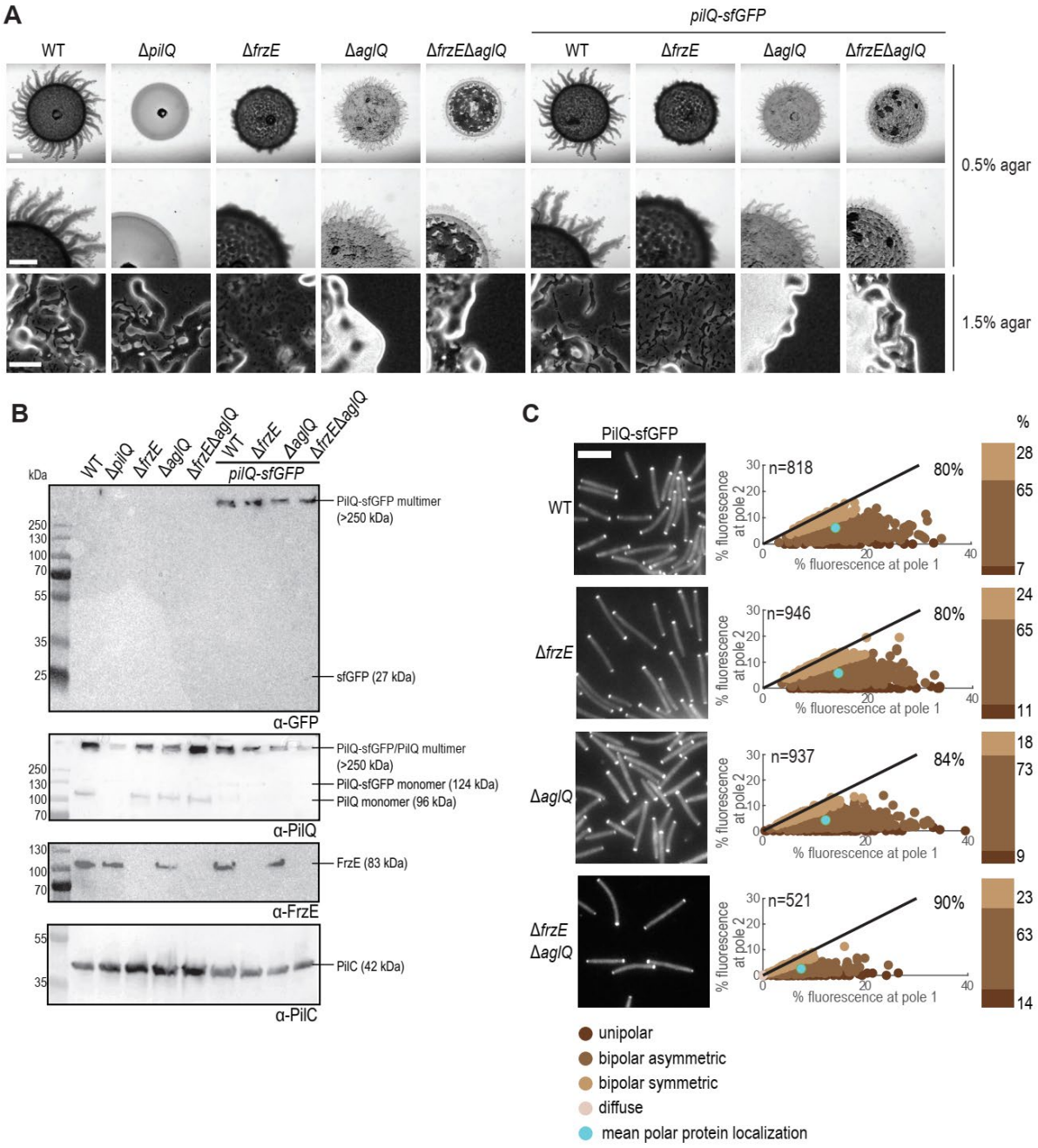

Figure 17 Functionality, accumulation and localization of PilQ-sfGFP. A. T4aP-dependent motility assay was performed on 0.5% agar (upper two rows) and gliding motility assay on 1.5% agar (bottom). Scale bars: 1 mm, 1mm and 100 µm from top to bottom. WT, Δ*pilQ*, Δ*frzE*, Δ*aglQ* and Δ*frzE*Δ*aglQ* strains were used as controls. **B.** Accumulation of PilQ and PilQ-sfGFP in the indicated strains analyzed by immunoblotting. Total cell extracts prepared from the same number of cells was loaded per lane. Antibodies used are indicted. The PilC immunoblot served as a loading control. **C.** Fluorescence microscopy of cells synthesizing PilQ-sfGFP. Exponentially growing cells were placed on chitosan-coated µ-dishes and imaged by fluorescence microscopy after 30 min at room temperature (RT). A representative snapshot is shown for each strain (Scale bar: 5 µm). Images were analyzed with a custom-made MATLAB script and the results shown as scatter plots in which by definition pole 1 refers to the pole with the highest polar fluorescent signal. Each dot

represents the polar localization pattern of one cell categorized as diffuse, unipolar, bipolar asymmetric and bipolar symmetric. The cyan dot shows the mean localization. The average cytoplasmic signal is given on the right top part of the scatter plot and the number of cells (n) at the top left part. The bars next to the scatter plots represent the percentage of cells sorted into the different localization patterns. The analysis of two biological replicates is shown.

5.2 Functionality, accumulation and localization of TsaP-mCherry

A newly constructed TsaP-mCherry fusion, based on a fusion published by (Siewering *et al.*, 2014), and encoded by the *tsaP-mCherry* allele at the native site was fully functional in motility assays (Figure 18A). In immunoblots, that all mutants accumulated TsaP-mCherry at similar levels and TsaP-mCherry accumulated at slightly higher levels than native TsaP (Figure 18B). Faint bands corresponding to free mCherry were also detected indicating that TsaP-mCherry was partially cleaved. Moreover, lack of FrzE was confirmed in the relevant strains (Figure 18B). As previously shown (Siewering *et al.*, 2014), fluorescence microscopy demonstrated that the polar localization of TsaP-mCherry in all four strains was predominantly bipolar symmetric, demonstrating that neither FrzE nor AglQ affects localization of TsaP-mCherry (Figure 18C).

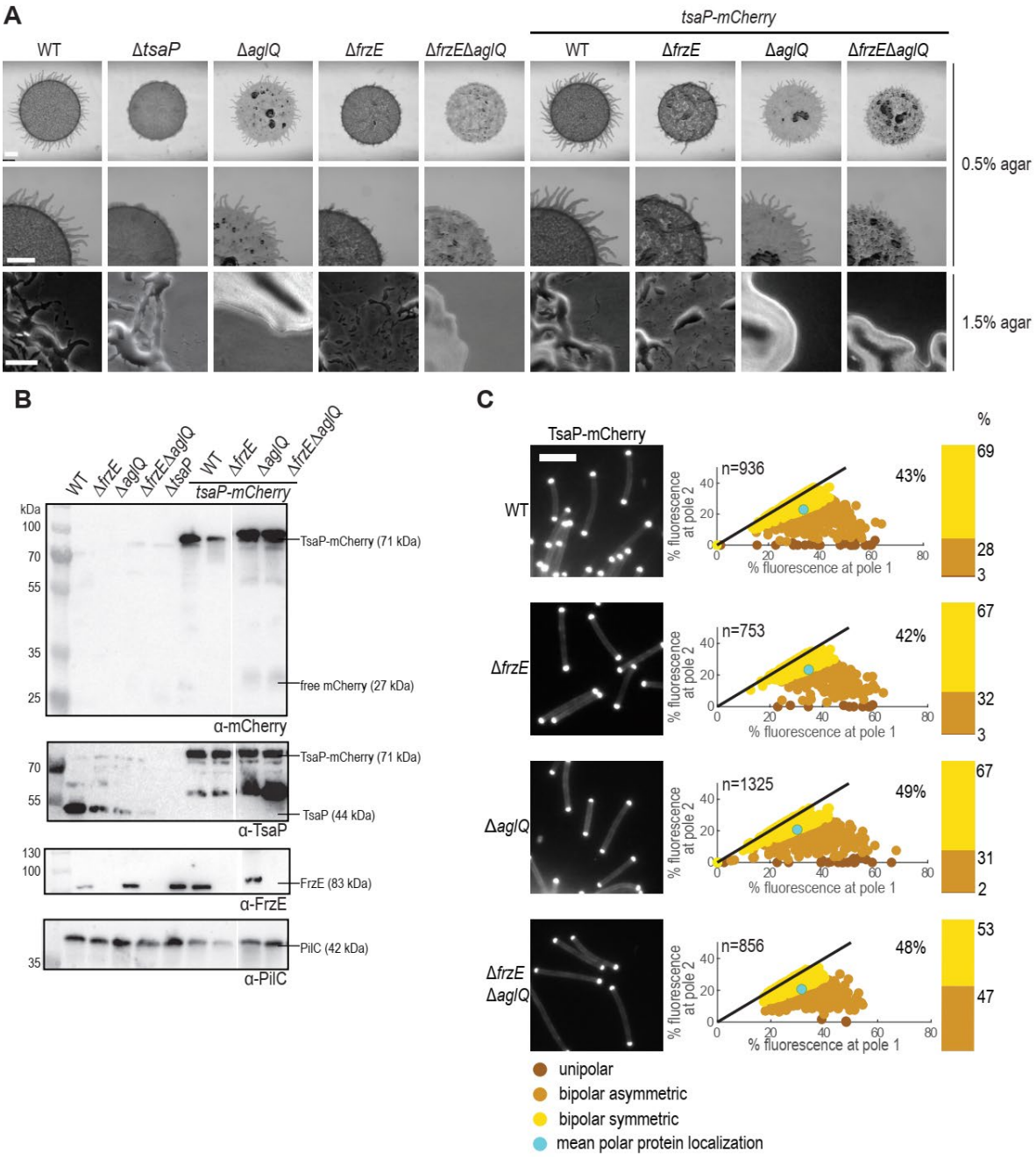

Figure 18 Functionality, accumulation and localization of TsaP-mCherry. A. Functional test of TsaP-mCherry in motility. Motility assays were performed as in Figure 17A. **B.** Immunoblot analysis of TsaP-mCherry accumulation. Experiments were done as in Figure 17B. **C.** Fluorescence microscopy of TsaP-mCherry. Experiments were done as in Figure 17C**.** The analysis of two biological replicates is shown.

5.3 Functionality, accumulation and localization of PilP-sfGFP

A newly generated PilP-sfGFP fusion expressed from *pilP-sfGFP* at the native site, which is based on a fusion published by (Friedrich *et al.*, 2014), was fully functional in supporting

T4aP-dependent motility (Figure 19A). In immunoblots, all strains accumulated PilP-sfGFP at similar levels, and PilP-sfGFP accumulated at a level similar to unlabeled PilP. Faint bands of free sfGFP could be detected using α-GFP antibodies, suggesting that PilP-sfGFP is partially cleaved (Figure 19B). Moreover, lack of FrzE was confirmed in the relevant strains (Figure 19B). In all four strains the polar localization of PilP-sfGFP was predominantly bipolar asymmetric (Figure 19C), demonstrating that neither lack of FrzE nor AglQ affects the localization of PilP-sfGFP.

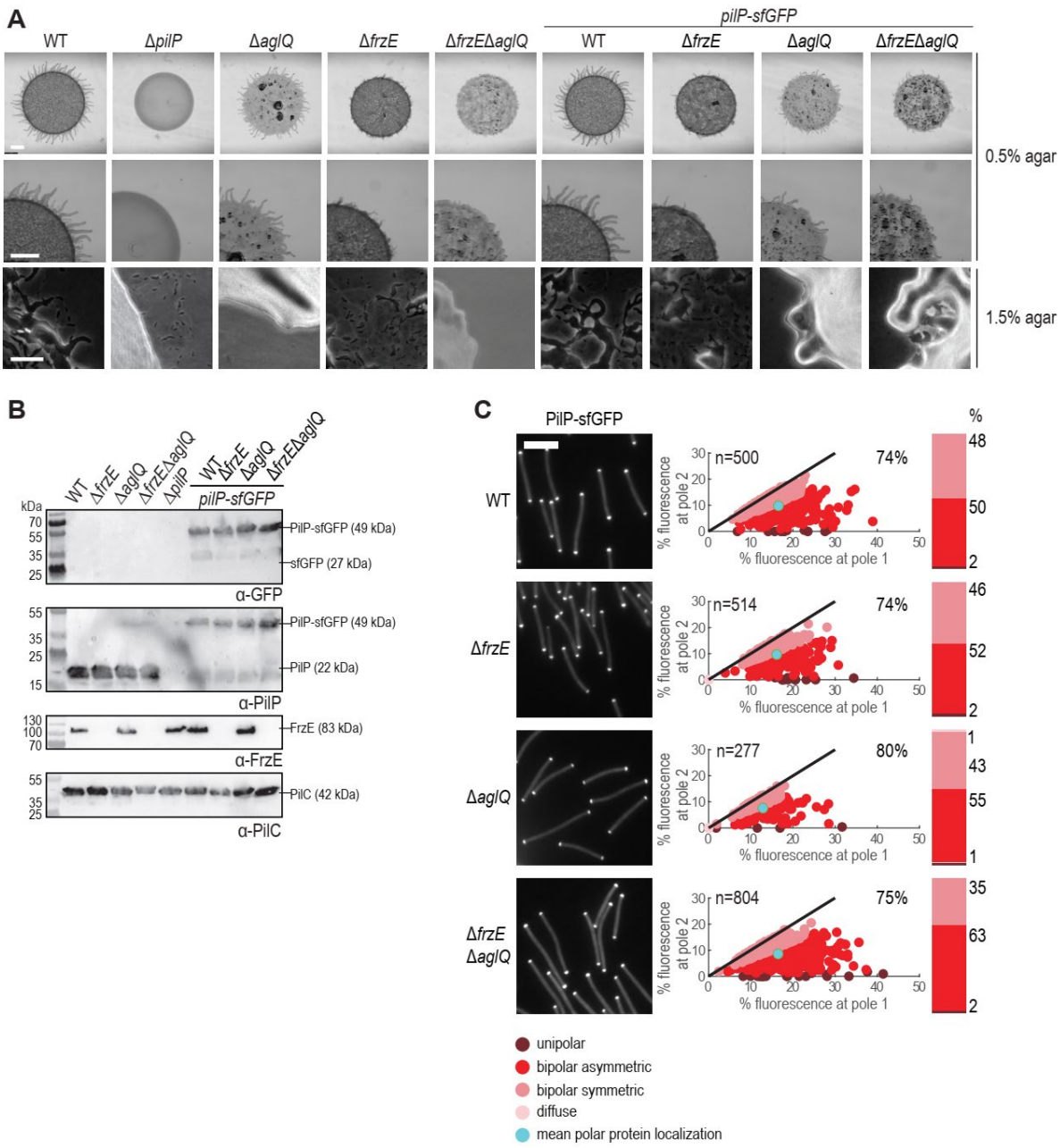

Figure 19 Functionality, accumulation and localization of PilP-sfGFP. A. Functional test of PilP-sfGFP in motility. Motility assays were performed as in Figure 17A. **B.** Immunoblot analysis of PilP-sfGFP accumulation. Experiments were done as in Figure 17B. **C.** Fluorescence microscopy of PilP-sfGFP. Experiments were done as in Figure 17C**.** The analysis of two biological replicates is shown.

5.4 Functionality, accumulation and localization of PilO-sfGFP

A PilO-sfGFP fusion expressed from *pilO-sfGFP* at the native site and generated on the basis of a PilO-sfGFP fusion, which was expressed ectopically in Friedrich *et al*., 2014,

was only partially active in WT and the Δ*frzE* mutant and did not support T4aP-dependent motility in the Δ*aglQ* and Δ*frzE*Δ*aglQ* mutants (Figure 20 20A). We conclude that the PilO-sfGFP fusion is only partially functional. In immunoblots, all strains accumulated PilO-sfGFP at similar levels, and PilO-sfGFP accumulated at slightly lower levels unlabeled PilO. Faint bands of free sfGFP could be detected using α-GFP antibodies, suggesting that PilO-sfGFP is partially cleaved (Figure 20B). Lack of FrzE was confirmed in the relevant strains (Figure 20B). In all four strains the polar localization of PilP-sfGFP was predominantly bipolar asymmetric (Figure 20C), demonstrating that neither lack of FrzE nor AglQ affects the localization of PilP-sfGFP. As previously described for WT (Friedrich *et al.*, 2014), polar localization of PilO-sfGFP was predominantly bipolar asymmetric in all four strains, demonstrating that FrzE or AglQ do not affect the polar PilO-sfGFP localization (Figure 20C).

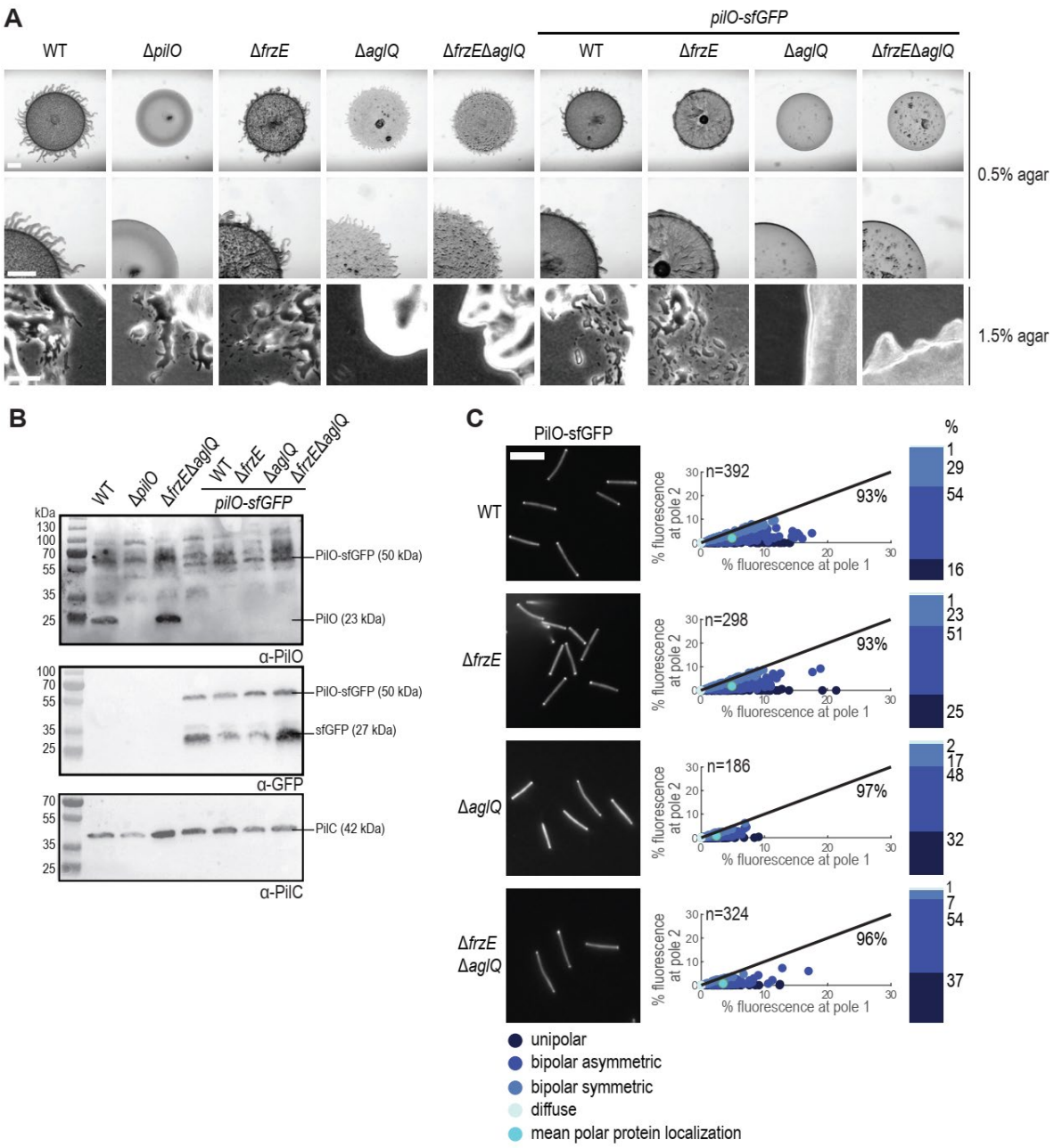

Figure 20 Functionality, accumulation and localization of PilO-sfGFP. A. Functional test of PilO-sfGFP in motility. Motility assays were performed as in Figure 17A. **B.** Immunoblot analysis of PilO-sfGFP accumulation. Experiments were done as in Figure 17B. **C.** Fluorescence microscopy of PilO-sfGFP. Experiments were done as in Figure 17C**.** The analysis of two biological replicates is shown.

5.5 Functionality, accumulation and localization of mCherry-PilM

As previously shown (Treuner-Lange *et al.*, 2020), mCherry-PilM expressed from the *mCherry-pilM* allele at the native site was fully active (Figure 21A). In immunoblots, all

strains accumulated mCherry-PilM at similar levels, but mCherry-PilM accumulated at a higher level than unlabeled PilM (Figure 21B). Using α-PilM antibodies, an additional band was detected and faint bands of free mCherry were also detected using α-mCherry antibodies, suggesting that mCherry-PilM is partially cleaved (Figure 21B). Moreover, lack of FrzE was confirmed in the relevant strains (Figure 21B). In all four strains the polar localization of mCherry-PilM was predominantly bipolar asymmetric (Figure 21C), demonstrating that neither lack of FrzE nor AglQ affects the localization of mCherry-PilM. Fluorescence microscopy demonstrated that mCherry-PilM localizes predominantly bipolar asymmetric in all four strains (Figure 21C). Thus, neither lack of FrzE nor AglQ affects mCherry-PilM localization.

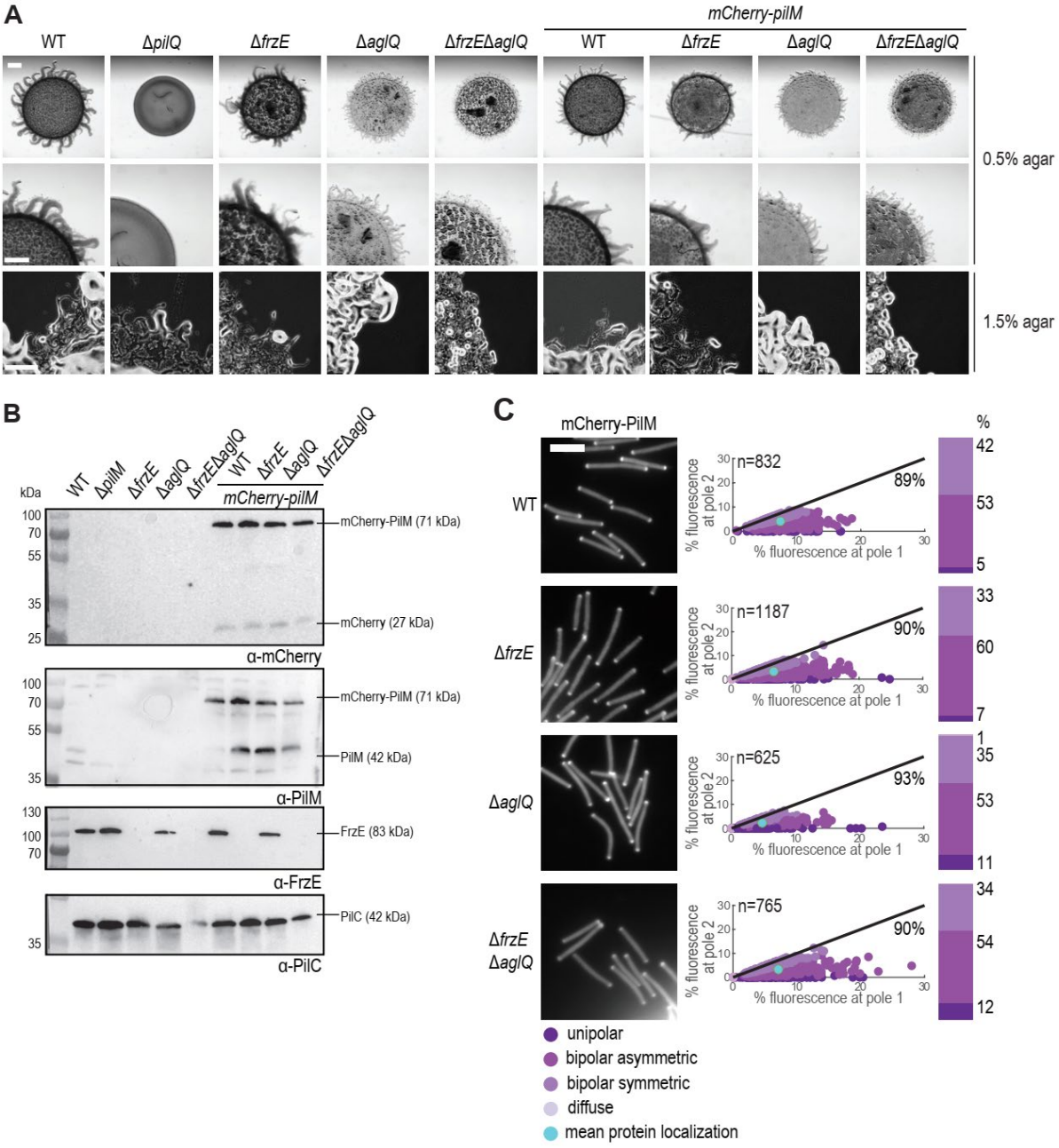

Figure 21 Functionality, accumulation and localization of mCherry-PilM. A. Functional test of mCherry-PilM in motility. Motility assays were performed as in Figure 17A. **B.** Immunoblot analysis of mCherry-PilM accumulation. Experiments were done as in Figure 17B. **C.** Fluorescence microscopy of mCherry-PilM. Experiments were done as in Figure 17C**.** The analysis of two biological replicates is shown.

5.6 Functionality, accumulation and localization of PilB-mCherry

A newly constructed PilB-mCherry fusion, based on (Potapova *et al.*, 2020), expressed from the *pilB-mCherry* allele at the native site was partially functional in supporting T4aP-

dependent motility (Figure 22A). PilB-mCherry accumulated at the same level in in all four strains and at the same level as unlabeled PilB (Figure 22B). Free mCherry was not detected, suggesting the fusion is not cleaved (Figure 22B). As previously reported for WT (Potapova *et al.*, 2020), PilB-mCherry was predominantly unipolar in all four strains (Figure 22C), demonstrating that lack of FrzE and/or AglQ does not affect the localization of PilB-mCherry.

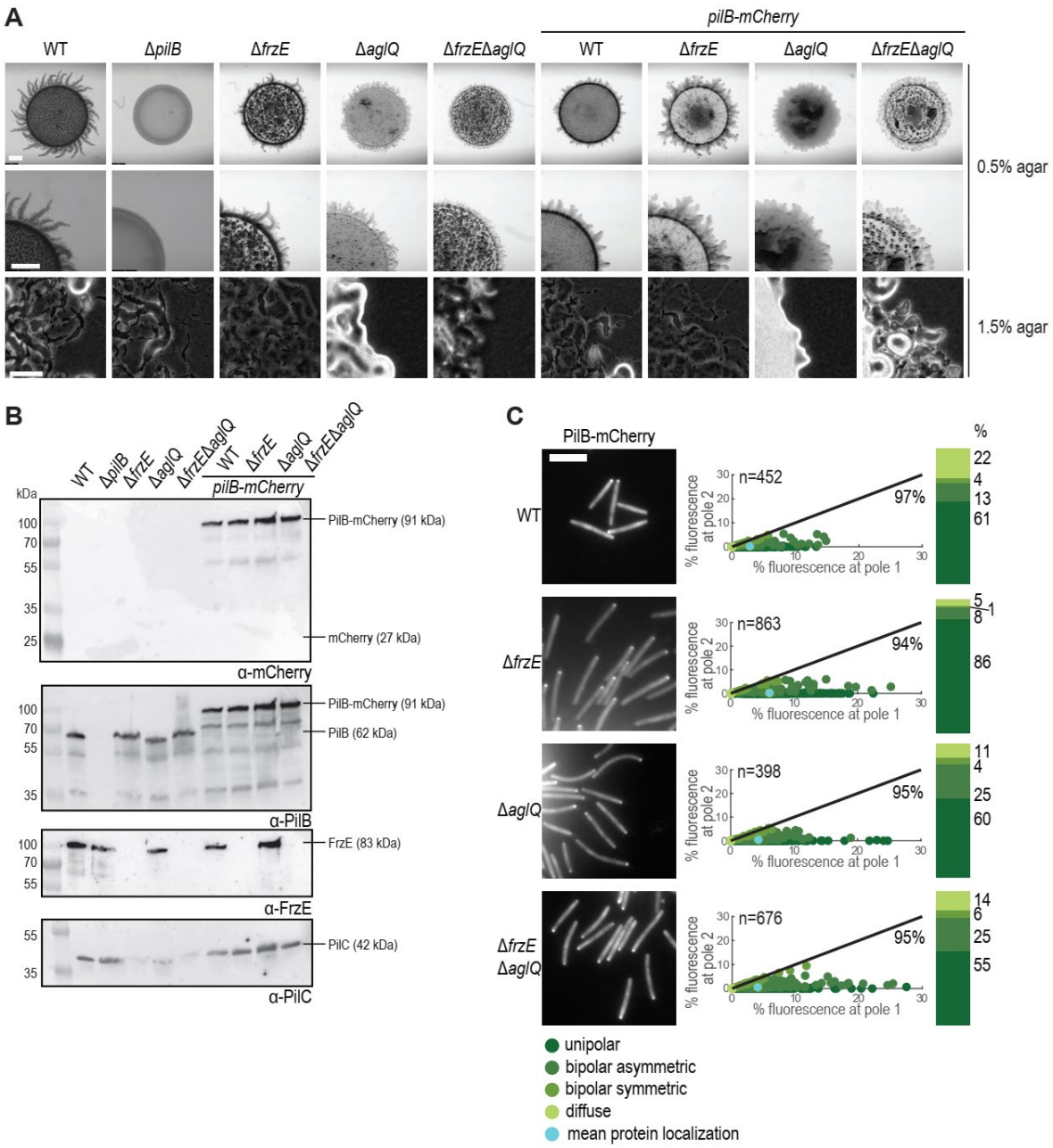

Figure 22 Functionality, accumulation and localization of PilB-mCherry. A. Functional test of PilB-mCherry in motility. Motility assays were performed as in Figure 17A. **B.** Immunoblot analysis of PilB-mCherry accumulation. Experiments were done as in Figure 17B. **C.** Fluorescence microscopy of PilB-mCherry. Experiments were done as in Figure 17C**.** The analysis of two biological replicates is shown.

5.7 Functionality, accumulation and localization of mCherry-PilT

A newly constructed mCherry-PilT fusion, based on (Potapova *et al.*, 2020), expressed from the *mCherry-pilT* allele at the native site is fully functional (Figure 23A). In all four strains, mCherry-PilT accumulated at the same level but at a slightly lower level than unlabeled PilT (Figure 23B). The detection of free mCherry suggest that mCherry-PilT was partially cleaved (Figure 23B). As previously shown in WT (Potapova *et al.*, 2020), mCherry-PilT localized predominantly in a bipolar asymmetric pattern in all four strains (Figure 23C), demonstrating that lack of FrzE and/or AglQ do not affect its localization.

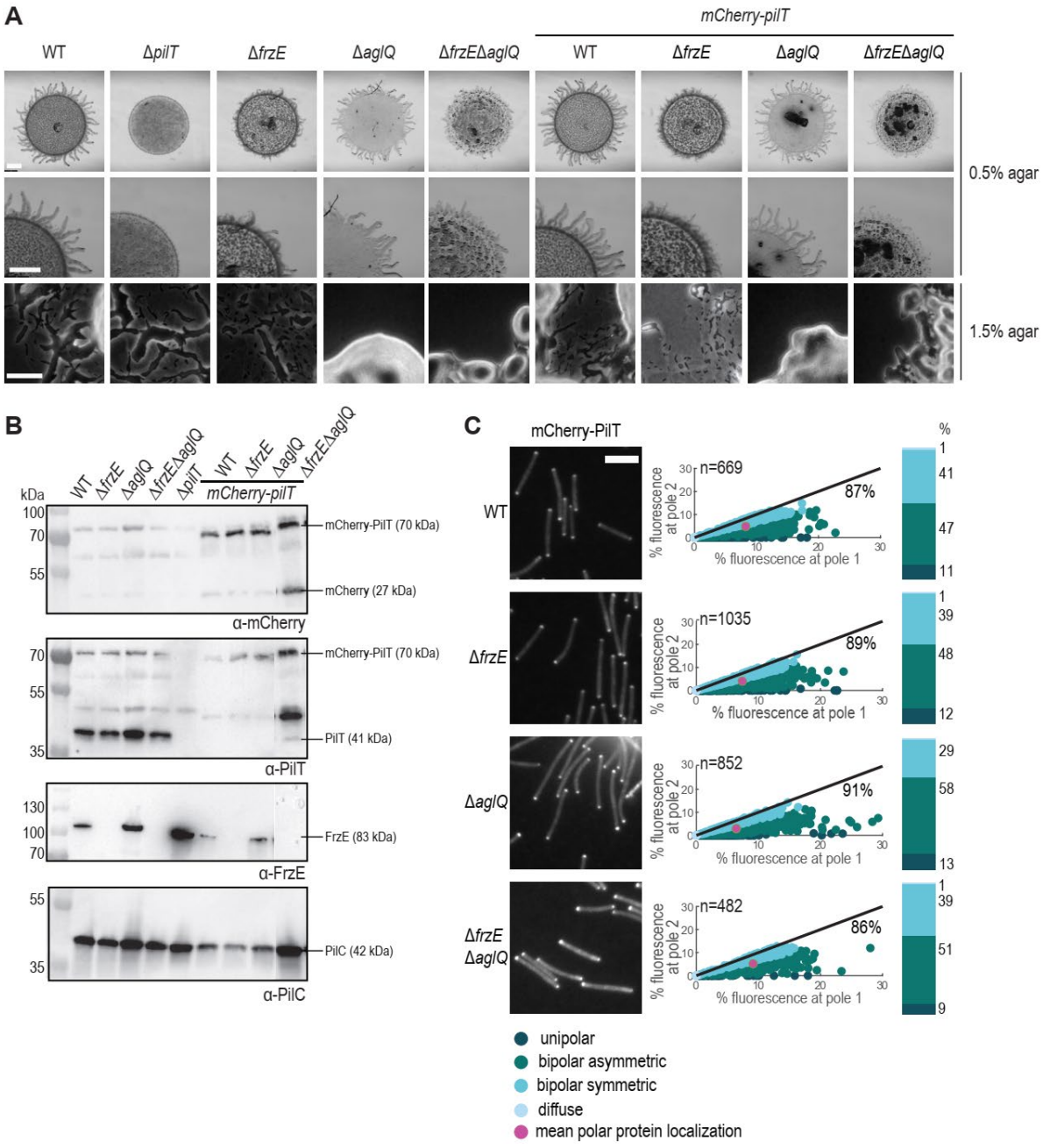

Figure 23 Functionality, accumulation and localization of mCherry-PilT. **A.** Functional test of mCherry-PilT in motility. Motility assays were performed as in Figure 17A. **B.** Immunoblot analysis of mCherry-PilT accumulation. Experiments were done as in Figure 17B. **C.** Fluorescence microscopy of mCherry-PilT. Experiments were done as in Figure 17C**.** The analysis of two biological replicates is shown.

5.8 Polar localization of PilB and PilT is strongly reduced in the absence of an assembled T4aPM

We previously showed that the polar localization of PilQ, TsaP, PilP, PilO and PilM reflects their incorporation into the T4aPM (Friedrich *et al.*, 2014, Herfurth *et al.*, 2023), while PilB and PilT were suggested to localize to the cell poles independently of the T4aPM (Friedrich *et al.*, 2014). However, in the case of PilB this was done using immunofluorescence microscopy, and in the case of PilT, this was done using a YFP-PilT fusion that accumulated at a much higher level than native PilT (Friedrich *et al.*, 2014). To assess PilB and PilT localization in the absence of an assembled T4aPM, we determined the accumulation and localization of the PilB-mCherry and mCherry-PilT fusions expressed from their native sites and accumulating at close to native levels (Figure 21B, 22B) in the absence of PilQ, which is essential for T4aPM assembly.

Neither PilB-mCherry nor mCherry-PilT accumulation was affected by the lack of PilQ (Figure 24B) (Friedrich *et al.*, 2014). However, in the absence of PilQ, and, thus, of the T4aPM, PilB-mCherry polar localization was strongly reduced and most cells did not have a polar cluster and in cells with a cluster, the cluster was very faint (Figure 24C). Similarly, mCherry-PilT also localized much more diffusely and unipolar in the absence of PilQ and the polar clusters were fainter than in WT (Figure 24C). We conclude that polar localization of PilB-mCherry and mCherry-PilT at native levels strongly depends on an assembled T4aPM.

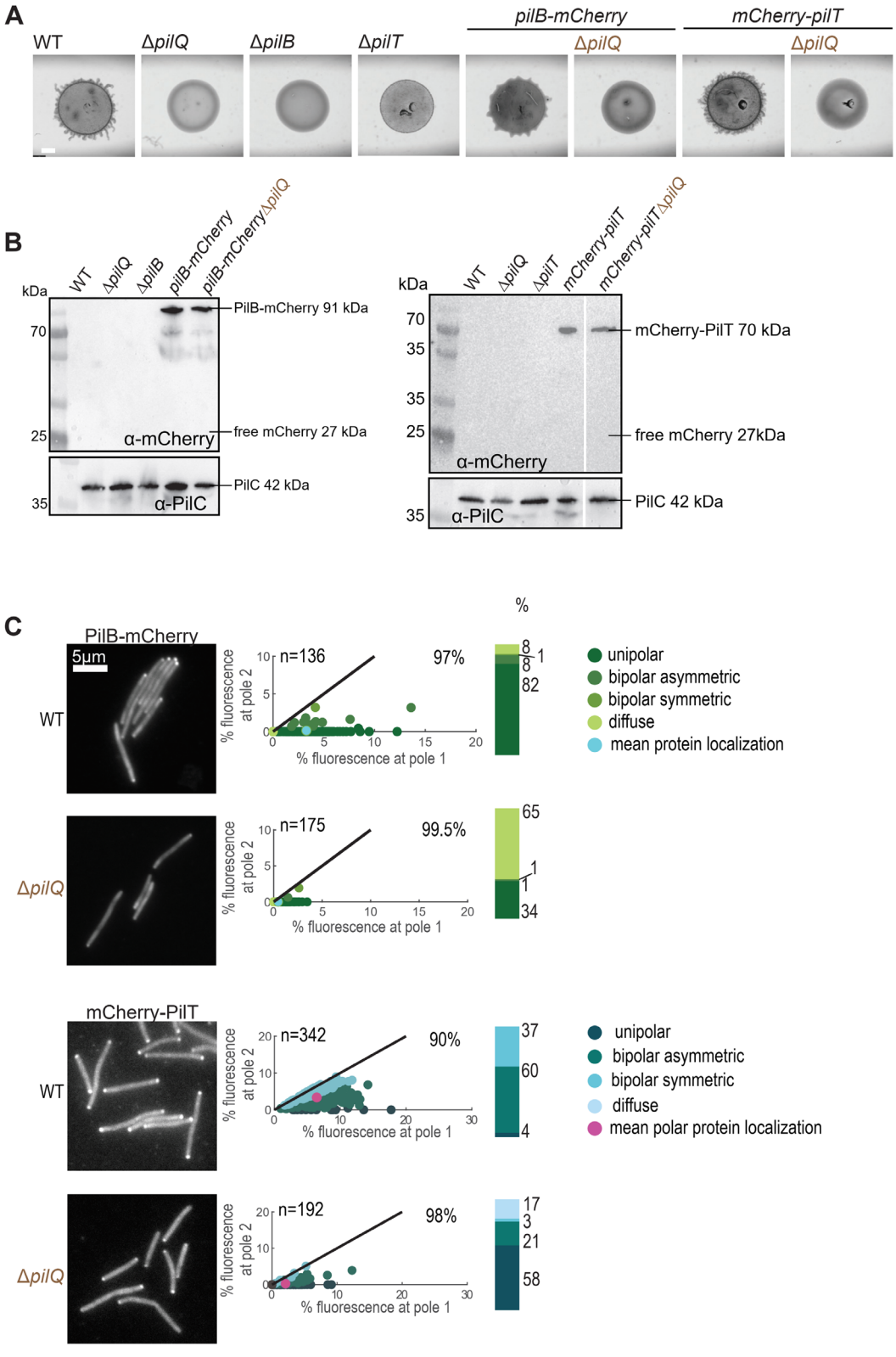

Figure 24 Polar localization of PilB-mCherry and mCherry-PilT is strongly reduced in the absence of assembled T4aPM. A. T4aP-dependent motility assay was performed on 0.5% CTT agar. Scale bar: 1mm. **B.** Immunoblot of PilB-mCherry and mCherry-PilT assembly. Total cell

extract from the same number of cells was loaded per lane. The α-PilC blots served as a loading control. **C**. Localization of PilB-mCherry and mCherry-PilT in the absence of PilQ. Microscopy and data analysis was performed as described in Figure 17C. The analysis of two biological replicates is shown.

5.9 Experimental and analytical setup for FRAP microscopy

Based on the above analyses, PilQ-sfGFP, TsaP-mCherry, PilP-sfGFP, mCherry-PilM and mCherry-PilT are fully functional and PilO-sfGFP and PilB-mCherry are partially functional. Moreover, neither accumulation nor localization of these proteins are affected by lack of FrzE and/or AglQ. Because the polar localization of PilQ, TsaP, PilP, PilO and PilM reflects their incorporation into the T4aPM (Friedrich *et al.*, 2014, Herfurth *et al.*, 2023) and PilB and PilT polar localization strongly depends the T4aPM, and, therefore, their incorporation into the T4aPM (5.8). We reasoned that we could use FRAP analysis to assess how stably these different building blocks are incorporated into the T4aPM.

To this end, we used the workflow outlined in Figure 25. Specifically, after the acquisition of a pre-bleach image, a cell of interest was photobleached in a 0.9×0.9 µm circular-shaped polar region. A fluorescence microscopy image was acquired immediately after photobleaching (defined as 0s) and the fluorescence recovery was followed over time, similarly as in (Schumacher *et al.*, 2017, Kiekebusch *et al.*, 2012). To quantify fluorescence, cells were segmented into the leading pole, the lagging pole, and the cytoplasmic region. Polar regions were defined as the regions of a cell within a distance of 10% of the cell length from a tip of the cell, and the cytoplasm as the remaining 80%. Subsequently, for each bleaching event, the normalized relative fluorescence in the bleached area was plotted as a function of time, followed by curve fitting using a single-exponential function. R^2 (coefficient of determination) and half-maximal recovery time ($t_{1/2}$) were calculated for each curve fit, and bleaching/recovery events with $R^2 < 0.35$ and $t_{1/2} > t_{measured}$ were excluded from further analyses. For the remaining bleaching events, the mean $t_{1/2}$ and the mean mobile fraction were determined by fitting the mean data from n cells to a single-exponential function and presented as mean±standard deviation (SD). To test for statistically significant differences between $t_{1/2}$ and mobile fraction for the same protein at the leading and lagging pole or between different proteins, we specifically compared $t_{1/2}$ and mobile fraction obtained for the n single cells.

Unless otherwise noted, we bleached either the leading or the lagging cell pole in the hypo-reversing Δ*frzE*Δ*aglQ* cells that only move by means of T4aP-dependent motility,

and then we followed the fluorescence recovery over time at the bleached pole. We also note that only unpiliated T4aPM machines are present at the lagging pole (Chang *et al.*, 2016). By contrast, at the leading pole, there is a mixture of piliated T4aPM with bound PilB or bound PilT as well as unpiliated T4aPM (Chang *et al.*, 2016) (Figure 15).

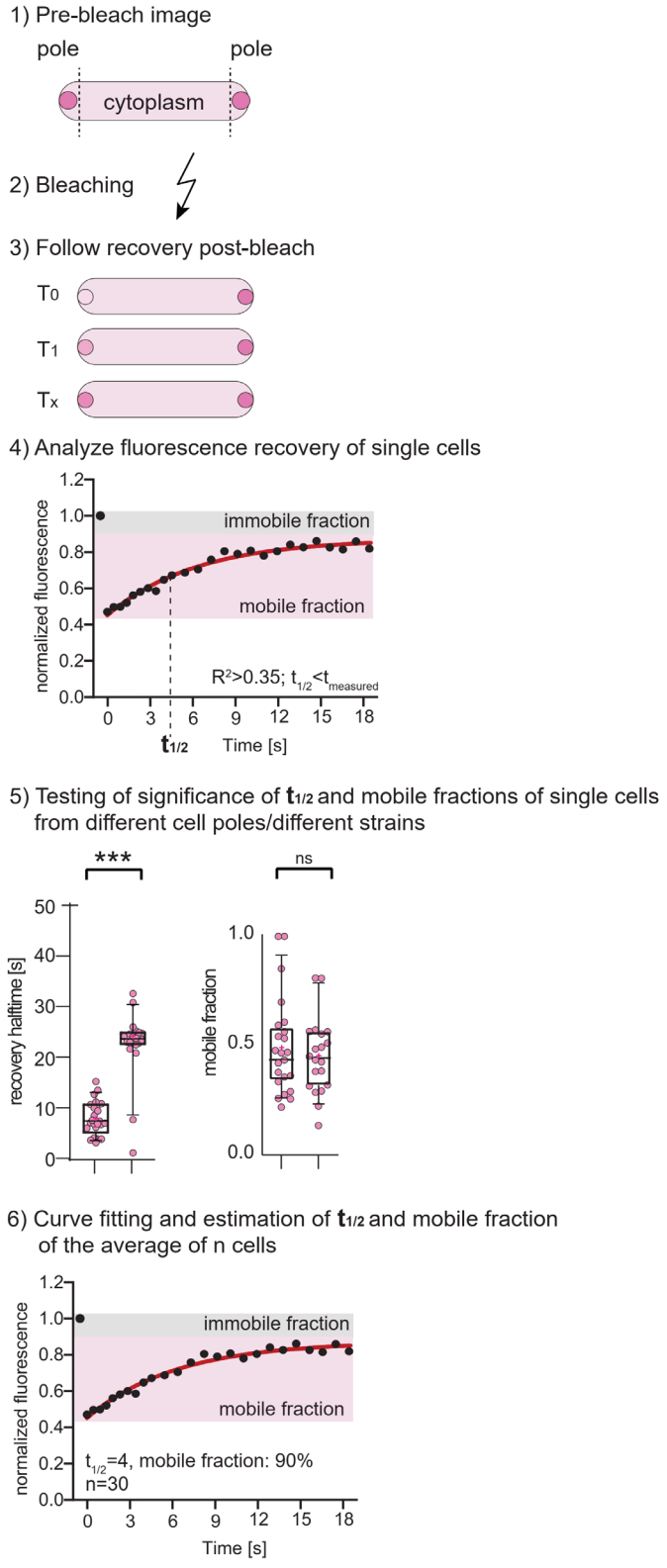

Figure 25 Overview of FRAP microscopy and data analysis. See text for details

5.10 PilQ, TsaP, PilP and PilO are stably incorporated into the T4aPM while PilM, PilB and PilT dynamically exchange subunits

At both, the leading and the lagging cell poles, bleached clusters of PilQ-sfGFP, TsaP-mCherry and PilP-sfGFP showed very little recovery within 30 min after the bleaching event (Figure 26).

Because PilO-sfGFP is only partially functional and *pilO-sfGFP*Δ*frzE*Δ*aglQ* cells were not moving on 0.5% agar (Figure 20A) and did not display single cell motility on chitosan coated µ-dishes (data not shown), we used the *pilO-sfGFP*Δ*frzE* strain, which can move by gliding motility, to be able to distinguish between leading and lagging poles of moving cells. Bleached PilO-sfGFP clusters at the leading and lagging poles showed very little recovery within 25 min after the bleaching event (Figure 26). We also observed that the polar clusters in the *pilO-sfGFP*Δ*frzE*Δ*aglQ* strain showed very little recovery within 25 min after the bleaching event (Figure 26).

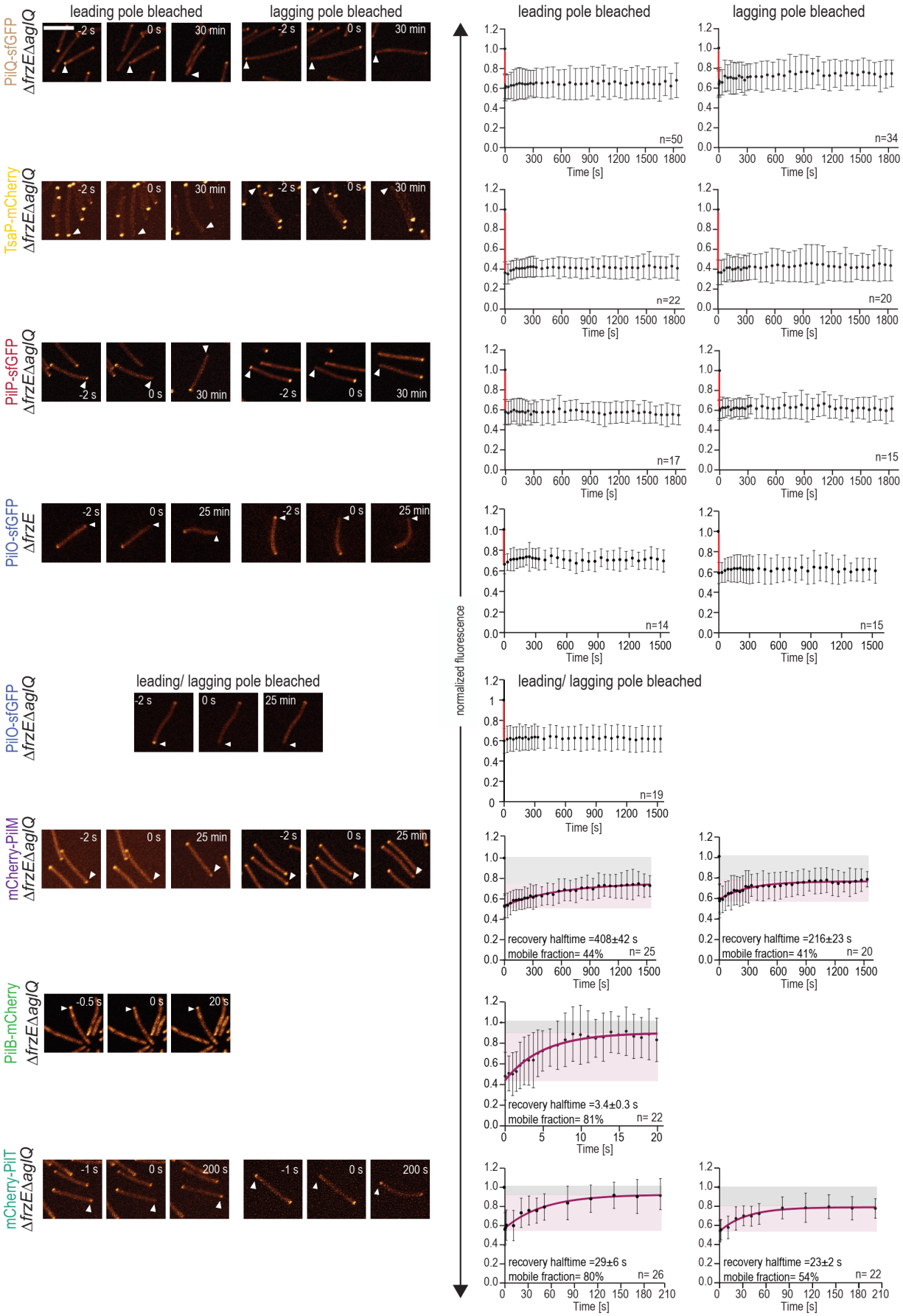
leading pole bleached
lagging pole bleached
PilQ-sfGFP ΔfrzEΔaglQ
TsaP-mCherry ΔfrzEΔaglQ
PilP-sfGFP ΔfrzEΔaglQ
PilO-sfGFP ΔfrzE
PilO-sfGFP ΔfrzEΔaglQ
leading/ lagging pole bleached
mCherry-PilM ΔfrzEΔaglQ
PilB-mCherry ΔfrzEΔaglQ
mCherry-PilT ΔfrzEΔaglQ
-2 s
0 s
30 min
25 min
-0.5 s
20 s
-1 s
200 s
normalized fluorescence
Time [s]
n=50
n=34
n=22
n=20
n=17
n=15
n=14
n=19
recovery halftime =408±42 s
mobile fraction= 44%
n= 25
recovery halftime =216±23 s
mobile fraction= 41%
n= 20
recovery halftime =3.4±0.3 s
mobile fraction= 81%
n= 22
recovery halftime =29±6 s
mobile fraction= 80%
n= 26
recovery halftime =23±2 s
mobile fraction= 54%
n= 22

Figure 26 FRAP microscopy of T4aPM components. Cells were placed on chitosan-coated µ-dishes which allowed their movement as single cells. Left panels, representative images of pre-bleach, post-bleach (0 sec) and the last frame acquired for cells bleached at either the leading or lagging pole. Arrowheads point to the bleached polar cluster. Scale bar: 5 µm. Right panels, average normalized fluorescence intensity as a function of time. Recovery half-maximal recovery time ($t_{1/2}$) was determined by fitting the mean data to a single-exponential function and is presented as mean±SD; n, number of bleaching events included in analysis. The mobile fraction is indicated with a pink background.

Upon bleaching of mCherry-PilM clusters at the leading and lagging poles, their fluorescence partially recovered within 25 min with significantly different half-maximal recovery time ($t_{1/2}$) at the two poles of 408±42 sec (n=25, leading pole) and 216±23 sec (n=20, lagging pole) calculated from the mean curve fit (Figure 26) and 406±221 sec (leading pole) and 262± 197 sec (lagging pole) calculated based on the mean $t_{1/2}$ from individual curve fits (Figure 27). The mobile fraction of mCherry-PilM was not significantly different at the two poles.

Upon bleaching of PilB-mCherry clusters at the leading pole, fluorescence rapidly and almost completely recovered with a t1/2 of 3.4±0.3 sec (n=22) (Figure 26) and 5±3 sec calculated based on the $t_{1/2}$ from individual curve fits (Figure 27). The mobile fraction of PilB-mCherry reached almost 100%.

Upon bleaching of mCherry-PilT clusters, fluorescence rapidly and almost completely recovered at the leading pole with a $t_{1/2}$ of 29±6 sec (n=26) and partially recovered at the lagging pole with a $t_{1/2}$ of of 23±2 sec (n=22) (Figure 26) and 22±32 sec (lagging pole) and 27±38 (leading pole) calculated based on the $t_{1/2}$ from individual curve fits (Figure 27). The $t_{1/2}$ at the two poles were not significantly different, while the mobile fraction was significantly higher at the leading pole (0.9) compared to the lagging pole (0.6). These observations are in overall agreement with previous analyses of PilT exchange (Bulyha *et al.*, 2009, Bulyha *et al.*, 2013).

From these analyses, we conclude that PilQ-sfGFP and TsaP-mCherry, which together form the OM pore of the T4aPM and bind to PG, are stably incorporated into the T4aPM at both poles and do not dynamically exchange with cellular pools on the time-scale of this experiment (30 min). Similarly, PilP-sfGFP and PilO-sfGFP, which together form the alignment complex in the periplasm and IM, are stably incorporated into the T4aPM at both poles and do not dynamically exchange with cellular pools on the time-scale of this

experiment (25-30 min). By contrast, the three cytoplasmic components of the T4aPM dynamically exchange with cytoplasmic pools and as described in the following, they do so with significantly different dynamics: mCherry-PilM exchanges slowly in the minute range at the two poles. Importantly, $t_{1/2}$ is significantly higher at the leading pole, thus mCherry-PilM exchanges more slowly at the leading than at the lagging pole. PilB-mCherry exchanges rapidly and almost completely within a few seconds at the leading pole range. Of note, PilB-mCherry exchange is significantly faster compared to mCherry-PilM at the leading pole (Figure 27). mCherry-PilT also exchanges rapidly and almost completely but only within ~30 sec at the leading pole and this exchange is significantly slower than that of PilB-mCherry (Figure 27) but significantly faster than that of mCherry-PilM (Figure 27). Furthermore, PilB-mCherry and mCherry-PilT exchange with significantly higher mobile fractions than mCherry-PilM. Taken together, these results indicate that PilM, PilB and PilT exchange occurs independently of each other.

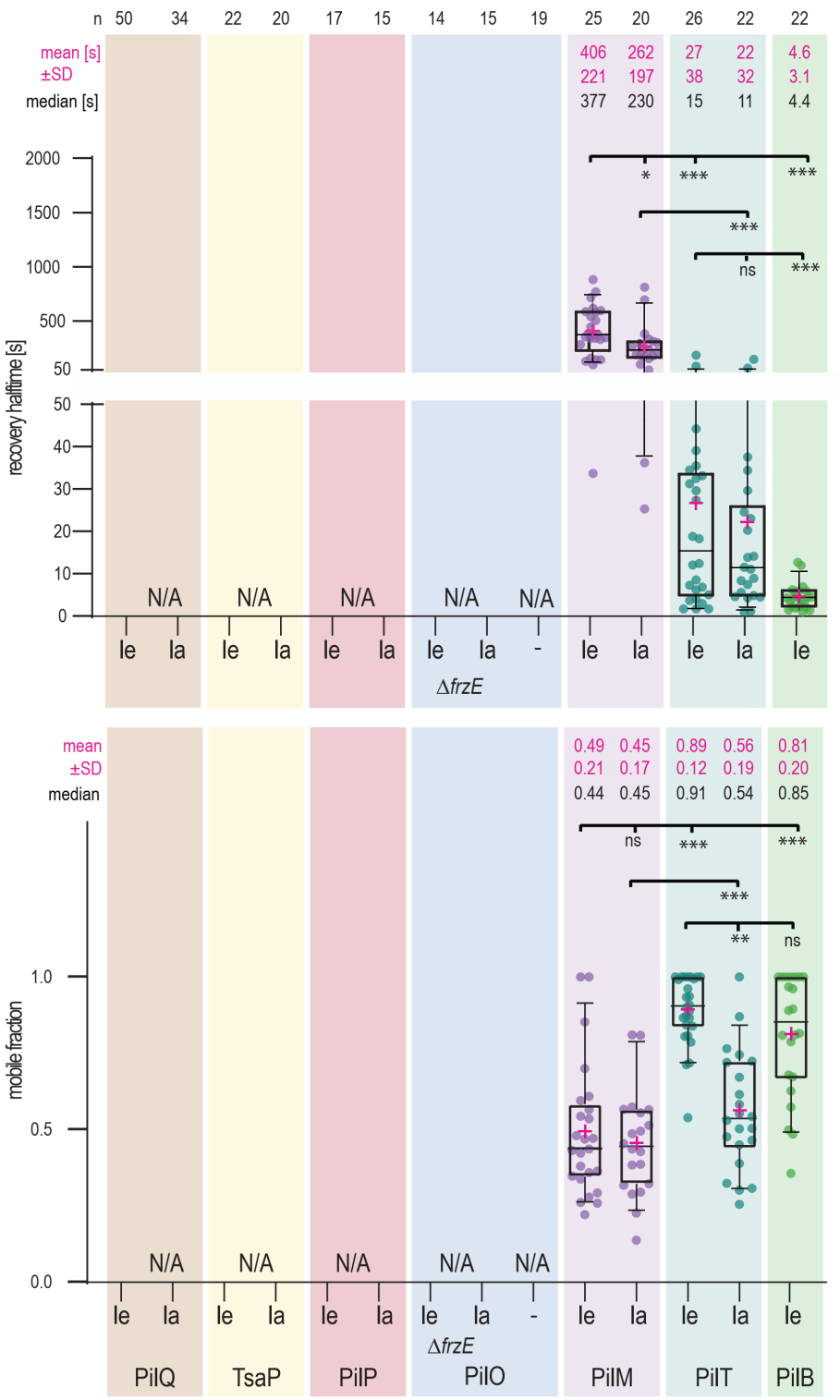

Figure 27 Boxplots of single-cell $t_{1/2}$ and mobile fractions of T4aPM components. A. $t_{1/2}$'s for single cells are shown in the upper and mobile fractions in the lower boxplot. The number of cells analyzed (n) is listed above the corresponding column. The box represent the 25th to 75th percentile

and whiskers the 10th and 90th percentile. Pink cross, the mean, thick black line, the median. The Mann-Whitney Rank-Sum test was used to test for significant differences. le, leading pole and la, lagging pole. N/A, not applicable; * $p \leq 0.05$, ** $p \leq 0.01$, ** $p \leq 0{,}001$, ns, not significantly different ($p > 0.05$).

5.11 Differential dynamics of cytoplasmic T4aPM components

To investigate whether the differential dynamic exchange of mCherry-PilM, PilB-mCherry and mCherry-PilT at the cytoplasmic base of the T4aPM at the leading pole could be correlated with the incorporation/removal of the major pilin PilA from the pilus base, we roughly estimated dwell times of mCherry-PilM, PilB-mCherry and mCherry-PilT. For this purpose, purified His6-tagged PilM, PilB, and PilT were used for quantitative immunoblot analyses to estimate the number of proteins in an average *M. xanthus* cell, as the exact number of T4aPM at the poles is not known yet.

Specifically, based on the localization of mCherry-PilM, PilB-mCherry and mCherry-PilT in an average *M. xanthus* cell based on the pre-bleach images in Figure 26, we estimated the fractions of each protein that localize in the cytoplasm and to the two poles. Then, we used the mean $t_{1/2}$, mobile fraction for each of the three proteins to approximately estimate mCherry-PilM, PilB-mCherry and mCherry-PilT dwell times similarly as it was calculated in (Milne-Davies *et al.*, 2021). First, we estimated the amount of protein exchanged at the given $t_{1/2}$ and then calculated how long one protein would take to be exchanged. E.g. 135 PilM localize to the leading pole of *M. xanthus* cells (Figure 28), of which 53% are bleached according to our FRAP Data (~72 molecules). Within 25 min ~40% of the fluorescence recovers (~29 molecules) and the half-maximum recovery is reached at ~408 seconds according to the average curve fitting at the leading cell pole (~14 molecules). Thus, we roughly estimate that one PilM would be exchanged in ~29 sec.

It is not known how many copies of PilM are incorporated into the T4aPM. Consequently, we estimated the dwell time of monomeric mCherry-PilM. We estimate dwell times of 29 sec and 20 sec for a PilM monomer at the leading and lagging poles. Because the active form of PilB and PilT is hexameric, we estimated the dwell times for hexameric PilB-mCherry and mCherry-PilT. We estimate a dwell time of 270 msec for hexameric PilB-mCherry and 8 sec and 9 sec per PilT hexamer at the leading and lagging cell pole (Figure 26B). It has previously been estimated that thousands of PilA subunits must be delivered to or be removed from the base of a T4aP within a second (Clausen *et al.*, 2009b). Based

on the estimated dwell times, we surmise that PilA delivery/removal occurs on a timescale much faster than the exchange of mCherry-PilM, PilB-mCherry and mCherry-PilT. We conclude that mCherry-PilM, PilB-mCherry and mCherry-PilT exchange does not reflect delivery/removal of PilA and that mCherry-PilM, PilB-mCherry and mCherry-PilT exchange reflects binding/unbinding to the T4aPM base independently of PilA delivery/removal. This conclusion is in agreement with the observation that mCherry-PilM and mCherry-PilT undergo exchange at the lagging pole.

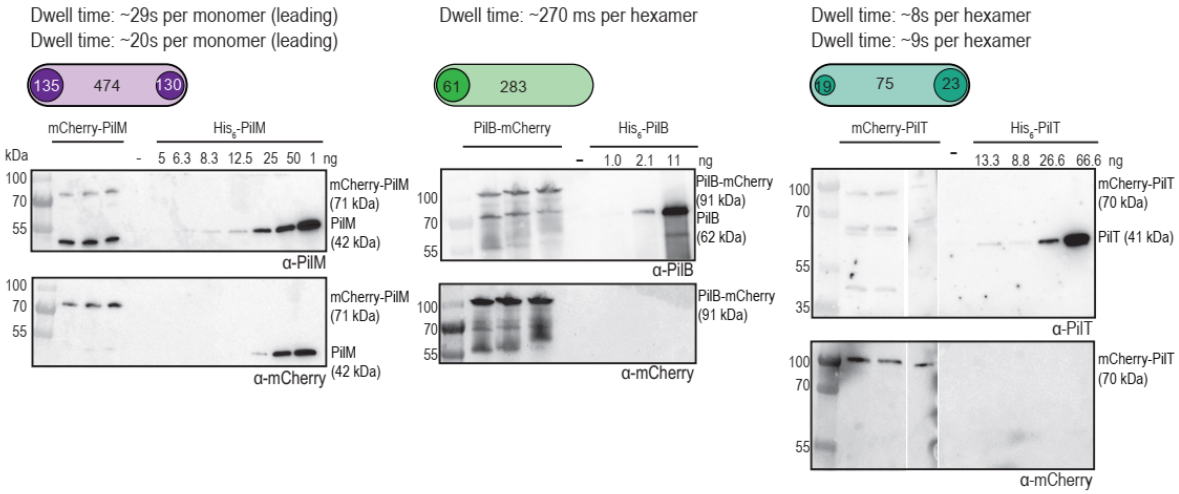

Figure 28 Estimation of dwell times of mCherry-PilM, PilB-mCherry and mCherry-PilT in polar clusters. Lower panels, quantitative immunoblot analyses of purified His6-PilM, His6-PilB and His6-PilT. The indicated amounts of purified proteins were loaded and compared to total cell extracts prepared from *M. xanthus* cells producing mCherry-PilM, PilB-mCherry or mCherry-PilT. In the three lanes with cell extracts, 12.5 µL of cell extract with an OD_{550}=14 (corresponding to 10^7 cells per µl) were loaded. The intensity of the signals for each sample was measured using Fiji and the protein amount in the cells estimated by correlating signal intensity to a standard curve based on the protein dilutions with a known amount of purified protein. For mCherry-PilM, PilB-mCherry and mCherry-PilT the bands corresponding to the full-length proteins were used for analysis. The immunoblots were probed with α-mCherry as control. Strong signals for high amounts of His6-PilM detected by α-PilM could not be fully removed from the immunoblot (left) by stripping, as signals for His6-PilM were still detected after stripping and incubation with α-mCherry.

5.12 PilB and PilT binding to the T4aPM slows down PilM dynamic exchange

mCherry-PilM exchanges significantly slower at the leading pole at the leading than at the lagging pole (Figure 26 and 27), suggesting a difference in mCherry-PilM exchange dynamics between different states of the T4aPM (piliated vs. unpiliated machines) and, thus, a correlation between mCherry-PilM exchange and T4aPM activity. To understand

which T4aPM components might affect mCherry-PilM exchange, we generated strains lacking PilB and/or PilT, or the IM platform proteins PilC. Fluorescence microscopy and immunoblot analyses documented that lack of neither PilB and/or PilT nor PilC significantly affected mCherry-PilM localization or accumulation (Figure 27A-B).

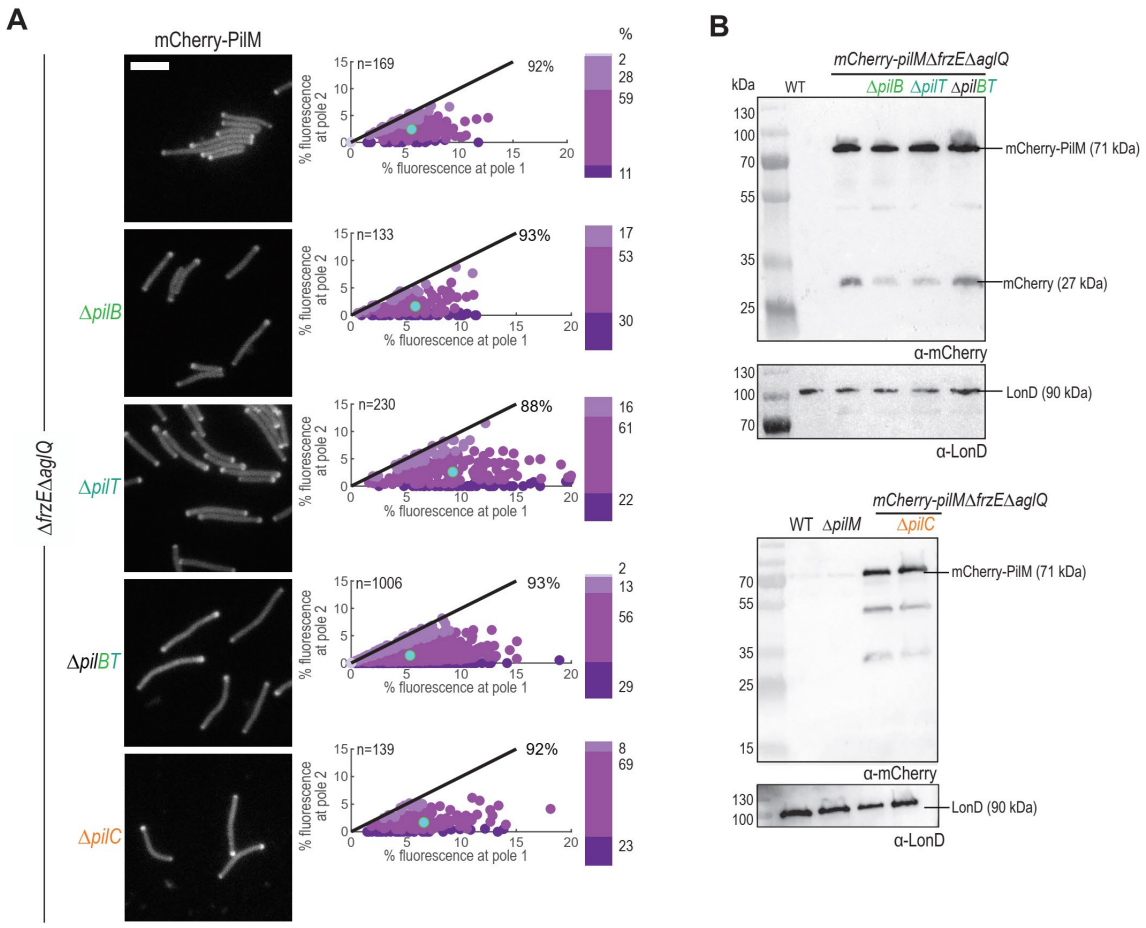

Figure 29 Localization and accumulation of mCherry-PilM. A. mCherry-PilM localization was studied by fluorescence microscopy. Scale bar: 5µm. Cells were treated and images analyzed as described in Figure 17C. **B.** Accumulation of mCherry-PilM in the indicated strains analyzed in immunoblot analyses. Total cell extract from the same number of cells was loaded per lane. Immunoblots probed with α-LonD antibodies served as loading controls.

Next, we performed FRAP experiments to assess the exchange dynamics of mCherry-PilM in the absence of PilB and/or PilT or PilC. Because these strains are non-motile by means of T4aP and all have the Δ*frzE*Δ*aglQ* genotype, we were not able to distinguish between leading and lagging cell poles. In the absence of PilB, mCherry-PilM exchanged

with similar $t_{1/2}$ as mCherry-PilM at the lagging pole of in WT (Figure 30). In the absence of PilT, mCherry-PilM exchanged with similar $t_{1/2}$ as the WT at the leading cell pole. In the absence of both PilB and PilT, mCherry-PilM exchanged with similar $t_{1/2}$ as mCherry-PilM at the lagging pole of in WT (Figure 30).

In *M. xanthus* cells, PilB binds to the cytoplasmic T4aPM base in the absence of PilT but PilT does not bind to the cytoplasmic base of the T4aPM in cells lacking PilB (Chang *et al.*, 2016). Moreover, T4aPM at the leading pole contain either bound PilB or PilT while T4aPM at the lagging pole contain neither bound PilB nor PilT (Chang *et al.*, 2016). Because (1) mCherry-PilM exchange in the absence of PilB is similar to that at of the T4aPM at the lagging pole in WT, (2) mCherry-PilM exchange in the absence of PilB as well as PilT is similar to that at of the T4aPM at the lagging pole in WT, and (3) mCherry-PilM exchange in the absence of PilT, we suggest that binding of PilB as well as binding of PilT to the T4aPM slows down mCherry-PilM exchange. In other words, binding of PilB or PilT to the T4aPM base stabilizes PilM binding at the T4aPM base.

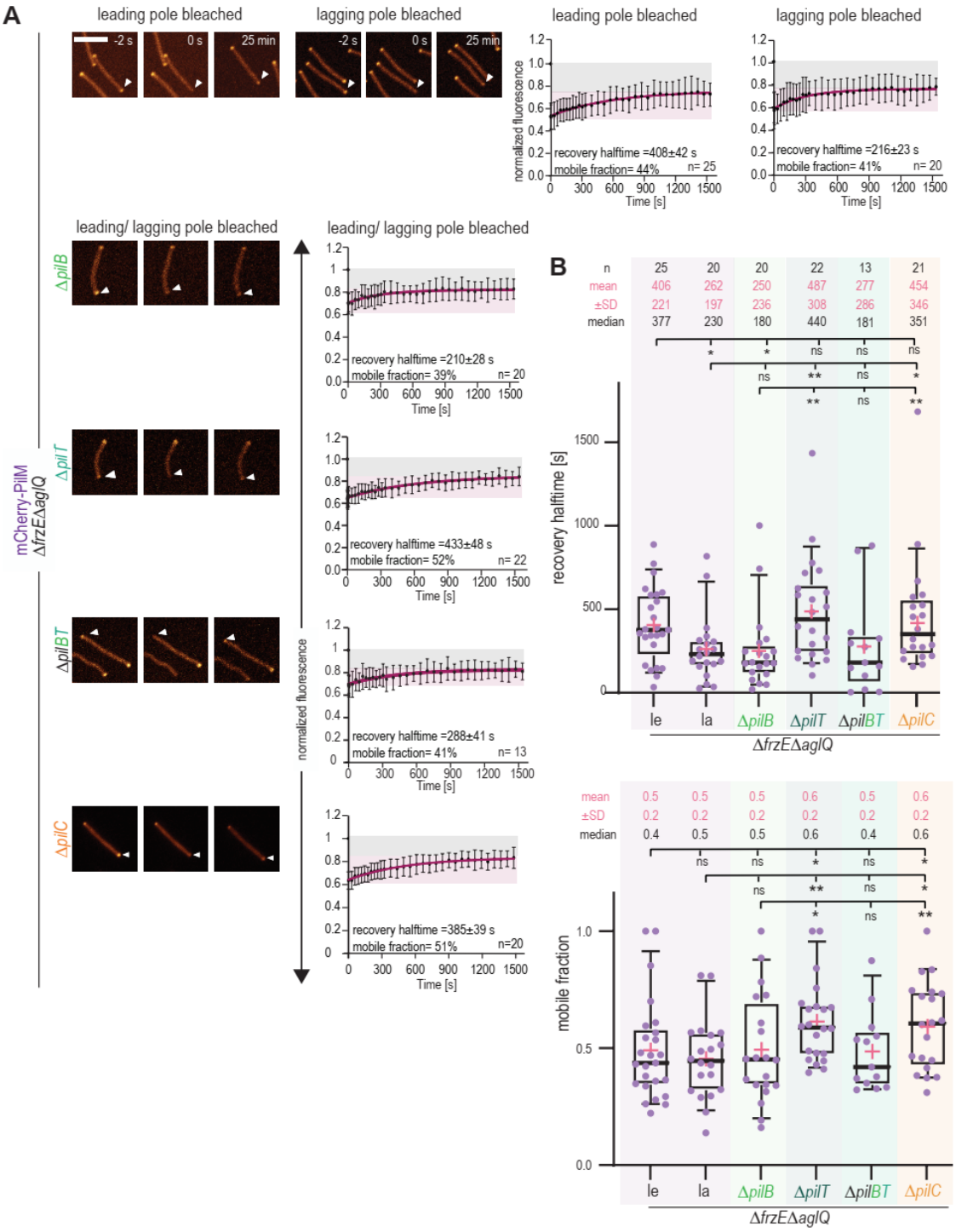

Figure 30 Dynamics exchange of mCherry-PilM in the absence of PilB, PilT or PilC. A. FRAP microscopy of mCherry-PilM at leading and lagging pole The experiments were performed and analyzed as described in Figure 26. Left panels, representative images of pre-bleach, post-bleach (0 sec) and the last frame acquired for cells bleached (25 min). **B.** Boxplots of the indicated strains'

single-cell $t_{1/2}$ (upper panel) and mobile fractions (bottom panel). Analyses were done as in Figure 27.

Lack of PilC resulted in mCherry-PilM exchange with a $t_{1/2}$ similar to that at the leading pole in WT and a slightly higher mobile fraction (Figure 30). This was surprising because PilB and PilT do not bind to the T4aPM in absence of PilC (Chang *et al.*, 2016).

5.13 PilM dynamic exchange is not essential for T4aPM function

PilM and PilN are encoded by neighboring genes. PilM interacts with the cytoplasmic N-terminal of PilN (Tammam *et al.*, 2013, Karuppiah & Derrick, 2011) and in the absence of PilN, PilM becomes unstable (Friedrich *et al.*, 2014, Bischof *et al.*, 2016) suggesting that PilM is recruited to the T4aPM by means of the interaction to PilN. PilO and PilN form heterodimers (Leighton *et al.*, 2016, Sampaleanu *et al.*, 2009) and PilO is stably incorporated into the T4aPM (see Figure 26 and 27). Therefore, we hypothesized that PilN would also be stably incorporated into the T4aPM; however, we have been unable to test this hypothesis because we do not have an active fluorescently-tagged PilN variant that accumulates stably. Therefore, to test whether the dynamic exchange of PilM at the T4aPM base is essential for T4aPM function, we generated fusions with or without mCherry in which the C-terminus of (mCherry-)PilM was fused directly to PilN ((mCherry-)PilM-N fusions). The two corresponding alleles were integrated at the native *pilM/pilN* site and replaced *pilM*$^{+}$ and *pilN*$^{+}$.

The mCherry-PilM-N (90 kDa) as well as the PilM-N (71 kDa) fusion accumulated in *M. xanthus* cells, but a truncated variant of mCherry-PilM-N was also detected by α-PilM, α-PilN and α-mCherry antibodies (Figure 31A). Moreover, mCherry-PilM-N localized similar to mCherry-PilM in a WT background (Figure 31B). Strikingly, cells producing mCherry-PilM-N or PilM-N as the only copies of PilM and PilN were still able to move by T4aP-dependent motility (Figure 31C).

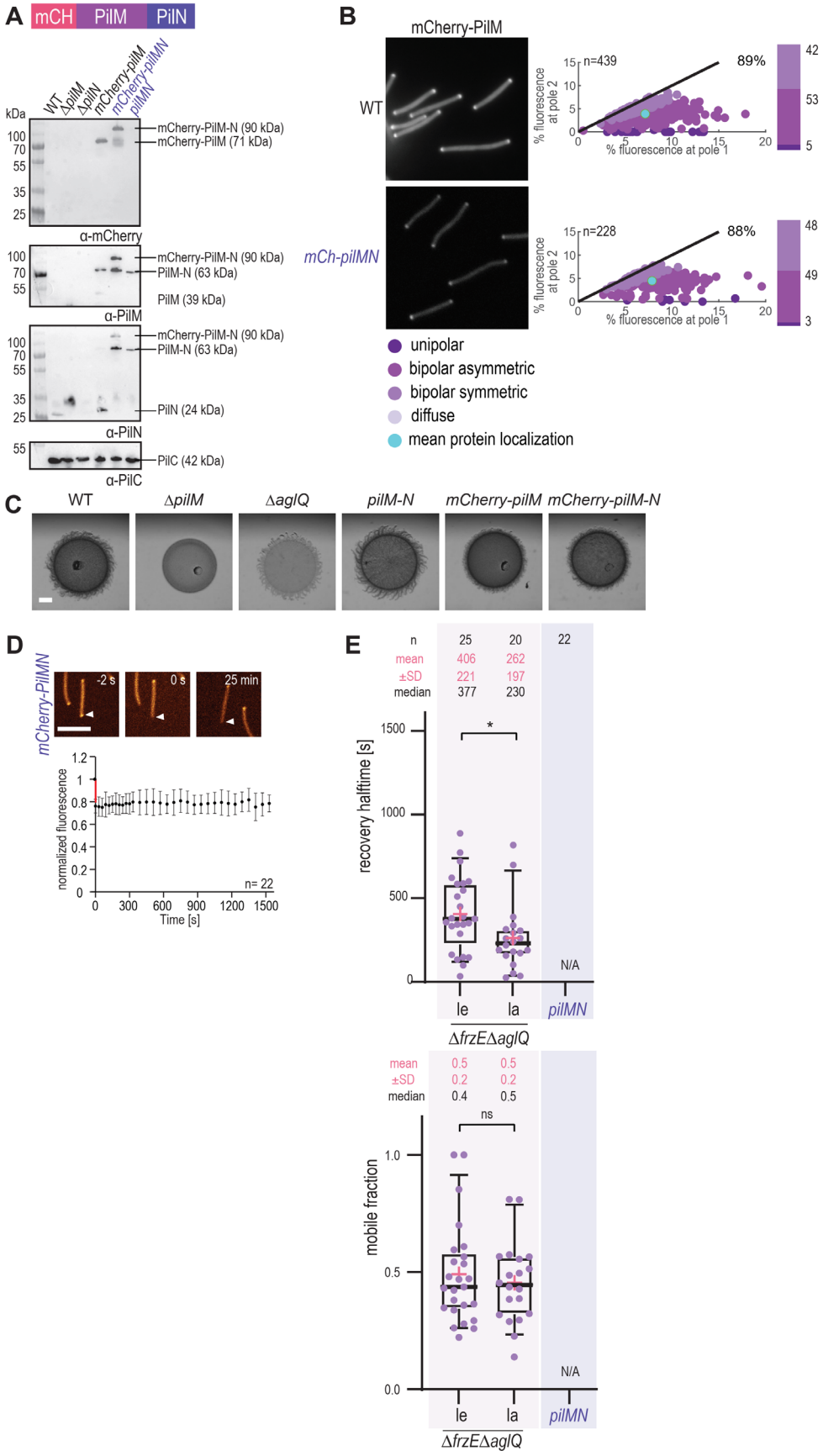
A
mCH
PilM
PilN
WT
ΔpilM
ΔpilN
mCherry-pilM
mCherry-pilMN
pilMN
kDa
100
70
55
35
25
mCherry-PilM-N (90 kDa)
mCherry-PilM (71 kDa)
α-mCherry
mCherry-PilM-N (90 kDa)
PilM-N (63 kDa)
PilM (39 kDa)
α-PilM
mCherry-PilM-N (90 kDa)
PilM-N (63 kDa)
PilN (24 kDa)
α-PilN
PilC (42 kDa)
α-PilC
B
mCherry-PilM
WT
mCh-pilMN
n=439
89%
n=228
88%
% fluorescence at pole 2
% fluorescence at pole 1
42
53
5
48
49
3
unipolar
bipolar asymmetric
bipolar symmetric
diffuse
mean protein localization
C
WT
ΔpilM
ΔaglQ
pilM-N
mCherry-pilM
mCherry-pilM-N
D
mCherry-PilMN
-2 s
0 s
25 min
normalized fluorescence
n= 22
Time [s]
E
n
mean
±SD
median
25
406
221
377
20
262
197
230
22
recovery halftime [s]
*
N/A
le
la
pilMN
ΔfrzEΔaglQ
0.5
0.5
0.2
0.2
0.4
0.5
ns
mobile fraction
N/A
le
la
pilMN
ΔfrzEΔaglQ

Figure 31 Dynamics exchange of mCherry-PilM is not essential for T4aPM function. A. Accumulation of PilM-N and mCherry-PilM-N in the indicated strains analyzed in immunoblot analyses. Total cell extract from the same number of cells was loaded per lane. A schematic overview of the mCherry-PilM-N fusion is shown above. The Immunoblot probed with α-PilC antibodies served as loading control. **B.** mCherry-PilM localization was studied by fluorescence microscopy. Scale bar: 5 µm. Cells were treated and images analyzed as described in Figure 17C. **C.** T4aP-dependent motility assay was performed on 0.5% agar for the indicated strains. Scale bar, 1 mm. **D.** FRAP microscopy of mCherry-PilM-N in WT. The experiments was performed and analyzed as described in Figure 26 **E.** Boxplots of the indicated strains' single-cell $t_{1/2}$ (upper panel) and mobile fractions (bottom panel). Analyses were done as in Figure 27.

Because the mCherry-PilM-N fusion was generated only in the WT background and cells reversed their direction of movement during the recovery phase of the FRAP experiment, it was not possible to clearly differentiate between leading and lagging poles. Nevertheless, upon bleaching of a polar mCherry-PilM-N cluster, we observed very little recovery within 25 min of the bleaching event (Figure 31). Previous FRAP measurements in WT cells synthesizing mCherry-PilM demonstrated that mCherry-PilM is also slowly exchanged in presence of FrzE and AglQ (Master thesis, Memduha Muratoglu, 2019). Thus, the stable incorporation of mCherry-PilM-N must be caused by PilN forming a stable unit within the T4aPM. In total, these observations strongly support that the dynamic exchange of PilM at the base of the T4aPM is not essential for T4aPM function. In this context, we also note that GspL in the T2SS is homologous to PilN and PilM and, thus, the PilM-N fusions are similar to GspL.

5.14 The stable incorporation of the PilQ secretin pore does not depend on TsaP or PilP

The PilQ secretin is stably incorporated into the T4aPM. We, therefore, asked whether PilQ is sufficient to form this stable unit or whether other components would be necessary for PilQ stabilization. TsaP forms a ring-like structure around the PilQ secretin (Siewering *et al.*, 2014, Chang *et al.*, 2016) and the secretin also interacts with PilP (Siewering *et al.*, 2014, Balasingham *et al.*, 2007, McCallum *et al.*, 2021, Chang *et al.*, 2016). We generated strains lacking TsaP or PilP in a *pilQ-sfGFP*Δ*frzE*Δ*aglQ* background to determine whether TsaP and/or PilP are required for the formation of the stable PilQ complex. The Δ*tsaP* and Δ*pilP* cells accumulated less PilQ-sfGFP compared to the parental strain (Figure 32B). Similarly, PilQ-sfGFP in both strains only generated low fluorescence intensity polar clusters and had less polar localization in the absence of TsaP and PilP (Figure 32A). Both strains are non-motile precluding the distinction between the leading and lagging poles in FRAP experiments. We observed that the bleached PilQ-sfGFP clusters in both

strains did not recover within 30 min after the bleaching event as previously observed at both poles in the presence of TsaP and PilP (Figure 32C). We conclude that neither TsaP nor PilP affect PilQ-sfGFP are not important for the stability of the PilQ secretin of the T4aPM.

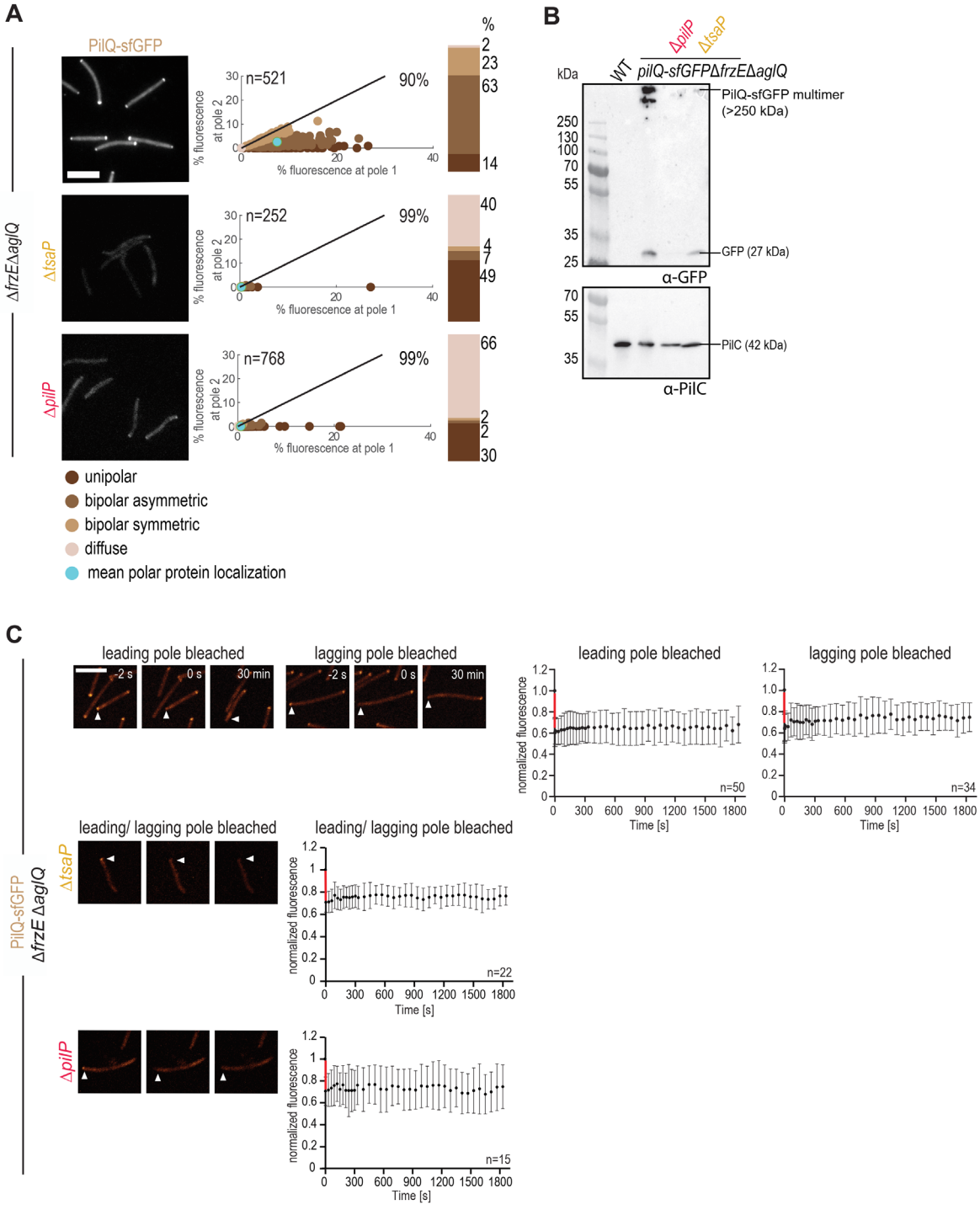

Figure 32 FRAP microscopy, accumulation and localization of PilQ-sfGFP in the absence of TsaP or PilP. A. Fluorescence microscopy and analysis of PilQ-sfGFP. Scale bar, 5µm. Microscopy and data analyses was performed as described in (Figure 17C). **B.** Accumulation of PilQ-sfGFP tested by immunoblot analysis. Total cell extract from the same number of cells was loaded per lane. **C.** FRAP microscopy of PilQ-sfGFP. Data from Figure 26 are included for

comparison.The experiment and analyses were performed and as described in Figure 26. Left panels, representative images of pre-bleach, post-bleach (0 sec) and the last frame acquired for cells bleached (30min).

5.15 PilC and PilM stabilize the periplasmic PilP ring

PilP forms a periplasmic ring, which connects the OM secretin to the periplasmic cage formed by PilN and PilO. PilN, in turn, interacts via its cytoplasmic N-terminus with PilM. FRAP analyses demonstrated that PilP-sfGFP is stably incorporated into the T4aPM (Figure 26). PilP accumulation relies on the presence of PilQ, and polar localization of PilP is abolished in the absence of PilN and/or PilO (Friedrich *et al.*, 2014). Therefore, we asked whether PilP-sfGFP dynamics is altered in the absence of the IM platform forming PilC and the cytoplasmic PilM. In agreement with previous analyses (Friedrich *et al.*, 2014), PilP-sfGFP accumulation and localization were unaffected in by lack of PilC or PilM (Figure 33A, B). Both strains are non-motile precluding the distinction between the leading and lagging poles in FRAP experiments. FRAP microscopy in strains lacking PilC or PilM demonstrated that PilP-sfGFP clusters recovered within 30 min after the bleaching event with similar characteristics (Figure 36C, D). We conclude that PilC and PilM are essential for the stable incorporation of PilP-sfGFP in the T4PaM even though no direct interaction of PilP to PilC or PilM is known so far.

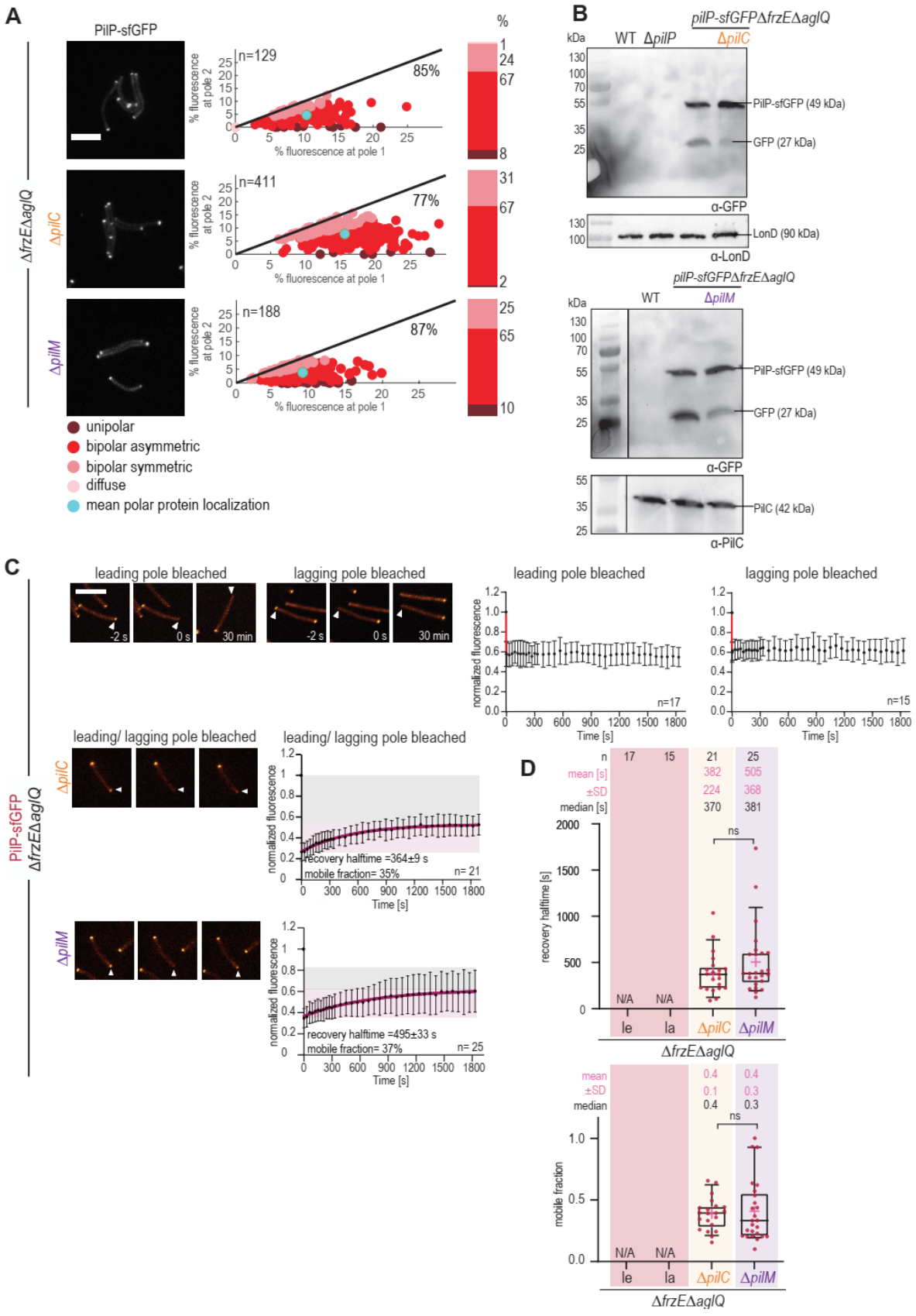
A
PilP-sfGFP
ΔfrzEΔaglQ
ΔpilC
ΔpilM
n=129
85%
n=411
77%
n=188
87%
% fluorescence at pole 2
% fluorescence at pole 1
%
1
24
67
8
31
67
2
25
65
10
unipolar
bipolar asymmetric
bipolar symmetric
diffuse
mean polar protein localization
B
pilP-sfGFPΔfrzEΔaglQ
kDa
WT
ΔpilP
ΔpilC
PilP-sfGFP (49 kDa)
GFP (27 kDa)
α-GFP
LonD (90 kDa)
α-LonD
pilP-sfGFPΔfrzEΔaglQ
WT
ΔpilM
PilP-sfGFP (49 kDa)
GFP (27 kDa)
α-GFP
PilC (42 kDa)
α-PilC
C
PilP-sfGFP
ΔfrzEΔaglQ
ΔpilC
ΔpilM
leading pole bleached
lagging pole bleached
-2 s
0 s
30 min
normalized fluorescence
Time [s]
n=17
n=15
leading/ lagging pole bleached
recovery halftime =364±9 s
mobile fraction= 35%
n= 21
recovery halftime =495±33 s
mobile fraction= 37%
n= 25
D
n
mean [s]
±SD
median [s]
17
15
21
25
382
505
224
368
370
381
ns
recovery halftime [s]
N/A
le
la
ΔpilC
ΔpilM
ΔfrzEΔaglQ
mean
±SD
median
0.4
0.4
0.1
0.3
0.4
0.3
mobile fraction

Figure 33 Accumulation and localization and dynamics of PilP-sfGFP in the absence of PilC or PilM. A. Localization of PilP-sfGFP. Experiment and analyses were done as described in 17C, representative snapshot is shown for each strain; Scale bar, 5 µm. **B.** Accumulation of PilP-sfGFP tested by immunoblot analysis. Total cell extract from the same number of cells was loaded per lane. As a loading control, the blots were probed with α-LonD or α-PilC. **C.** FRAP microscopy of PilP-sfGFP. Data from Figure 26 are shown for comparison. The experiment was performed and analyzed as described in Figure 26. Left panels, representative images of pre-bleach, post-bleach (0 sec) and the last frame acquired for cells bleached (30 min). **D.** Boxplots of single cell $t_{1/2}$ (upper) and mobile fractions (lower). Cells were analyzed as described in Figure 27.

5.16 PilC but not PilM stabilizes the incorporation of PilO in the T4aPM

IM PilO is stably incorporated into the T4aPM and is part of the alignment complex formed by PilMNOP (Tammam *et al.*, 2011, Leighton *et al.*, 2016, Chang *et al.*, 2016). PilO accumulation depends on PilQ, PilP and PilN (Friedrich *et al.*, 2014). We asked whether the stable incorporation of PilO-sfGFP depends on the IM platform protein PilC and/or cytoplasmic PilM. PilO-sfGFP accumulation was not affected by the absence of PilC but was decreased in the absence of PilM (Figure 34B). Localization of PilO-sfGFP was not affected by the lack of PilC. However, in the absence of PilM, polar localization of PilO-sfGFP was more unipolar (Figure 34A). Both strains are non-motile precluding the distinction between the leading and lagging poles in FRAP experiments. FRAP microscopy of PilO-sfGFP demonstrated that the absence of PilC resulted in PilO-sfGFP exchange. By contrast, PilO-sfGFP exchange was not observed in the absence of PilM (Figure 34C, D). Thus, PilC but not PilM stabilizes PilO-sfGFP incorporation in the T4aPM.

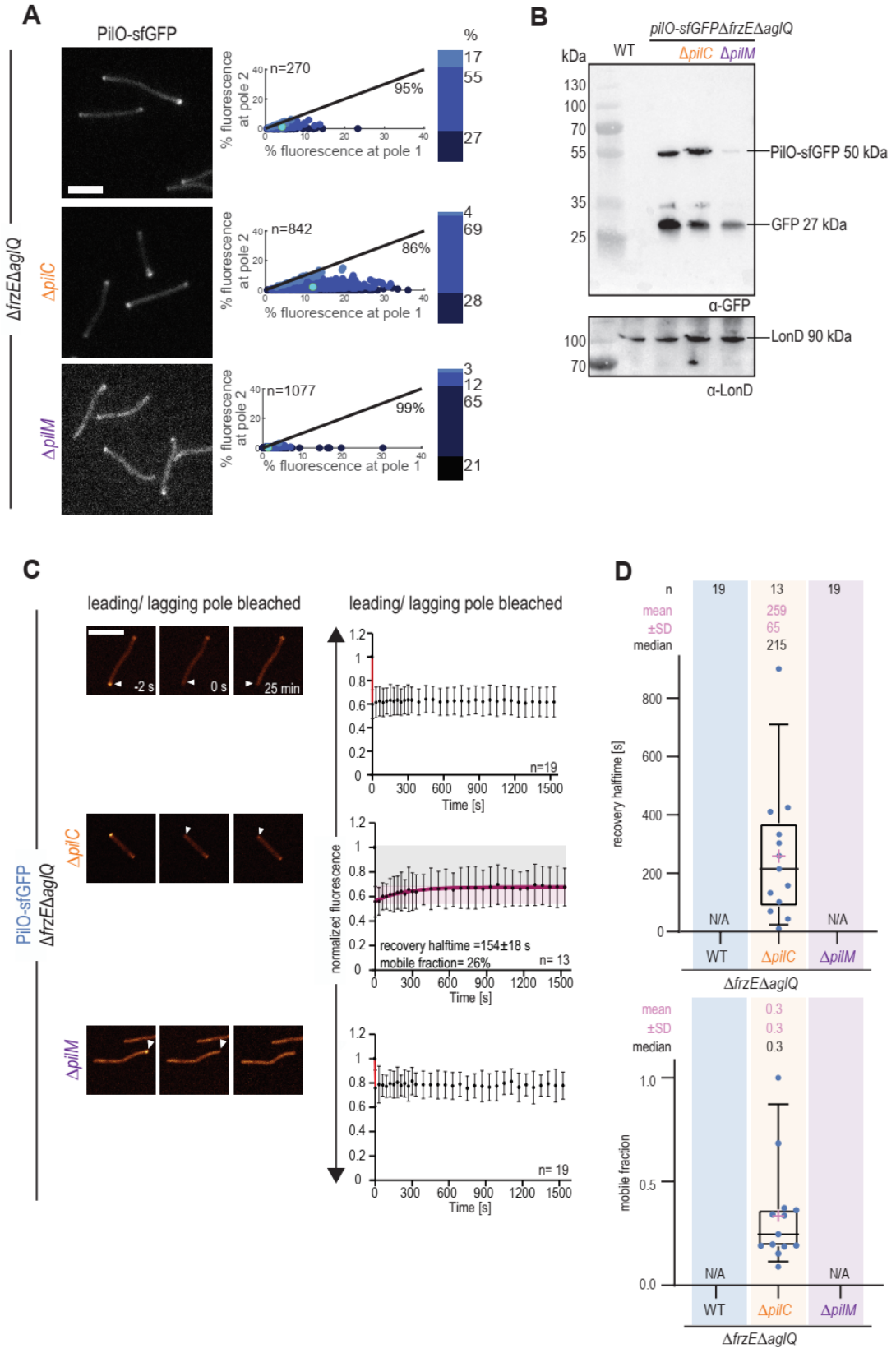
A
PilO-sfGFP
ΔfrzEΔaglQ
ΔpilC
ΔpilM
% fluorescence at pole 2
% fluorescence at pole 1
n=270
95%
%
17
55
27
n=842
86%
4
69
28
n=1077
99%
3
12
65
21
B
pilO-sfGFPΔfrzEΔaglQ
kDa
WT
ΔpilC
ΔpilM
130
100
70
55
35
25
PilO-sfGFP 50 kDa
GFP 27 kDa
α-GFP
100
70
LonD 90 kDa
α-LonD
C
leading/ lagging pole bleached
leading/ lagging pole bleached
-2 s
0 s
25 min
PilO-sfGFP
ΔfrzEΔaglQ
ΔpilC
ΔpilM
normalized fluorescence
n=19
recovery halftime =154±18 s
mobile fraction= 26%
n= 13
n= 19
Time [s]
D
n
mean
±SD
median
19
13
259
65
215
19
recovery halftime [s]
N/A
N/A
WT
ΔpilC
ΔpilM
ΔfrzEΔaglQ
mean
±SD
median
0.3
0.3
0.3
mobile fraction
N/A
N/A
WT
ΔpilC
ΔpilM
ΔfrzEΔaglQ

Figure 34 Accumulation localization and FRAP microscopy of PilO-sfGFP. A. Localization of PilO-sfGFP. Experiments and analyses were done as in Figure 17C. A representative snapshot is shown for each strain (Scale bar, 5 µm). **B.** Accumulation of PilO-sfGFP tested by immunoblot analysis. Total cell extract from the same number of cells was loaded per lane. The blot probed with α-LonD served as a loading control. **C.** FRAP microscopy of PilO-sfGFP. Data from Figure 26 are shown for comparison. The experiment was performed and analyzed as described in Figure 26. Left panels, representative images of pre-bleach, post-bleach (0 sec) and the last frame acquired for cells bleached (25 min). **D.** Boxplots of single-cell $t_{1/2}$ (upper) and mobile fractions (lower) as in Figure 27.

6 Discussion

Here, we used FRAP microscopy to systematically study the T4aPM as a representative of a large family of prokaryotic cell-envelope spanning nano-machines, including the T2SS, other T4P systems, and the archaeal flagellum. Components of the T4aPM were labeled with fluorescent proteins tested for functionality, accumulation, and localization in genetic background, which generally allowed to distinguish between the leading and lagging poles and allowed cells to only move by T4aP. We found different components of the machine to have individual dynamics and that those T4aPM components can affect the stabilities and dynamics of others.

In particular, we found the OM pore complex consisting of PilQ and TsaP and the most components of the alignment complex consisting of PilP, PilN and PilO to form a stable unit. The three cytoplasmic components PilM, PilB and PilT exchange subunits with differential dynamics.

6.1 The differential dynamics of T4PM components

Secretins form large OM pores to allow substrate translocation in T4P systems, the T2SS and the T3SS (Silva *et al.*, 2020). T4aPM, T2SS, and some T3SS are known to assemble outside-in, starting with the secretin (Friedrich *et al.*, 2014, Korotkov *et al.*, 2012, Deng *et al.*, 2017). Thus, secretins can be seen as a fundamental building block of these cell envelope-spanning multi-protein complexes and as these proteins are in the T4aPM the first component to assemble, one might see them as an anchor for the rest of the T4aPM. We have demonstrated that once assembled the secretin does not exchange subunits in T4aPM and also no new T4aPMs assemble at the poles of *M. xanthus* cells within a timescale of 30 minutes. This result agrees with previous observations indicating that the

OM pore made by secretins is very stable. Of note, the secretin could still be detected as an oligomer after boiling samples in SDS- buffer in this study as in several other cases (Burkhardt *et al.*, 2011, Friedrich *et al.*, 2014, Nouwen *et al.*, 1999). In conclusion, once the PilQ pore is made, it forms a stable unit, which must ensure function over a life-cycle of a cell.

The ring formed by TsaP around the secretin is thought to assist anchoring of the secretin PilQ to the PG via its LysM domain and to help align PilQ with the IM components of the T4aPM. CryoET of Δ*tsaP* mutants showed that lack of TsaP caused a disengagement of the OM channel from the mid-periplasmic ring in unpiliated T4aPM (Chang *et al.*, 2016). However, TsaP was also shown to bind peptidoglycan, most likely by its LysM domain (Siewering *et al.*, 2014). In *Caulobacter crescentus* DipM, which is involved in cell division, carries two LysM tandems at its N-terminus. While DipM-mCherry fluorescent signals did not recover fluorescence intensity in FRAP microscopy, a variant lacking one LysM tandem was mobile, demonstrating the importance of LysM domains for protein mobility (Poggio *et al.*, 2010). Therefore, it is likely that the LysM domain of TsaP contributes to the stability of TsaP in the T4aPM.

The lipoprotein PilP is anchored in the IM via its lipidation site. PilP connects the OM pore to the IM components of the T4aPM by directly interacting with the N0 domain of PilQ and PilN and PilO in the IM (Tammam *et al.*, 2013, Tammam *et al.*, 2011). To answer the question how PilP stability within the T4aPM is established one might wonder if lipoproteins in general might form stable units and if the lipidation site of PilP might be essential for its stability within the T4aPM. In *P. aeruginosa* PilP was shown to form a complex with PilN and PilO heterodimers and the lipidation site of PilP was demonstrated to not be essential for T4aPM function (Tammam *et al.*, 2011). It was suggested that the complex formed by PilPNO must be stable so that the lipid anchor of PilP is dispensable for the function of the T4aPM (Tammam *et al.*, 2011). Therefore, PilP's lipidation site and association with the IM is unlikely responsible for its stability within the T4aPM. Also, other lipoproteins have been suggested to be mobile and exchange subunits including the pilotin SctG of the T3SS (Wimmi *et al.*, 2022).

In the IM, PilO and PilN heterodimers form a cage-like structure (Chang *et al.*, 2016). Only both proteins together form a complex with PilP, which connects the alignment complex to the OM complex (Tammam *et al.*, 2011, Ayers *et al.*, 2009). Our results demonstrate that PilN and PilO form stable complexes in the T4aPM as well. In conclusion, PilQ and

TsaP form a stable OM pore complex, which is connected to PilP, PilN and PilO, which form a stable part of the alignment complex. This stable multiprotein complex is formed at both cell poles of *M. xanthus* cells and most likely ensures function of the T4aPM and thus enables T4aP-dependent motility for a life cycle of a cell. Considering the forces, that the T4aPM generates to retract a T4aP, with up to 150 pN (Clausen *et al.*, 2009b), it seems reasonable that a stable unit is essential to withstand these high forces and hold the interconnected rings in place to allow continuous and fast extension and retraction cycles.

The cytoplasmic ring of the T4aPM consists of PilM subunits (Chang *et al.*, 2016). Here, we found PilM to be slowly exchanged at both cell poles of *M. xanthus* cells. The protein exchange at the leading pole is slower than at the lagging pole as the recovery halftimes at the leading pole are significantly slower. This indicates that protein exchange is faster at the lagging pole with unpiliated machines than the leading pole with a mixture of piliated extending, piliated retracting and unpiliated machines.

In *M. xanthus,* the two ATPases PilB and PilT power extension and retraction cycles of the T4aP (Jakovljevic *et al.*, 2008). Both ATPases belong to the superfamily of secretion ATPases, also found in T2SS and archaeal surface structures (Planet *et al.*, 2001, Peabody *et al.*, 2003). While all of the other components of the T4aPM remain stationary at both poles, PilB switches from the old leading to the new leading pole. PilT localizes bipolar asymmetric with a large cluster at the lagging pole and also switches poles upon reversals (Bulyha *et al.*, 2009). Our finding that PilB-mCherry and mCherry-PilT polar clusters recover fluorescence intensity rapidly after photobleaching and thus rapidly exchange proteins at the poles is in accordance with the model in which PilB and PilT must bind and unbind from the T4aPM to power extension and retraction of the pilus fiber (Bulyha *et al.*, 2009, Jakovljevic *et al.*, 2008, Koch *et al.*, 2021). Previously, FRAP microscopy with a YFP-PilT fusion was performed in *M. xanthus* cells. Although the experimental setup was different because YFP-PilT was not expressed at native levels and a pre-bleaching of the cytoplasmic background was necessary, YFP-PilT clusters recovered within 3 minutes, which is a very similar range compared to the mCherry-PilT recovery observed in this study.

6.2 PilM exchange in the cytoplasmic ring is activity dependent but not essential for T4aPM function.

In the case of the T4aPM of *M. xanthus*, at the leading cell pole, the two ATPases PilB and PilT must bind and unbind to the T4aPM to power extension and retraction of the pilus fiber (Jakovljevic *et al.*, 2008). It was suggested that in the absence of PilB, PilT also does not bind to the base of the T4aPM (Chang *et al.*, 2016). As we found PilM exchange to significantly differ between leading and lagging cell poles of *M. xanthus* cells, we next tested whether the absence of PilB or PilT and both ATPases affects the PilM dynamic exchange. In the absence of PilB the dynamics the mCherry-PilM of exchange was similar to the subunit exchange at the lagging pole of a strain in which the ATPases are present. In turn, in the polar clusters of cells lacking PilT exchanged mCherry-PilM significantly slower compared to PilM exchange in cells lacking PilB, and had and had a higher mobile fraction. At the same time, the PilM exchange dynamics were similar to the exchange of mCherry-PilM at the leading cell pole of strains in the presence of the two ATPases. As expected in absence of both ATPases mCherry-PilM had similar exchange dynamics as in the strain only lacking PilB. Thus, in the presence of both ATPases, mCherry-PilM exchange is slower, whereas, in the absence of both ATPases, mCherry-PilM exchange is faster. The lack of PilT but the presence of PilB led to half-maximal recovery times similar to the leading pole when both ATPases were present. Therefore, extension and retraction ATPases must slow down PilM exchange and in conclusion, the cytoplasmic ring made by PilM must be more stable in machines actively extending or retracting pilus fibers.

Next, we asked if the dynamic PilM exchange is required for the T4aPM function. We assumed that fusing PilM to the N-terminus of PilN, to which it interacts (Karuppiah & Derrick, 2011), might stabilize the PilM ring, as PilN forms heteromers with PilO, which in turn forms a stable unit in the T4aPM. Therefore, PilM and mCherry-PilM were fused to PilN resembling GspL, a hybrid homolog of PilM and PilN in the T2SS (McCallum *et al.*, 2016). The mCherry-PilM-N fusion localized similarly to mCherry-PilM and did not show fluorescence recovery as mCherry-PilM in FRAP experiments. This first suggests that PilN indeed forms a stable unit as PilO and by fusing PilM to PilN we were able to stabilize the cytoplasmic ring. However, strains expressing mCherry-PilM-N or PilM-N were not impaired in T4aP-dependent motility. Thus, the dynamic PilM exchange is not essential for the T4aPM function. The exact benefit of the subunit exchange of the PilM ring is thus not clear yet. However, the advantage of slow subunit exchange in the cytoplasmic ring of

the injectisome is also changing dynamics based on secreting or non-secreting conditions and by the presence of an active ATPase YscN. But, the exchange rates do also not correlate with the rate of effector secretion and thus the advantage of subunit exchange is not clear yet (Diepold *et al.*, 2015). The exchange of PilM might simply be a result of the PilM-PilN binding affinity.

Possibly, in the T2SS, which evolutionary branched from T4aPM (Denise *et al.*, 2019), GspL, which is a hybrid homolog of PilM and PilN might be an evolutionary result of PilM and PilN fusion as the subunit exchange was possibly not essential for function of the T2SS.

6.3 The function of the T4aPM

The IM proteins PilN and PilO were suggested to interact with the major pilin (Georgiadou *et al.*, 2012) and PilO-PilC interactions were also suggested based on BACTH assays, the question was raised if and how the IM cage made by PilO and PilN is involved in pilus assembly (Georgiadou *et al.*, 2012). Different scenarios are conceivable. (I) The PilN-O cage is flexible, and conformational changes allow the major pilin to enter and exit the cage. This scenario was suggested in a model of the T4aPM of *M. xanthus* based on cryoET and homology modeling (Chang *et al.*, 2016). (ii) Protein exchange of PilN or PilO causes gaps which allow entry or exit of the major pilin. (iii) The major pilin is delivered or removed with PilN or PilO during protein exchange. In a model of the T2SS, the PilO homolog PulM was suggested to deliver the major pseudo-pilin dynamic association to the T2SS (Dazzoni *et al.*, 2023).

As we found PilO and PilN to be stably incorporated into the T4aPm and not exchanging subunits we suggest that conformational changes of the IM cage must allow PilA entry and exit to and from the cage as suggested in the first scenario. This finding also excludes the possibility in which the major pilin is delivered to the base of the pilus fiber by PilO, as it was suggested for PulM in the T2SS (Dazzoni *et al.*, 2023).

We also found significantly different recovery halftimes and mobile fractions for PilM, PilB and PilT. Based on the quantitative immunoblot analyses and fluorescence intensities of leading and lagging poles of the pre-bleach images in FRAP microscopy, we determined the amount of these three proteins at the poles of *M. xanthus* cells. Taken together with the average recovery halftimes of the FRAP experiments, dwell times of PilM, PilB and

PilT at the leading cell poles were roughly estimated as 29s per monomer, 8s and 270ms per hexamer, respectively. Demonstrating that these three dynamically exchanging components of the T4aPM exchange independently of each other, and are unlikely to form sub-complexes. Furthermore, these dwell times are on a scale of hundreds of miliseconds and seconds, whereas previous studies suggest thousand PilA subunits to be removed and likewise incorporated at the pilus base within one second (Clausen *et al.*, 2009a). Therefore, it is unlikely that any of studied components here (PilQ, TsaP, PilP, PilO, PilM, PilB or PilT) is responsible for the delivery of the major pilin to the T4aPM. Additionally as one major pilin subunits corresponds to an axial rise of 10.5 Å within the T4aP, and considering the addition of 1000 subunits per second, dwelling of a PilB hexamer for 270ms at the base of one T4aPM, would allow to extend one pilus for 284 nm, which is in a similar range as measured pilus length e.g. in *P. aeruginosa* (Simsek *et al.*, 2023, Kolappan *et al.*, 2016, Clausen *et al.*, 2009a).

Even though both ATPases exchange rapidly at the cell poles, PilB is exchanged much faster than PilT. This is in agreement with estimated unbinding rates of PilB and PilT from *P. aeruginosa*, which were determined as 1.6 and 9.1 sec, respectively. Our findings would support the suggestion that pilus synthesis is limited by the slow unbinding of the retraction ATPase (Koch *et al.*, 2021). However, it must be considered that 2% of mCherry-PilT localizes to the cell poles of *M. xanthus* cells even in the absence of the T4aPM, whereas only 0.5% of mCherry-PilB still localizes to the cell poles (3.14). This suggests that a fraction of polar localizing ATPases, especially PilT is not bound to the T4aPM.

6.4 Comparison of the T4aPM dynamics to other trans-envelope complexes

Protein exchange in other large trans-envelope complexes has been studied before. In this study, we systematically studied which components of the T4aPM form stable complexes and which of them exchange subunits dynamically, by FRAP microscopy. We have demonstrated that the T4aPM components either form a stable complex or show differential dynamics. Similarly, the *E. coli* flagellum and the *Y. enterocolitica* injectisome are known to have stably incorporated or dynamically exchanging components (Delalez *et al.*, 2010, Li & Sourjik, 2011, Bai *et al.*, 2014, Leake *et al.*, 2006, Fukuoka *et al.*, 2010, Delalez *et al.*, 2014, Diepold *et al.*, 2015, Wimmi *et al.*, 2022, Milne-Davies *et al.*, 2021).

As we found the secretin of the T4aPM PilQ to be stably incorporated into the T4aPM, YscC, the secretin of the *Y. enterocolitica* injectisome also forms a stable complex in the T3SS as well (Diepold *et al.*, 2015).

The cytoplasmic ring was also found to exchange subunits in the *E. coli* flagellum and the injectisome of *Y. enterocolitica*. In the case of the flagellum, FliM exchange depends on the binding of CheY, which in turn changes the rotational direction of the flagellum (Delalez *et al.*, 2010). Thus, FliM exchange in the flagellum has a regulatory role. In the case of the injectisome of *Y. enterocolitica,* the C-ring made by YscQ is exchanging subunits faster under secreting conditions than under non-secreting conditions, and the presence of a functional ATPase (YscN) has a stabilizing effect on the exchange of YscQ (Diepold *et al.*, 2015). Similarly, subunit exchange in the T4aPM differs between 'active' and unpiliated machines, exchange dynamics change in presence of the ATPases powering pilus extension and retraction but the function of the machines is not impaired when the subunit exchange is prohibited by fusion to PilN.

Previously FliI, the ATPase of the bacterial flagellar export apparatus, was shown to exchange proteins with a rate of approximately six proteins per minute. FliI exchange rates were compared to flagellar export rates (Aizawa & Kubori, 1998). The ATPase FliI was suggested to act as a substrate loader and deliver the substrate to the export apparatus (Bai *et al.*, 2014). In case of the T4aPM the ATPases PilB and PilT also exchange subunits at the cell poles of *M. xanthus* cells. This exchange most likely reflect binding and unbinding of PilB and PilT to the base of the T4aPM to power extension and retraction and the ATPases unlikely deliver any substrate to the machine, as discussed above.

In contrast to our finding, that the dynamically exchanging components of the T4aPM must exchange independently of each other, in both other systems, the flagellum and the injectisome components were found to form sub-complexes. In the case of the flagellum, FliI can either form a ring as $FliI_6$ and also sub-complexes with e.g., FliH ($FliH_2FliI$). The two complexes were suggested to act as a static substrate loader or dynamic substrate carrier, respectively. Here, protein exchange of FliI was suggested to be important to deliver cargo to the export gate or initiate or enhance the efficiency of flagellin export (Bai *et al.*, 2014). In the injectisome of *Y. enterocolitica*, YscQ, which forms the cytoplasmic ring, was found to exchange subunits, and the dynamics of this exchange were found to differ in secreting and non-secreting conditions (Diepold *et al.*, 2015). As YscQ was found in sub-complexes with other injectisome components such as YscQc, SctL, and YscN

(Lara-Tejero *et al.*, 2011, Diepold *et al.*, 2017), it is conceivable that these interaction partners exchange as sub-complexes (Rocha *et al.*, 2018). Furthermore, YscQ is known to interact with effectors and chaperones (Lara-Tejero *et al.*, 2011). Thus, YscQ exchange might be beneficial for delivery of these to increase the local concentration of cargo and enhance secretion (Milne-Davies *et al.*, 2021).

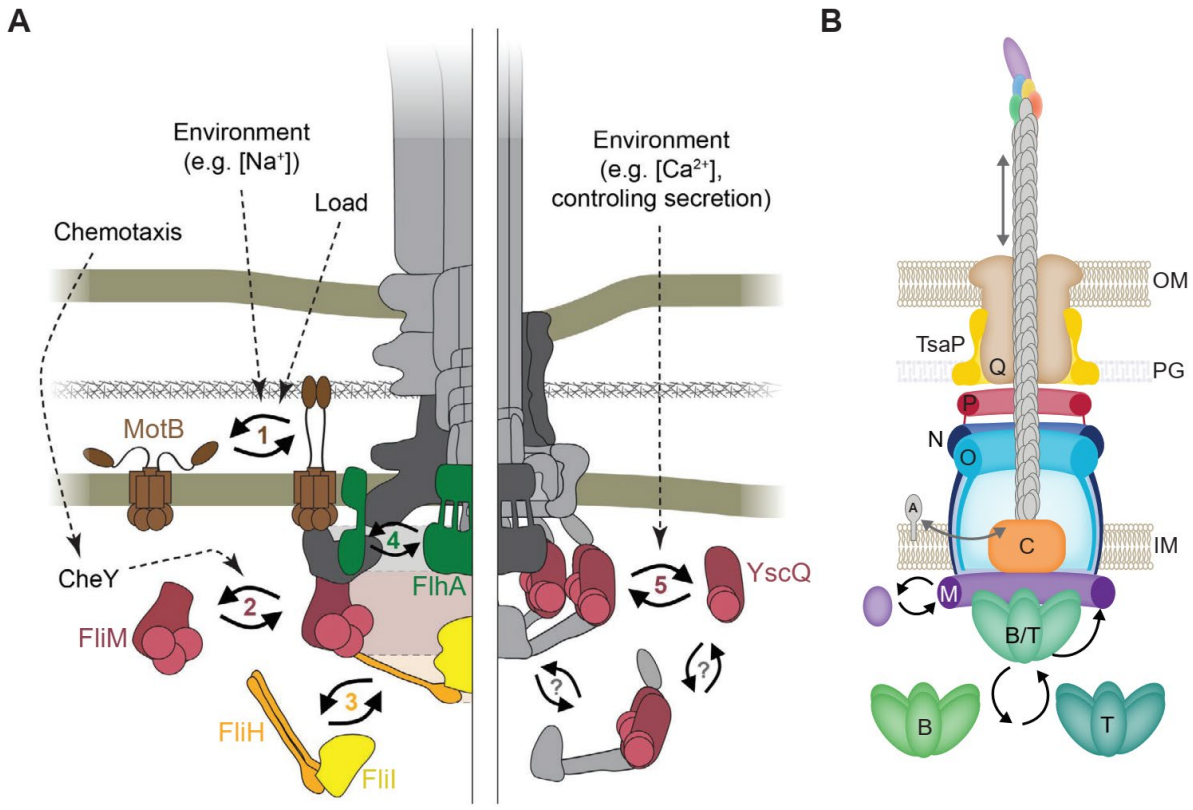

Figure 35 Summary of component exchange in the T4aPM and comparison to the bacterial flagellum and the injectisome. A. Summary of protein exchange in the bacterial flagellum and the injectisome. Schematic overview of the flagellum (left) and the injectisome (right). Protein exchange is marked by colors and protein found to not be exchanged are shown in grey (FliG, FliH and YscV and YscC). Dashed arrows indicate external factors influencing the protein exchange (Milne-Davies *et al.*, 2021). **B.** Overview of the stable and the dynamically exchanging units in the T4aPM. Arrows forming a circle show protein exchange. Grey arrows indicate PilA incorporation and removal from the base of the pilus fiber and pilus extension and retraction.

6.5 Stability in the OM pore complex and parts of the alignment complex

To learn if this stability within the OM pore complex of the T4aPM depends on interaction partners, we also performed FRAP microscopy in strains expressing PilQ-sfGFP but

lacking TsaP and PilP. Even though the accumulation of PilQ-sfGFP was lower in the absence of each of the two proteins and its localization was reduced, only no to little recovery in FRAP measurements suggests that TsaP and PilP do not affect the stability of the secretin pore made by PilQ-sfGFP in the T4aPM.

If the TsaP stable unit in turn depends on other T4aPM components, can be studied in the future by systematic FRAP microscopy of deletion mutants of T4aPM components, as TsaP was shown to accumulate and localize as in wildtype in Δ*pil* strains except of Δ*pilQ* and Δ*tgl*, in which TsaP levels were reduced (Siewering *et al.*, 2014). One can speculate that a strong interaction of TsaP to PilQ and/or to itself leads to the stable ring formation and as discussed obove, that TsaP's LysM domains might contribute to its stable incorporation into the T4aPM.

The stability of the PilP ring in the T4aPM seems to depend on direct interaction partners of PilP. However, in *M. xanthus* PilP does not accumulate in the absence of PilQ and does not localize polarly in the absence of PilN or PilO (Friedrich *et al.*, 2014). Therefore, we studied if the stability of the PilP-sfGFP ring depends on the presence of PilM or PilC by FRAP microscopy. Indeed, PilP-sfGFP polar clusters recovered fluorescence intensity in the absence of PilM or PilC. Thus, PilP must be stabilized by PilM and PilC. As no direct interactions of PilP to PilC or PilM were shown to date, this might be an indirect effect, e.g., PilC might destabilize PilO to which it was suggested to interact with (Georgiadou *et al.*, 2012); or PilM might influence PilN, and in both cases, the result might be a destabilization of the PilPNO complex, resulting in the mobility of PilP.

As PilC and PilM affect PilP stability in the T4aPM, we also studied whether PilO-sfGFP stability in the T4aPM depends on PilC or PilM. Interestingly, the FRAP microscopy experiments demonstrated that PilC but not PilM is necessary for PilO to form a stable unit in the T4aPM. As PilN and PilO together are known to interact with PilP, and PilC affects PilO stability, it is likely that PilC affects PilP stability in the T4aPM in an indirect manner. However, it was surprising that the absence of PilM mobilizes PilP but not PilO, as they are known to form a complex (Tammam *et al.*, 2011). PilN, PilO, and PulM and PulL of the T2SS were shown to form either heterodimers (PilN-PilO, PulM-PulL) and homodimers (Leighton *et al.*, 2016, Dazzoni *et al.*, 2023). This discrepancy between PilP and no PilO mobilization by lack of PilM might be caused by different states of homo or heteromer formation by PilO and PilN (Leighton *et al.*, 2016), and needs further investigation.

Part II

7 Introduction

7.1 Introduction to the bacterial cell envelope

Bacteria can survive many environmental conditions. The first protective barrier of bacterial cells the cell envelope. Besides its protective function, it also allows cells to interact with their environment as well as with eukaryotic cells and other bacteria.

The cell envelope of Gram-positive bacteria consist of a single phospholipid membrane that is surrounded by a thick layer of PG and contains wall teichoic acids (WTA) and lipoteichoic acids (LTA) that are coupled to the PG and membrane lipids. The cell envelope of Gram-negative bacteria consists of an IMIM, composed of phospholipids, a thin PG layer and an OMO) that offers additional protection. The inner leaflet of the OM is made of phospholipids and the outer leaflet is composed of lipopolysaccharide (LPS) (Silhavy *et al.*, 2010, Whitfield & Trent, 2014).

7.1.1 Introduction to glycans

Bacteria produce a variety of intracellular and extracellular glycans. In Gram-negative bacteria, these include PG, secreted polysaccharide (SPS), capsular polysaccharides (CPS), lipopolysaccharides (LPS), lipooligosaccharides (LOS), glycoproteins and intracellular storage polysaccharides (Tytgat & Lebeer, 2014). Gram-positive bacteria possess lipoglycans or glycosylated teichoic acids (TA), but lack LPS and LOS (Figure 34) (Tytgat & Lebeer, 2014). The glycoconjugates found on the cell envelope build a strain-specific barcode, mediating specific interactions with the environment e.g. other bacterial cells or the host organism (Tytgat & Lebeer, 2014).

Cell surface polysaccharides are large polymers of sugar monomers and are distinguished as CPS and SPS. They differ from each other in their degree of attachment to the cell surface. SPS are secreted to the extracellular environment or loosely attached to the cell surface via electrostatic interactions. CPS is often bound more closely and covalently to the cell surface and can also form a thick glycan layer or capsule around the cell, SPS is often found as free EPS or slime around the cells (Knirel & Valvano, 2013, Tytgat & Lebeer, 2014).

A variety of organisms produce SPS and the polysaccharides in these biopolymers were shown to vary immensely in composition and structure (Roca *et al.*, 2015). The function of SPS is just as varied. It can be important for biofilm formation adhesion and protection against environmental conditions as well as for motility of microorganisms (Wolfaardt *et al.*, 1999, Hu *et al.*, 2016, Nwodo *et al.*, 2012).

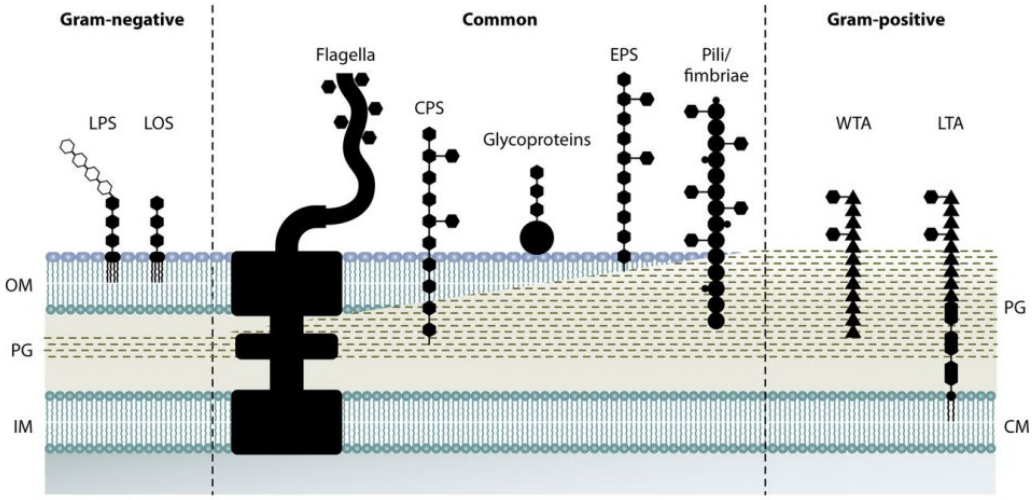

Figure 36 Bacterial glycoconjugates. LPS and LOS are found in Gram-negative bacteria. Gram-positive bacteria are known to glycosylate their TAs (e.g. WTA and LTA). Both types of bacteria can glycosylate large appendages (e.g. flagella, pili or fimbriae) and possess CPS, SPS and glycoproteins. PG is an important component of the bacterial cell wall. Round dots represent proteins and triangles represent ribotol phosphate or glycol phosphate moieties (Tytgat & Lebeer, 2014).

7.1.2 Synthesis of cell-surface polysaccharides

Polysaccharides represent the most abundant biomolecules in nature and are involved as key players in a variety of important biological processes. Repeated monosaccharide units linked by glycosidic bonds form long polysaccharides. These can differ in their monosaccharide composition, their glycosidic linkage, their level of polymerization, thus polysaccharides can widely vary in their structure and biological function (Silva *et al.*, 2014, Wang *et al.*, 2016a).

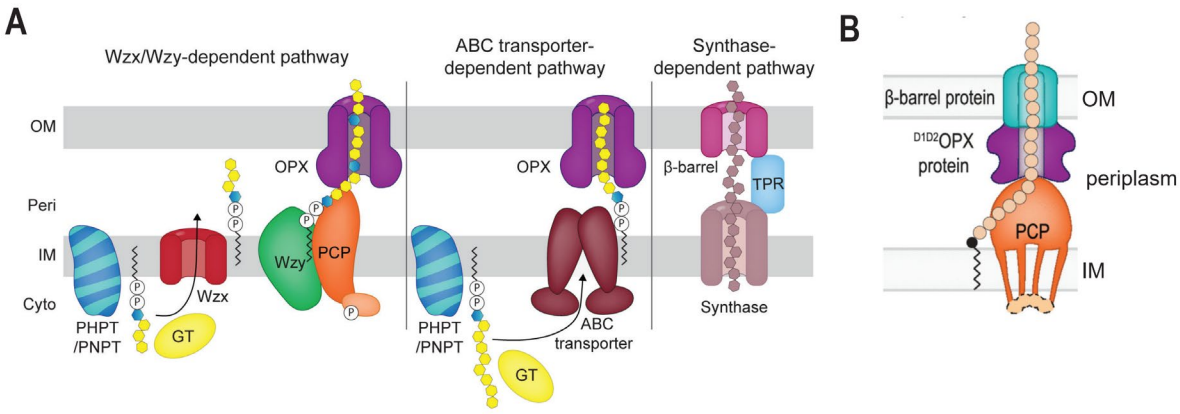

Figure 37 Overview of surface polysaccharide synthesis pathways in Gram-negative bacteria. A. The Wzx/Wzy dependent pathway, the ABC-transporter dependent pathway and the Synthase dependent pathway are depicted. For simplicity, only one GT is shown as example in the scheme. Adapted from (Perez-Burgos & Søgaard-Andersen, 2020). **B.** Overview of the composite OPX/β-barrel translocon. The OPX protein lacks the OM part, a β-barrel protein constitutes the OM part of the composite OPX/β-barrel protein translocon. Adapted from (Schwabe *et al.*, 2022).

There are generally different pathways for synthesis of cell-surface polysaccharides in bacteria, the Wzx/Wzy-, the ABC transporter and the synthase dependent pathway (Figure 37) (Whitfield *et al.*, 2020, Perez-Burgos & Søgaard-Andersen, 2020).

The Wzx/Wzy dependent pathway is involved in synthesis of polysaccharides and glycoconjugates. The synthesis of the repeat unit starts with the transfer of a phosphorylated monosaccharide from an activated uridine diphosphate-sugar to a molecule of the lipid carrier, an undecaprenyl phosphate, forming an undecaprenyl diphosphate-sugar. This reaction can be catalyzed by two different types of enzymes: the polyisoprenyl-phosphate hexose-1-phosphate transferases (PHPTs) or the polyisoprenyl-phosphate N-acetylhexosamine-1-phosphate transferases (PNPTs) (Lukose *et al.*, 2017, Valvano, 2011). Glycosyltransferases (GTs) add sugars to the undecaprenyl diphosphate-sugar molecule to synthesize the repeat unit. The lipid-linked units are translocated across the IMIM by the Wzx flippase. A Wzy polymerase with the help of a polysaccharide co-polymerase (PCP) polymerizes the units into longer polysaccharide chains in the periplasm and translocation across the OM is ensured by an OPX protein (Whitfield *et al.*, 2020, Perez-Burgos & Søgaard-Andersen, 2020). The translocation across the OM can also be provided another system comprising a composite OPX/β-barrel translocon (Schwabe *et al.*, 2022).

In the ABC-transporter dependent pathway the full-length polysaccharide molecule is synthesized by sequential action of different GTs in the cytoplasm. An ABC transporter then ensures translocation of the polysaccharide across the IMIM. Afterwards, the polysaccharide is transported across the OM by an OPX protein or a composite OPX/β-barrel translocon (Greenfield & Whitfield, 2012, Whitfield *et al.*, 2020, Perez-Burgos & Søgaard-Andersen, 2020, Schwabe *et al.*, 2022).

In the synthase dependent pathway a synthase complex spans the cell envelope and catalyzes initiation, polymerization and transport of glycans. In this pathway, polymerization and transport of the polysaccharide chain across the cell envelope occur simultaneously (Whitfield *et al.*, 2020, Perez-Burgos & Søgaard-Andersen, 2020).

7.1.3 Surface polysaccharides of *M. xanthus*

M. xanthus cells are surrounded by an extracellular matrix (ECM), which consists of a polysaccharide referred to as exopolysacchride (EPS), proteins, extracellular lipids, OM vesicles (OMV) and also extracellular DNA (Behmlander & Dworkin, 1994, Muñoz-Dorado *et al.*, 2016). In addition to EPS, *M. xanthus* cells synthesize three other cell-surface polysaccharides: biosurfactant polysaccharide (BPS), spore coat polysaccharides and the O-antigen of LPS. While EPS, BPS and the O-antigen of LPS are important for motility and development (Bowden & Kaplan, 1998, Islam *et al.*, 2020, Lu *et al.*, 2005, Perez-Burgos *et al.*, 2020a, Perez-Burgos *et al.*, 2019), the spore coat polysaccharide is specifically needed for sporulation (Holkenbrink *et al.*, 2014, Perez-Burgos *et al.*, 2020b, Müller *et al.*, 2012). Moreover, moving *M. xanthus* cells leave a slime trail behind. This trail was shown to contain polysaccharides and OMV, but its exact function and composition remains unknown (Ducret *et al.*, 2013a, Ducret *et al.*, 2012).

7.1.4 *M. xanthus* EPS synthesis and function

According to current models, EPS is loosely associated to the cell surface (Berleman *et al.*, 2016, Gloag *et al.*, 2016, Hu *et al.*, 2013).EPS is synthesized via a Wzx/Wzy dependent pathway and its components are encoded by the *eps* locus (Islam *et al.*, 2020, Perez-Burgos *et al.*, 2020a, Lu *et al.*, 2005, Zhou & Nan, 2017). EpsZ is the PHPT, which initiates synthesis of the EPS repeat unit. The five GTs (i.e. EpsU, EpsH, EpsE, EpsD and EpsA) are thought to extend the repeat unit. Next, individual repeat units are translocated

across the IMIM by the Wzx_{EPS} flippase. The Wzy_{EPS} polymerase and EpsV, a PCP protein, polymerize the repeat units. The polysaccharide can then be translocated across the OM via the composite translocon formed by the OPX protein EpsY and EpsX (Perez-Burgos *et al.*, 2020a, Islam *et al.*, 2020, Schwabe *et al.*, 2022).

EPS is important for cell-cell cohesion, T4aP-dependent motility and development under submerged conditions (Arnold & Shimkets, 1988, Hu *et al.*, 2012, Shimkets, 1986, Perez-Burgos *et al.*, 2020a, Yang *et al.*, 1998). However, the exact function of EPS in the *M. xanthus* is not clear.

The dependency of T4aP-dependent motility on EPS seems to involve various processes. First, EPS^{-} strains containing mutations in genes of the Dif chemosensory system make T4aP at WT levels or are hyperpiliated but have reduced T4P-dependent motility (Li *et al.*, 2003, Yang *et al.*, 2000). Exogenous EPS restored the hyperpiliation phenotype of the EPS^{-} *dif* mutants (Hu *et al.*, 2011, Li *et al.*, 2003). It was also reported that T4aP as well as PilA bind EPS (Hu *et al.*, 2012, Li *et al.*, 2003). As *dif* mutants with an EPS^{-} phenotype possess T4aP but have reduced T4aP-dependent motility, these observations led to the suggestion that EPS might stimulate T4aP retraction (Hu *et al.*, 2012, Li *et al.*, 2003). Second, mutants lacking components of the pathway for EPS synthesis have a defect in T4aP assembly, suggesting that EPS or the EPS biosynthetic machinery is important to stimulate T4aP extension (Perez-Burgos *et al.*, 2020a). Third, *dif* mutants reverse with a decreased frequency, compared to WT (Shi *et al.*, 2000, Kearns *et al.*, 2000), while an *epsZ* mutant hyperreverses (Zhou & Nan, 2017). Thus, it was suggested, that EPS is also important for regulation of the reversal frequency. These observations were done in different strains and under differing conditions, but altogether support the idea that EPS *per se* or the EPS biosynthetic pathway interfere with the T4aPM by different mechanisms.

7.1.5 Regulation of EPS synthesis

Different regulators of EPS synthesis are known in *M. xanthus*. The Dif chemosensory system is one of the best-studied pathways involved in EPS regulation (Yang *et al.*, 1998, Yang & Li, 2005). It consists of DifA (methyl-accepting chemotaxis protein [MCP]), DifE (CheA-type histidine kinase), DifC (CheW coupling protein), a single-domain response regulator EpsW, the single-domain response regulator DifD and CheC-like phosphatase DifG. Upon activation of the Dif pathway, the DifE phosphorylates EpsW and DifD

(Bellenger *et al.*, 2002, Black *et al.*, 2015, Lancero *et al.*, 2005, Yang *et al.*, 1998, Yang & Li, 2005). DifD has been suggested to act as a phosphate sink for the phosphate flow from DifE (Black *et al.*, 2010, Black & Yang, 2004) and DifG is responsible for dephosphorylating DifD (Black & Yang, 2004).

An interaction between DifE and the NtrC-like transcriptional regulator Nla19 has also been suggested. However, it is not clear if DifE phosphorylates Nla19 (Lancero *et al.*, 2005). While DifA, DifE, DifC and EpsW are known as positive regulators of EPS synthesis, DifD, DifG and Nla19 are negative regulators (Perez-Burgos & Søgaard-Andersen, 2020), but it is still an open question how the Dif chemosensory system regulates EPS synthesis.

Additionally, mutants lacking components of the T4aPM that are unable to make T4aP also lack EPS, while a mutant lacking the retraction ATPase PilT is hyperpiliated and has increased levels of EPS (Black *et al.*, 2006, Black *et al.*, 2017, Bretl *et al.*, 2016, Shimkets, 1986, Dana & Shimkets, 1993). It was suggested that the extension ATPase PilB builds a link between the T4aPM and EPS synthesis (Black *et al.*, 2017) and that the activity of the Dif chemosensory system is regulated by the T4aPM (Black *et al.*, 2006, Black *et al.*, 2017, Wu & Kaiser, 1995). StkA, which is a DnaK homolog, is a negative regulator of EPS synthesis and was shown to act between the T4aPM and the Dif pathway (Black *et al.*, 2006, Moak *et al.*, 2015, Dana & Shimkets, 1993).

Another key player for regulation of EPS synthesis is the second messenger c-di-GMP. A strain lacking the diguanylate cyclase DmxA has higher c-di-GMP levels during growth and increased EPS accumulation (Skotnicka *et al.*, 2016b). Also, lack of other proteins associated to c-di-GMP (e.g. SgmT, DigR, TmoK) lead to increased EPS synthesis during growth (Skotnicka *et al.*, 2016a, Overgaard *et al.*, 2006). Additionally, the diguanylate cyclase DmxB, which is responsible for increasing the c-di-GMP level during development, is important for increased EPS synthesis upon starvation (Skotnicka *et al.*, 2016c). C-di-GMP has also been suggested to bind to Nla24, which is an NtrC-like transcriptional regulator encoded by the *eps* locus, to stimulate the transcription of the *eps* genes (Skotnicka *et al.*, 2016c).

In addition to these regulators, many other proteins have been implicated with the regulation of EPS synthesis (Perez-Burgos & Søgaard-Andersen, 2020). Interestingly, among the remaining regulators, FrzS and SgmO (also referred to as RasA) are encoded

by neighboring genes (Pham *et al.*, 2005a). FrzS is a pseudo-response regulator, which was suggested to regulate T4aP-dependent motility by stimulating EPS production (Berleman *et al.*, 2011). Additionally, it interacts with the small GTPase MglA (Mauriello *et al.*, 2010), which is important to establish polarity in *M. xanthus* (Leonardy *et al.*, 2010b, Carreira *et al.*, 2022).

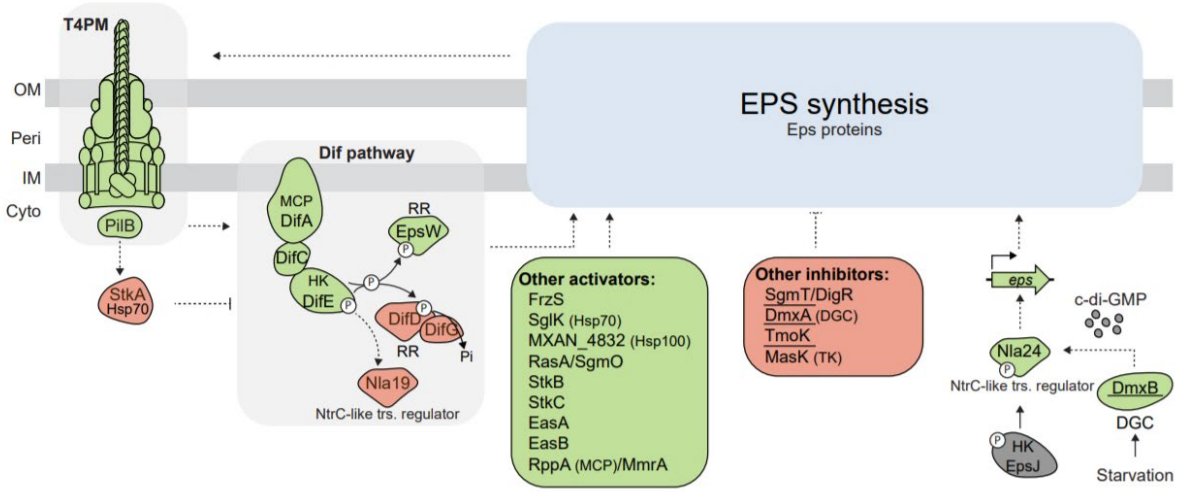

Figure 38 Regulation of EPS biosynthesis in *M. xanthus*. The T4aPM, Dif pathway and c-di-GMP and related proteins are involved in regulation of EPS synthesis. Additionally other activators and inhibitors of EPS synthesis in *M. xanthus* are known. Positive regulators are shown in green and negative regulators in red (Perez-Burgos & Søgaard-Andersen, 2020).

8 Scope of this study

Here, we focus on SgmO, a suggested regulator of EPS synthesis. Insertional mutants of *sgmO* were shown to have a defect in EPS accumulation, T4aP-dependent motility, and development (Pham *et al.*, 2005a, Youderian & Hartzell, 2006). Here, we aim to investigate the role of SgmO in the EPS synthesis.

9 Results

9.1 Bioinformatics analyses

Previously it was noted that SgmO does not possess any known protein domains that would hint at its function (Pham *et al.*, 2005a). However, using the SMART database

(Letunic & Bork, 2018), KEGG database (Kanehisa & Goto, 2000), Pfam database (Mistry *et al.*, 2021), and HHpred, a structural-based recognition server (Zimmermann *et al.*, 2018), we identified a HEAT repeat, two low complexity regions and a domain of unknown function (DUF1641) in SgmO. The amino acid composition of SgmO contains 10% of Leu and 14% of Ala residues. SignalP-5.0 identified no signal peptides or transmembrane helices. Analysis of the secondary structure of SgmO with Phyre^2 (Kelley *et al.*, 2015) predicted that SgmO consists mostly of α-helices. Alphafold predictions of SgmO confirmed this (Figure 39A, D).

Using a reciprocal best BlastP hit method (KEGG SSDB database) (Kanehisa & Goto, 2000), we found that *sgmO* is conserved in the genomes of all fully sequenced myxobacterial genomes, while the synteny of flanking genes is less conserved (Figure 39C).

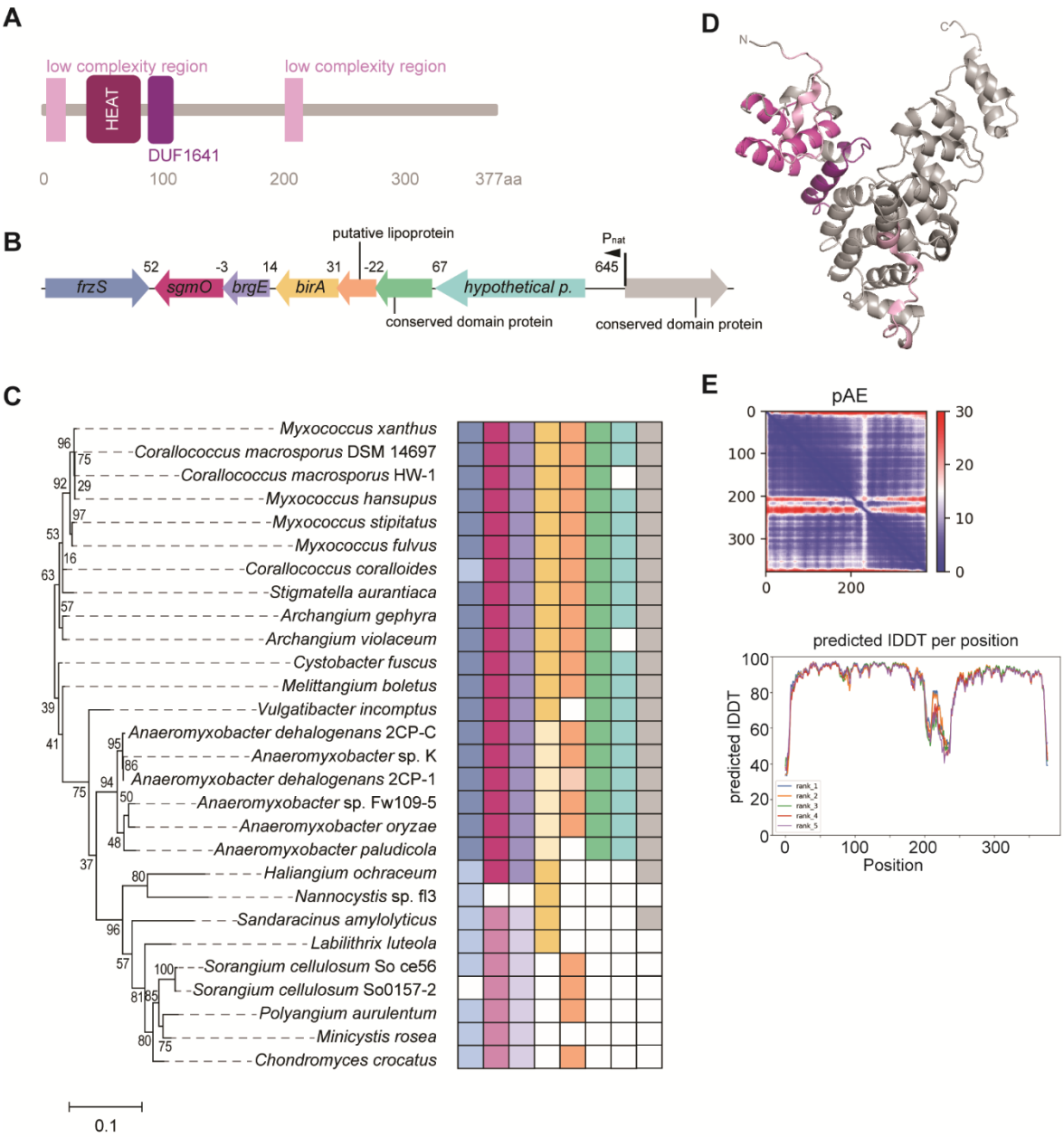

Figure 39 Bioinformatics analyses of *sgmO* A. Domain architecture of SgmO. Low complexity regions, HEAT repeat region and DUF1641 are indicated. The protein is drawn to scale (0-377aa). **B.** Genetic neighborhood and **C.** conservation of *sgmO* in different myxobacterial genomes. *sgmO* and neighboring genes in *M. xanthus* are drawn to scale. Numbers between the arrows indicate the distance between the corresponding genes. A reciprocal best BLASTP hit method was used to identify orthologs in all fully sequenced genomes of myxococcota. A 16S rRNA tree of these speciesis shown on the left. Conserved genes in the genetic neighborhood of *sgmO* are shown in the corresponding color. Light coloring indicated that the gene is present but not in the *sgmO* genetic neighborhood. White, the gene was not identified. **D.** Alphafold prediction of SgmO, the domains are colored as in A. **E.** Predicted aligned error (pAE) and predicted LDDT for full-length *M. xanthus* SgmO.

9.2 Phenotypic analyses of *sgmO* mutant

An in-frame deletion mutant of *sgmO* was constructed to study the function of SgmO. Cells were tested for T4aP-dependent and gliding motility, as well as for EPS accumulation by supplementing 0.5% agar plates with trypan blue or congo red which binds to EPS resulting in either a blue or a red color. Wildtype cells were used as a positive control, while the Δ*pilA* and Δ*aglQ* strains were used as a negative control for T4aP-dependent and gliding motility. Δ*difE* and Δ*epsZ* cells did not synthesize EPS (Perez-Burgos *et al.*, 2020a) and were used as a negative control for EPS accumulation.The Δ*sgmO* mutation caused a defect in EPS synthesis and T4aP-dependent motility, but cells were able to move by gliding motility (Figure 40A).

The motility and EPS defects of the Δ*sgmO* mutant were complemented by ectopically expressing *sgmO* under the control of the putative native promoter from a plasmid integrated into a single copy at the Mx8 *attB* site (Figure 40A).

To investigate if the lack of SgmO is only causing a defect in T4aP-dependent motility or also affecting gliding motility, double deletions of Δ*sgmO and pilA* or *aglQ* were created and cells spotted on 0.5% and 1.5% agar. The Δ*sgmO*Δ*pilA* strain was affected in T4aP-dependent motility but could move by means of gliding motility similarly to a Δ*pilA* mutant. In contrast, a Δ*sgmO*Δ*aglQ* strain was not moving under both conditions, while a Δ*aglQ* mutant moved by T4aP-dependent motility but not by gliding motility. This together indicates that lack of SgmO is primarily affecting T4aP-dependent motility (Figure 40B).

Because mutants lacking components of the EPS machinery showed a reduction in the assembly of T4aP, we next performed a shearing assay to test the T4aP levels of Δ*sgmO* mutants. Immunoblot assays of the sheared pili fraction using antibodies against the major pilin, PilA, showed that Δ*sgmO* cells have a reduced level of T4aP compared to WT. Similarly, the cellular fraction of PilA was reduced in the Δ*sgmO* mutant. The decreased level of PilA in the cellular fraction is comparable to the one for the Δ*pilB* mutant. The defects were restored in the complementation strain (Figure 40C).

To test if the Δ*sgmO* mutant was able to develop, we investigated the Δ*sgmO* strain on agar and in submerged conditions.

WT cells were able to form aggregates at 24 h that led to the formation of mature fruiting bodies, as well as heat and sonication resistant spores. In contrast, the Δ*sgmO* mutant

cells have reduced formation of fruiting bodies with reduced sporulation under both conditions. Because a *difE* mutant neither develops on agar nor under submerged conditions (Yang *et al.*, 1998, Yang *et al.*, 2000), the Δ*difE* mutant was used as a negative control for development. The ectopic expression of SgmO from the putative native promoter recovered the ability of a Δ*sgmO* mutant to develop (Figure 40D).

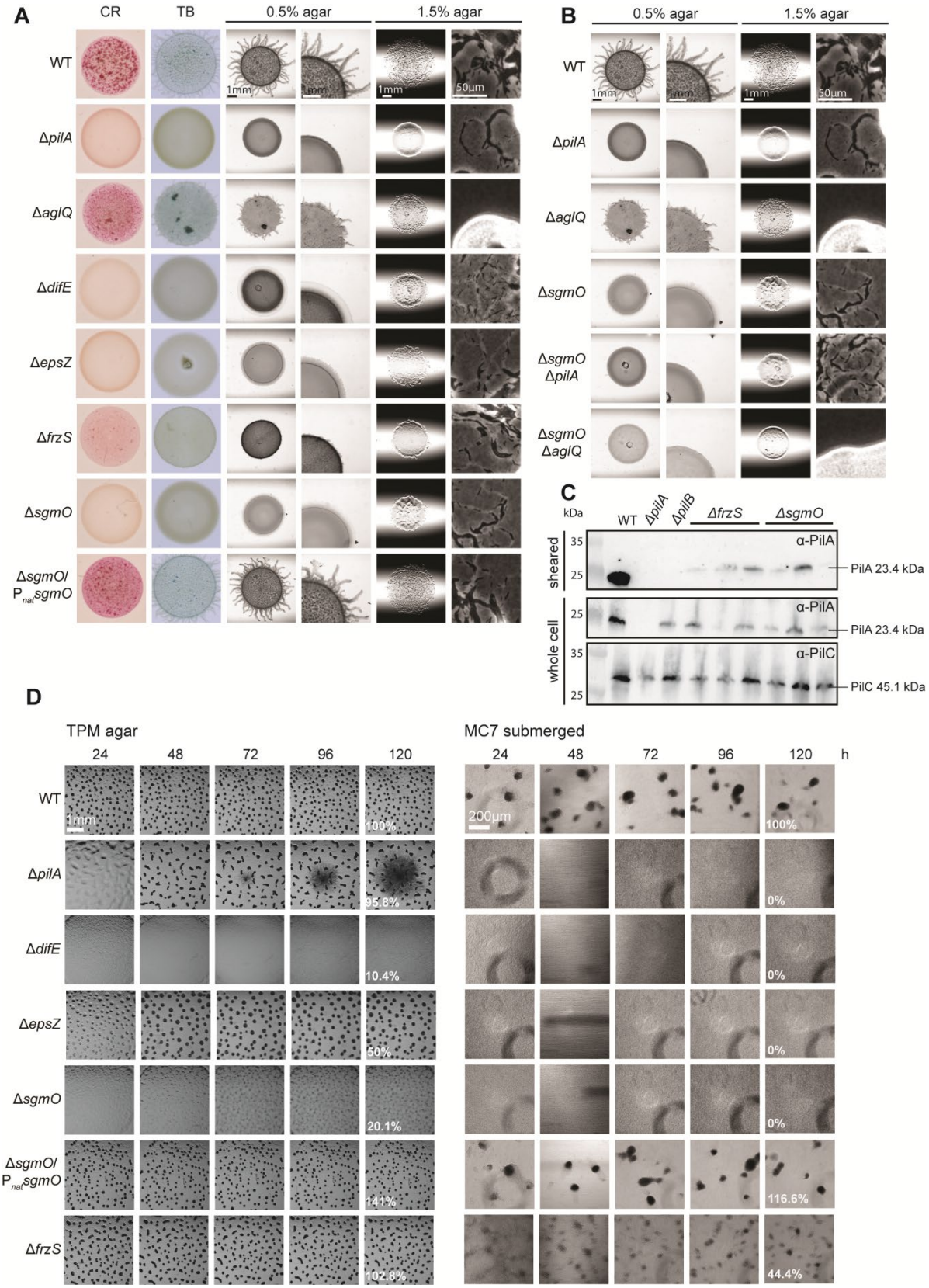
A
CR
TB
0.5% agar
1.5% agar
WT
ΔpilA
ΔaglQ
ΔdifE
ΔepsZ
ΔfrzS
ΔsgmO
ΔsgmO/ P natsgmO
1mm
50μm
B
0.5% agar
1.5% agar
WT
ΔpilA
ΔaglQ
ΔsgmO
ΔsgmO ΔpilA
ΔsgmO ΔaglQ
C
kDa
WT
ΔpilA
ΔpilB
ΔfrzS
ΔsgmO
sheared
whole cell
35
25
α-PilA
PilA 23.4 kDa
α-PilC
PilC 45.1 kDa
D
TPM agar
MC7 submerged
24
48
72
96
120
h
WT
ΔpilA
ΔdifE
ΔepsZ
ΔsgmO
ΔsgmO/ P natsgmO
ΔfrzS
1mm
200μm
100%
95.8%
10.4%
50%
20.1%
141%
102.8%
0%
116.6%
44.4%

Figure 40 Phenotypic analyses of *sgmO* mutants A. Colony-based motility assay of the Δ*sgmO* mutant. T4aP-dependent and gliding motility were tested on 0.5% and 1.5% agar, respectively. EPS accumulation was tested on 0.5% agar containing congo red (CR) and trypan blue (TB). Images were recorded after 24 h. Scale bars: 1mm, 1mm, 1 mm and 50µm (left to right). **B.** Colony-based motility assay of the Δ*sgmO* Δ*pilA* and Δ*sgmO* Δ*aglQ* mutants. T4aP-dependent and gliding motility were tested on 0.5% and 1.5% agar, respectively. Images were recorded after 24 h. Scale bars: 1mm, 1mm, 1mm and 50µm (left to right). **C.** Shear-off assay. Samples of sheared fraction and total cells were prepared and SDS-PAGE and immunoblot analysis was performed to determine the PilA levels in different strains. As a negative control, samples of ∆*pilA* cells were used. The membrane on the top is showing the results of the sheared fraction, while the two images at the bottom correspond to the whole cell fraction probed with α-PilA (middle) or α-PilC antibodies as loading control (bottom). Protein sizes are indicated. **D.** Development assay of the ∆*sgmO* mutant. OD_{550}=7 samples were spotted on TPM agar (left) and submerged with MC7 buffer (right). Images of spots and wells were taken at the indicated time points. At 120 h, samples were collected and treated with heat and sonicated. Heat and sonication resistant spores were counted and indicated as a percentage of wildtype. Scale bars: 1mm, 200µm (from left to right).

9.3 Functionality and localization of SgmO fluorescent fusions

Determining the localization pattern of proteins can help to understand their function. Thus, N- and C-terminal fluorescent fusions of SgmO to mCherry were created and ectopically expressed under the control of the native promoter in the ∆*sgmO* strain. Both fluorescent fusions were tested for functionality by performing T4aP-dependent motility and measuring the EPS level. Both fusions were partially functional since the T4aP-dependent motility defect of the ∆*sgmO* strain was not fully rescued. However, expression of mCherry-SgmO rescued the EPS biosynthesis defect while expression of SgmO-mCherry did not (Figure 41A). Importantly, immunoblot assays with α-mCherry antibodies showed that both fusion proteins accumulate and are stable since no free mCherry was detected. Interestingly, mCherry-SgmO accumulated at lower levels than SgmO-mCherry despite the fact that its expression complements the motility and EPS defects of the Δ*sgmO* mutant better (Figure 41B).

Next, we analyzed the localization of the SgmO fusions. In both cases, the SgmO fluorescent fusion localized diffusely. Some bright spots within the cells were observed. However, they are likely inclusion bodies because the fluorescence signals of these spots were also visible in the GFP channel (Figure 41C).

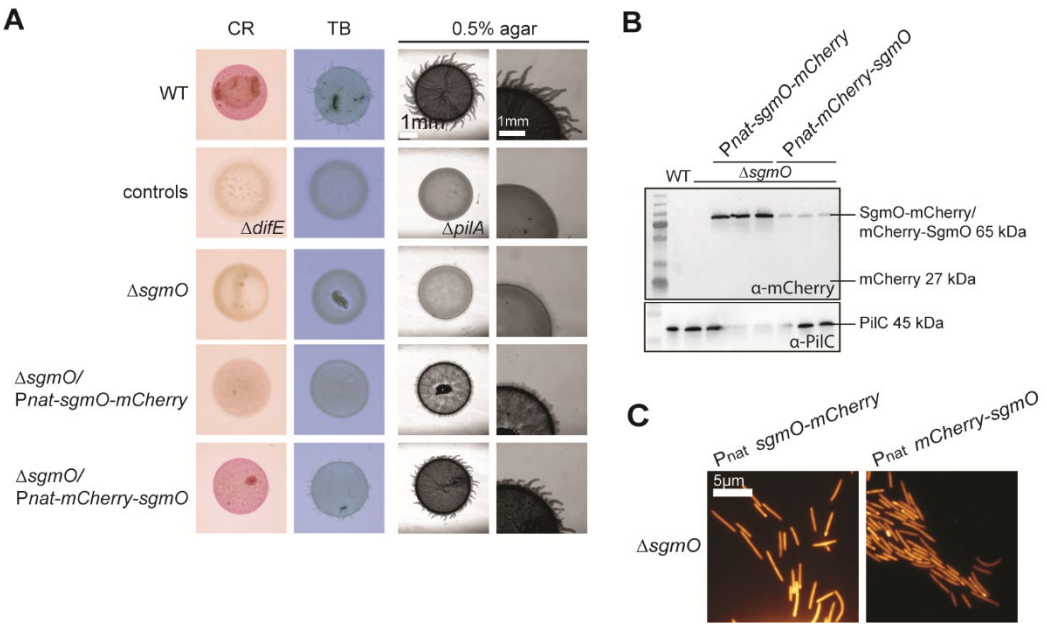

Figure 41 Functionality, accumulation and localization of SgmO fluorescent fusions. A. Colony-based motility assay of Δ*sgmO* strains that ectopically express mCherry fusions. T4aP-dependent motility was tested on 0.5% (right panels), EPS accumulation was tested on 0.5% agar containing congo red (CR) (left) and trypan blue (TB) (middle). Images were recorded after 24 h. Scale bar: 1mm. **B.** Accumulation of SgmO fluorescent fusions. Immunoblot analysis was performed with samples of Δ*sgmO*/P_{nat}-*sgmO-mCherry* and Δ*sgmO*/P_{natm}Cherry-*sgmO*. Expected protein sizes are indicated on the right side and a protein ladder is on the left. The membrane was additionally incubated with α-PilC antibodies as loading control. **C.** Fluorescence microscopy was performed on 1% TPM-agarose slides with exponentially growing cultures. Images in TXR channel are shwon. Scale bar: 5µm.

Since localization of the SgmO fluorescent fusions did not give a significant insight into the putative role of SgmO, we next looked into the genetic neighborhood of *sgmO.*

9.4 *sgmO* is encoded in an operon

Two genes in the genetic region of *sgmO* (Figure 39B), *frzS* and *brgE*, were implicated with EPS synthesis and T4aP-dependent motility (Berleman *et al.*, 2011), or development (Pham *et al.*, 2005b). Downstream of *brgE*, *birA* encodes a BirA family transcriptional regulator, biotin operon repressor/biotin[acetyl-CoA-carboxylase] ligase. In *E. coli,* BirA is a bifunctional protein that catalyzes both the ligation of a biotin moiety onto a specific Lys residue of the biotin carboxyl carrier protein and represses the biotin biosynthetic operon by binding to an operator site (Barker & Campbell, 1981) and is, thus, involved in the regulation of biotin synthesis (Chakravartty & Cronan, 2013, Wilson *et al.*, 1992). The three

genes downstream of *birA* encode a putative lipoprotein, a conserved domain protein, and a hypothetical protein.

Since these genes are found in close proximity, we hypothesized that they might form an operon. Therefore, operon mapping was performed, for which total RNA was isolated from *M. xanthus* DK1622and reverse transcribed to generate cDNA using a reverse transcriptase. As a negative control, PCRs were also performed with samples in which no reverse transcriptase was added. gDNA was used as a positive control that the intergenic primers were functional. All primers could bind to gDNA, and the fragments with expected sizes could be amplified (Figure 42). At the same time, no fragments could be amplified from RNA samples that were not transcribed to cDNA. In the reactions performed on cDNA, fragments could be amplified, indicating that *sgmO* is encoded in an operon with *brgE*, *birA*, *mxan_4153*, *mxan_4154 and mxan_4155*. The in-frame deletion mutants of *brgE*, *birA*, *mxan_4153*, *mxan_4154 and mxan_4154* need to be generated to study if the function of the encoded proteins is connected to SgmO.

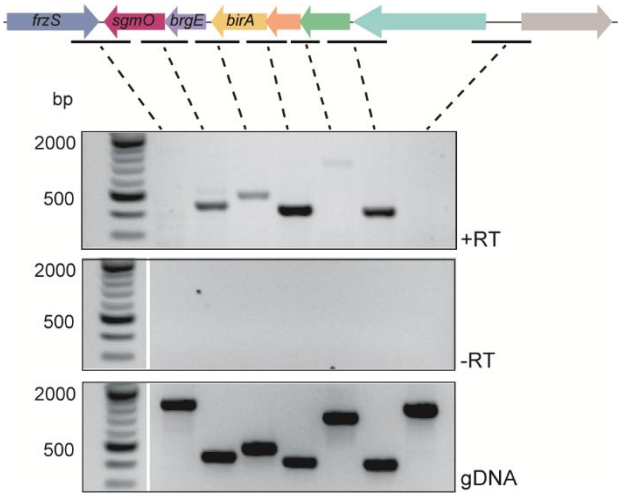

Figure 42 Operon mapping of *sgmO*. RNA of *M. xanthus* DK1622 was isolated and used for operon mapping. Black lines below the gene cluster indicate amplified regions and were numbered from one to seven. As a positive control for the reaction, genomic *M. xanthus* DK1622 DNA was used. As a negative control, samples in which the reverse transcriptase was omitted were used.

10 Discussion

10.1 SgmO- a regulator of EPS synthesis in *M. xanthus*

SgmO was identified as a regulator of EPS synthesis as part of the characterization of its neighboring gene *brgE,* which is necessary for fruiting body formation and sporulation (Pham *et al.*, 2005b, Youderian & Hartzell, 2006). Similarly, SgmO, is required for EPS synthesis and, therefore also for development, as well as T4aP dependent motility and cell-cell cohesion (Pham *et al.*, 2005a). Of note, SgmO does not possess any conserved motifs and does not bear sequence homology to any known genes according to the literature (Pham *et al.*, 2005a, Pham *et al.*, 2005b).

brgE and *sgmO* are transcribed in the opposite directions compared to the the downstream *frzS* gene (Ward *et al.*, 2000, Pham *et al.*, 2005b). The interesting genetic neighborhood, as well as the phenotype of the Δ*sgmO* mutant, emphasize SgmO as a player in the regulation of EPS synthesis. It is an open question, how SgmO is involved in this process and if it interacts with its genetic neighbors *brgE* or *frzS*. Studying SgmO could give an insight into the connection between the T4aPM, the Dif chemosensory system, and EPS synthesis. Alternatively, it could reveal a yet unknown pathway of EPS biosynthesis regulation.

In this study, we confirmed that lack of SgmO leads to defects in EPS synthesis, T4aP-dependent motility and development. Additionally, we observed that Δ*sgmO* cells had reduced T4aP. Because EPS/the EPS machinery (Δ*eps* mutants) is important for stimulation of T4aP formation and T4aP-dependent motility (Perez-Burgos *et al.*, 2020a) and because EPS is important for cell-cell cohesion (Arnold & Shimkets, 1988), the motility and developmental defects of the Δ*sgmO* mutant can be widely explained by lack of EPS. Next, to test if, as the Δ*eps* mutants, T4P extension in the ∆*sgmO* strains is reduced, or whether the ∆*sgmO* cells are hyperretracting T4P a ∆*sgmO*∆*pilT* strain, lacking the retraction ATPase, needs to be generated. Additionally, localization studies of components of the T4aPM in the Δ*sgmO* mutant would allow to conclude if the observed decreased level of T4aP in the Δ*sgmO* mutant might be caused by reduced assembly of the T4aPM.

Recently, the synthesis pathway of EPS has been uncovered in *M. xanthus* (Perez-Burgos *et al.*, 2020a). Moreover, EPS synthesis in *M. xanthus* is regulated in a very complex manner, which includes the Dif chemosensory pathway, and that T4P assembly and EPS

synthesis regulate each other (Perez-Burgos & Søgaard-Andersen, 2020, Li *et al.*, 2003, Hu *et al.*, 2012). It is unclear at this moment at which stage of the cascade SgmO acts.

Additional epistasis experiments could help to understand if SgmO is acting downstream of T4aPM and upstream of the Dif chemosensory pathway, in between the Dif chemosensory pathway and the EPS biosynthetic machinery or if it is part of a yet unknown pathway. For this purpose, new mutants need to be generated. It was shown that a lack of the DnaK homolog StkA restores EPS to a *pilA* deletion mutant but not to a *difA* deletion mutant (Moak *et al.*, 2015). This indicated that StkA acts downstream of T4P but upstream of the Dif chemosensory pathway. Thus, it would be interesting to create a Δ*sgmO*Δ*stkA* mutant. If this strain would restore EPS biosynthesis, this would suggest that SgmO acts upstream of the Dif pathway.

On the contrary, if a Δ*sgmO*Δ*stkA* mutant does not synthesize EPS, it would suggest that SgmO acts downstream of the Dif pathway. It was also shown that a Δ*difD*Δ*difG* double mutant overproduces EPS, and DifD and DifG are negative regulators of EPS synthesis (Black & Yang, 2004). In case a Δ*sgmO*Δ*difD*Δ*difG* triple mutant would restore EPS biosynthesis, it would indicate that SgmO acts upstream of the Dif chemosensory pathway and in case not, that SgmO acts between the Dif pathway and the EPS biosynthetic machinery.

Operon mapping indicated that *sgmO* is encoded in an operon with *brgE, birA*, *mxan_4153*, *mxan_4154,* and *mxan_4155*. It is, therefore, possible that the proteins encoded by the operon act in the same pathway, together with SgmO, to regulate EPS biosynthesis.

It is known that *brgE* is important for the development of *M. xanthus* cells (Pham *et al.*, 2005b). However, whether this mutant also has an EPS accumulation defect that might affect motility and development was not studied. *birA* encodes a bifunctional protein, a biotin ligase and a repressor of the biotin operon in *E. coli* (Barker & Campbell, 1981). Further experimental analyses could help to understand if SgmO could be biotinylated by BirA.

It would be interesting to generate mutants with single in-frame deletions in *brgE, birA*, *mxan_4153*, *mxan_4154* and *mxan_4155* to compare them to the Δ*sgmo* strain. Also, pull-down experiments could help to elucidate with which proteins SgmO interacts to understand its function.

Finally, because FrzS was reported as a regulator of EPS synthesis (Berleman *et al.*, 2011), a Δ*frzS* mutant was included in the motility, developmental and EPS accumulation assays. While Δ*sgmO* cells completely lack EPS, the Δ*frzS* mutant synthesizes EPS anbeit at a lower level than WT. The Δ*frzS* mutant colonies also show reduced T4aP-dependent motility but are not as smooth as the Δ*sgmO* strain. The two strains also differ in their phenotypes during development. While the Δ*frzS* mutant forms fruiting bodies, the ∆*sgmO* mutant forms some aggregates on TPM agar and fails entirely to develop under submerged conditions. This might point to *frzS* and *sgmO* not acting together. Because FrzS was shown to localize to the cell poles of *M. xanthus* cells (Mignot *et al.*, 2005), FrzS localization could be studied in a ∆*sgmO* strain to learn if lack of SgmO somehow affects FrzS localization.

11 Materials and Methods

11.1 Chemicals and equipment

The Reagents, enzymes, kits and antibiotics used in this study are listed in Table 1. The equipment used for this study is listed in Table 2 and the software used for Data analysis is listed in Table 3.

Table 1 Reagents, enzymes, kits and antibiotics

Reagent	Manufacturer
Chemicals	Roth (Karlsruhe), Merck (Darmstadt), Sigma-Aldrich (Taufkirchen)
Media components, agar	Roth (Karlsruhe), Merck (Darmstadt), Difco (Heidelberg), Invitrogen (Darmstadt)
5x DNA loading buffer	New England Biolabs (NEB), (Frankfurt am Main)
2-log DNA ladder	New England Biolabs (NEB), (Frankfurt am Main)
Oligonucleotides	Eurofins MWG Operon (Ebersberg)

Rabbit antisera	Eurogentec (Seraing, Belgium)
Anti-GFP monoclonal antibodies	Roche Diagnostics GmbH (Mannheim)
Anti-mCherry antibodies	BioVision
Goat anti-rabbit IgG, goat anti-rabbit IgG DyLight 549	Pierce™ Thermo Scientific™ (Dreieich)
Anti-mouse with se, horseradish peroxidase linked	GE Healthcare Europe GmbH (Freiburg)
SDS gel electrophoresis size standards PagerulerTM Plus Prestained Protein Ladder	Pierce™ Thermo Scientific™ (Dreieich)
Nitrocellulose membrane	GE Healthcare Europe GmbH (Freiburg)
Luminata Western HRP Substrate	Millipore Merck Chemicals GmbH (Schwalbach)
Enzymes	
Restriction Enzymes	Fermentas (St. Leon-Rot), New England Biolabs (Frankfurt am Main)
Antarctic phosphatase	New England Biolabs (Frankfurt am Main)
T4 DNA Ligase	New England Biolabs (Frankfurt am Main)
Phusion High-Fidelity DNA polymerase	Thermo Scientific (Dreieich)
Q5 High-Fidelity DNA polymerase	New England Biolabs (Frankfurt am Main)
5 PRIME MasterMix	5 PRIME GmbH (Hamburg)
Antibiotics	
Gentamycin sulfate Kanamycin sulfate Ampicillin sodiumsulfate Oxytetracycline dehydrate Tetracycline hydrochloride	Roth (Karlsruhe)
Kits	
Purification of chromosomal DNA	Epicentre Biotechnologies (Wisconsin,USA)
NucleoSpin® Plasmid Kit NucleoSpin® Gel and PCR Clean-up Ki	Macherey-Nagel (Düren)

Table 2 Equipment

Application	Device	Manufacturer
PCR	MasterCycler Epigrade MasterCycler Personal	Eppendorf (Hamburg)
Gelectrophoresis	E835	Consort (Ottawa, CN)
DNA illumination	UVT_20 LE, UB Transilluminator 312nm	Herolab (Wiesloch) INTAS Science Imaging Instruments GmbH (Göttingen)

DNA illumination and documentation	E-BOX VX2 imaging system, GelStick Touch IMAGER	PeqLab (Eberhardzell) INTAS Science Imaging Instruments GmbH (Göttingen)
Thermomixer	Thermomixer F 1.5 Thermomixer C Thermomixer Compact	Eppendorf (Hamburg)
Electroporation	GenePulser Xcell	Bio-Rad (München)
Protein electrophoresis	Mini-PROTEAN® 3 cell	Bio-Rad (München)
Western blotting	TransBlot®TurboTM Transfer System	Bio-Rad (München)
Chemiluminescence detection	Luminescent image analyzer LAS-4000	Fujifilm (Düsseldorf)
Microscopes	Nikon Ti-E microscope with Perfect Focus System (PFS), temperature control, CFI PL APO 100x/1.45 Lambda oil, Hamamatsu Flash 4.0 camera	Nikon (Düsseldorf), Hamamatsu Photonics (Hersching)
	DMI6000B inverted microscope with AFC temperature control, HCX PL APO 100x/1.47 oil, HCX PL APO 100x/1.47 oil, Hamamatsu Flash 4.0 camera	Leica (Wetzlar) Hamamatsu Photonics (Hersching)
	M205FA Stereomicroscope	Leica (Wetzlar)
Determination of optical densities, nucleic acids/protein absorption	Ultrospec 2100 pro Spectrophotometer, Nanodrop ND-1000 UV-Vis spectrophotometer	GE Healthcare Europe GmbH (Freiburg) Nanodrop (Wilmington)

Table 3 Software

Application	Software	Manufacturer
Checking of DNA and proteins sequences, *in silico* plasmid cloning, sequence assembly	DNASTAR	DNASTAR, Inc (Madison, USA)
Data analysis of microscopy pictures	Metamorph® v 7.7.5.0	Molecular Devices (Union City, CA)
Detection of cells on microscopy pictures	Oufti	Jacobs-Wagner Lab (Paintdakhi *et al.*, 2016)
Calculation of fluorescence signals	MATLAB R2016b/R2018a	The MathWorks, Inc (Natcik, USA)

Curve fitting, plotting of data and statistical testing	Sigma Blot 14.0 Graph Pad Prism 9.0.2	Systat Software Inc. (San Jose, USA) Dotmatics (San Diego, USA).

11.2 Media

All media and solutions were autoclaved for 20 min, 121 °C, and 1 bar over-pressure. Antibiotics and other additives were filtered using sterile 0.22 µm pore-size filters (Millipore Merck, Schwalbach) and were added to pre-cooled media at around 55 °C

E. coli cells were grown on LB-medium (Luria Bertani). For preparation of agar-plates, 1.5% agar was added to the medium. *M. xanthus* cells were grown on 1% CTT medium in liquid cultures or on agar-plates. For preparation of agar-plates, 1.5% agar was added to the medium. Motility assays of *M. xanthus* cells were performed on soft (0.5%) or hard (1.5%) agar plates. Media compositions are described in Table 4.

Table 4 Bacterial growth media

Media	**Composition**
E. coli	
LB medium	1% (w/v) NaCl, 1% (w/v)tryptone, 0.5% (w/v) yeast-extract
LB agar	LB medium, 1% (w/v) agar
M. xanthus	
CTT medium	1% (w/v) Bacto-casintone. 10mM Tris-HCl pH 8.0 1mM potassium phosphate buffer pH 7.6, 8mM $MgSO_4$
CTT agar	CTT medium, 1.5% agar
Motility assays Soft agar Hard agar	 0.5% CTT medium, 0.5% agar; 0.5% CTT medium, 1.5% agar (Hodgkin & Kaiser, 1977)
Microscopy media	

MC7 buffer	10 mM MOPS, pH 7.0, 1 mM CaCl2
Chitosan 100x solution	2M acetic acid 15mg/ml chitosan
TPM-agar	10 mM Tris-HCl, pH 7.6, 1 mM KH2PO4, pH 7.6, 8 mM MgSO4, 1.5% agar

Additives used for *E. coli* and *M. xanthus* cells are listed in Table 5.

Table 5 Additives

Additive	**final concentration**	**dissolved in**
E. coli		
Kanamycin sulfate	50 µg/ml	H_2O
Tetracyclin dehydrate	25 µg/ml	99.9 % ethanol
M. xanthus		
Gentamycin sulfate	10 µg/ml	H_2O
Kanamycin sulfate	50µg/ml	H_2O
Oxytetracyline	10 µg/ml	0.1M HCl

11.3 Microbiological methods

11.3.1 Strain construction and growth conditions

All *M. xanthus* strains used in this study are derivatives of the wild-type strain DK1622 (Kaiser, 1979). Strains, plasmids, and oligonucleotides used in this work are listed in Table 6, 7, and 9. *M. xanthus* cells were grown at 32°C in 1% CTT (1% [wt/vol] Bacto Casitone, 10 mM Tris-HCl [pH 8.0], 1 mM K_2HPO_4-KH_2PO_4 [pH 7.6], and 8 mM $MgSO_4$) liquid medium or on 1.5% agar supplemented with 1% CTT (Shi & Zusman, 1993). In-frame deletions or insertions were generated as described previously (Shi *et al.*, 2008). Plasmids were introduced in *M. xanthus* by electroporation and integrated by homologous recombination at the endogenous locus. All in-frame deletions and plasmid integrations were verified by PCR. Plasmids were propagated in *E. coli* Mach1 and DH5α.

E. coli cells were grown in LB-medium or on plates containing LB supplemented with 1.5% agar at 37°C. Antibiotics were used when appropriate (Denman, 1983). All DNA fragments generated by PCR were verified by sequencing.

11.3.2 *E. coli* strains

E. coli strains used for cloning are listed in Table 1Table 6.

Table 6 *E. coli* strains

Strain	Characteristics	Reference
NEB® Turbo	F' *proA*$^{+}$*B*$^{+}$ *lacI*^{q} Δ*lacZM15 / fhuA2* Δ*(lac-proAB) glnV galK16 galE15 R(zgb-210::Tn10)*Tet^{S} *endA1 thi-1* Δ*(hsdS-mcrB)5*	New England Biolabs (NEB), (Frankfurt am Main)
Top10	F- mcrA Δ(mrr-hsdRMS-mcrBC) Φ80lacZΔM15 ΔlacX74 recA1 araD139 Δ(ara leu) 7697 galU galK rpsL (StrR) endA1 nupG	Invitrogen™ life technologies (Karlsruhe)
Mach1	Δ*rec*A1398 *endA*1 *tonA* φ80Δ*lacZ*M15 Δ*lacX*74 hsdR(rK- mK+)	Invitrogen™ life technologies (Karlsruhe)

11.3.3 *M. xanthus* strains

M. xanthus strains used in study are listed in Table 7.

Table 7 *M. xanthus* strains

Strain	Genotype	Reference
DK1622	wild-type	(Kaiser, 1979)
DK10416	Δ*pilB*	(Wu & Kaiser, 1997)
SA3002	Δ*pilM*	(Bulyha *et al.*, 2009)
DK10409	Δ*pilT*	(Wu & Kaiser, 1997)
SA3001	Δ*pilO*	(Friedrich *et al.*, 2014)
SA3005	Δ*pilP*	(Friedrich *et al.*, 2014)
DK8615	Δ*pilQ*	(Wall *et al.*, 1999)
SA6011	Δ*tsaP*	(Siewering *et al.*, 2014)
SA9303	Δ*frzE*	This work
DK10410	Δ*pilA*	(Wu & Kaiser, 1997)
SA5649	Δ*difE*	Dorota Skotnicka
SA7400	Δ*epsZ*	(Perez-Burgos *et al.*, 2020a)
SA5293	Δ*aglQ*	(Jakobczak *et al.*, 2015)
SA7135	Δ*frzE*Δ*aglQ*	(Szadkowski *et al.*, 2019)
SA7192	*pilQ-sfGFP*	(Potapova *et al.*, 2020)
SA7896	*mCherry-pilM*	(Treuner-Lange *et al.*, 2020)
SA9300	*pilB-mCherry*	This study
SA9307	*mCherry-pilT*	This study
SA9314	*pilO-sfGFP*	This study

SA9315	*pilP-sfGFP*	This study
SA9316	*tsaP-mCherry*	This study
SA9304	*pilB-mCherry ΔfrzE*	This study
SA9310	*pilB-mCherry ΔaglQ*	This study
SA9311	*pilB-mCherry ΔfrzE ΔaglQ*	This study
SA9329	*mCherry-pilT ΔfrzE*	This study
SA9323	*mCherry-pilT ΔaglQ*	This study
SA9326	*mCherry-pilT ΔfrzE ΔaglQ*	This study
SA9305	*mCherry-pilM ΔfrzE*	This study
SA9312	*mCherry-pilM ΔaglQ*	This study
SA9313	*mCherry-pilM ΔfrzE ΔaglQ*	This study
SA9337	*pilO-sfGFP ΔfrzE*	This study
SA9338	*pilO-sfGFP ΔaglQ*	This study
SA9339	*pilO-sfGFP ΔfrzE ΔaglQ*	This study
SA9330	*pilP-sfGFP ΔfrzE*	This study
SA9324	*pilP-sfGFP ΔaglQ*	This study
SA9327	*pilP-sfGFP ΔfrzE ΔaglQ*	This study
SA9331	*tsaP-mCherry ΔfrzE*	This study
SA9325	*tsaP-mCherry ΔaglQ*	This study
SA9328	*tsaP-mCherry ΔfrzE ΔaglQ*	This study
SA9306	*pilQ-sfGFP ΔfrzE*	This study
SA9308	*pilQ-sfGFP ΔaglQ*	This study
SA9309	*pilQ-sfGFP ΔfrzE ΔaglQ*	This study
SA9349	*pilQ-sfGFP ΔfrzE ΔaglQ ΔtsaP*	This study
SA9348	*pilQ-sfGFP ΔfrzE ΔaglQΔpilP*	This study
SA9344	*pilP-sfGFP ΔfrzE ΔaglQΔpilC*	This study
SA9345	*pilP-sfGFP ΔfrzE ΔaglQΔpilM*	This study
SA9350	*pilO-sfGFP ΔfrzE ΔaglQΔpilC*	This study
SA9351	*pilO-sfGFP ΔfrzE ΔaglQΔpilM*	This study
SA9346	*mCherry-pilMΔfrzEΔaglQΔpilB*	This study
SA9347	*mCherry-pilMΔfrzEΔaglQΔpilT*	This study
SA9352	*mCherry-pilMΔfrzEΔaglQΔpilBΔpilT*	This study
SA9353	*pilM-pilN*	This study
SA9354	*mCherry-pilM-pilN*	This study
SA12037	*pilB-mCherryΔpilQ*	María Pérez-Burgos
SA9342	*mCherry-pilTΔpilQ*	This study
SA9317	*ΔsgmO*	This study
SA9318	*ΔfrzS*	This study
SA9322	*ΔsgmO/Pnat-sgmO*	This study
SA9333	*ΔsgmO/Pnat-mCherry-sgmO*	This study
SA9332	*ΔsgmO/Pnat- sgmO-mCherry*	This study
SA9319	*ΔsgmOΔpilA*	This study
SA9320	*ΔsgmOΔaglQ*	This study

11.3.4 Cultivation and storage of bacteria

E. coli cells were cultivated on LB-agar plates at 37°C and grown in liquid LB-medium, shaking horizontally at 37°C with 220 rpm. Antibiotics were added with concentrations as listed in Table 5. The optical densities of cell cultures were photometrically determined at 600 nm. For short- term storage, the *E.coli* cells were grown on LB-agar plates and stored at 4°C. For long-term storage, stocks were taken from overnight liquid cultures with addition of 10% glycerol to the culture. The stocks were frozen in liquid nitrogen and stored at -80°C.

M.xanthus cells were cultivated on CTT-agar plates and incubated at 32°C in the dark. Liquid cultures were grown in CTT-medium, shaking horizontally at 32°C in the dark at 220 rpm. To prohibit contamination of *M. xanthus* cell cultures, liquid CTT-medium and CTT-agar was supplied with 10µg/ml gentamycin. The optical densities of liquid *M. xanthus* cell cultures were determined photometrically at 550 nm. For short-term storage *M. xanthus* cells were incubated on CTT-agar plates for up to two weeks at 18°C in the dark. For long-term storage, stocks were taken from overnight liquid cultures. The cells were harvested at 4700 rpm and resuspended in 1ml CTT with 15% glycerol. The stocks were fast frozen in liquid nitrogen and stored at -80 °C.

11.3.5 Motility assays

For motility assays, *M. xanthus* cells from exponentially growing cultures were harvested at 4000 g for 10 min at room temperature (RT) and resuspended in 1% CTT to a calculated density of 7×10^9 cells/ml. 5 µl aliquots of cell suspensions were placed on 0.5% agar plates supplemented with 0.5% CTT for T4P-dependent motility and 1.5% agar plates supplemented with 0.5% CTT for gliding motility (Shi & Zusman, 1993) and incubated at 32°C in the dark. After 24 hours, the colony and its edges were visualized using a Leica M205FA stereomicroscope and imaged using a Hamamatsu ORCA-flash V2 Digital CMOS camera (Hamamatsu Photonics). For higher magnifications of cells at colony edges on 1.5% agar, cells were visualized using a Leica DM6000B microscope and imaged using a Cascade II 1024 EMCCD camera (Photometrics).

11.3.6 EPS accumulation assays

To detect EPS accumulation, cells were grown in CTT medium and harvested at 4000g for 10 min at room temperature (RT) and resuspended in 1% CTT to a calculated density

of 7×10^9 cells/ml. 20 µl of the cell suspension was spotted on 0.5% agar plates, supplemented with 0.5% CTT and 40 µg/ml congo red or 20 µg/ml trypan blue. The plates were incubated at 32°C in the dark and imaged after 24 h (Perez-Burgos *et al.*, 2019).

11.3.7 T4P shearing assays

To shear off T4P, cells were grown on 1% CCT, 1.5% agar plates for three days at 32°C in the dark. The cells were scraped off the agar and resuspended in 1ml per 60mg cells. The suspension was vortexed for 10 min and incubated on ice for 10 minutes. Then, SDS samples for the total PilA level were taken (80 µl cellsuspension, 20µl 5xSDS sample buffer). The remaining suspension was centrifuged for 20 min at 13.000g at 4°C. The supernatant was centrifuged twice again for 10 min at 13.000g at 4°C. T4P in the supernatant were precipitated by adding 10x pili precipitation buffer (100mM TRIS-HCl pH:7.6, 150mM NaCl, 20%(w/v) PEG 6000, 1M $MgCl_2$) and incubated for >2h at 4°C followed by centrifugation for 30 min at 13.000g at 4°C. The pellet was resuspended in SDS sample buffer (1µl per mg vortexed cells). SDS samples of total cell and pili fraction were used further for SDS-PAGE and immunoblot analysis as described in 11.5.1 and 11.5.2.

11.3.8 Development assays

Development assays on TPM-agar and under submerged conditions in MC7 buffer were performed to study the development and fruiting body formation of *M. xanthus* cells. For this, exponentially growing cells were harvested at 4000g for 10 min at RT and resuspended in TPM to a calculated density of 7×10^9 cells/ml. 10 µl of the cell suspension was spotted on TPM agar, and 50 µl was resuspended in 350µl MC7 buffer and incubated in well-plates. Images of the colonies/ cell aggregates were acquired after 24, 48, 72, 96 and 120h. To count spores, the colonies were scratched from the agar using a pipet tip, and cell material was collected in an Eppendorf tube and resuspended in 500 µl MC7. To collect spores from submerged conditions, the MC7 buffer in the wells was harvested and added up to 500 µl. The collected spores were incubated for 2 h at 50°C (heat-shock) and sonicated for 30 seconds (50 W/ 75%). 5µl of this suspension were spotted on a Thoma counting chamber (Roth, Karlsruhe) and images were acquired using a Leica DM6000B microscope and a Cascade II 1024 EMCCD camera (Photometrics). The spores were counted manually.

11.3.9 Fluorescence microscopy and analysis

For microscopy, 200 µl of exponentially growing cells were resuspended in 1ml MC7 (10 mM MOPS [pH 7.0], 1 mM KH2PO4, 8 mM MgSO4, and 1 mM CaCl2) and spotted on chitosan-coated glass bottom µ-slides (ibidi) (Ducret *et al.*, 2013b) or 5µl of cells were spotted on a 1%TPM-agarose slide. Cells were incubated for 30 min in the dark at room temperature before imaging. Cells were observed using a Leica DMI6000B microscope with a Hamamatsu Flash 4.0 camera. Images were recorded with Leica MM AF software package and processed with Metamorph (Molecular Devices). Cells in phase contrast images were automatically detected using Oufti (Paintdakhi *et al.*, 2016). Fluorescence signals in segmented cells were identified and analyzed using a custom-made Matlab v2016b (MathWorks) script that divides a cell into polar region 1, polar region 2, and the cytoplasmic region. Polar regions are defined as the regions of a cell within a distance of 10 pixels, corresponding to 0.64 µm, from a tip of the cell. The cytoplasmic region includes all pixels of the cell with the exception of the polar regions. A polar cluster was identified when three or more connected pixels within a polar region had a fluorescence signal higher than a cell-specific threshold signal of two SDs above the average fluorescence signal in the cytoplasmic region. The fluorescence of a polar cluster was defined as the sum of the fluorescence signal of all connected pixels that exceeded the threshold value in that polar region. The cytoplasmic signal was defined as the sum of the fluorescence signal of all pixels between the two polar regions. For each cell with polar cluster(s), an asymmetry index (ω) was calculated as

$$\omega = \frac{(\text{total fluorescence at pole 1} - \text{total fluorescence at pole 2})}{(\text{total fluorescence at pole 1} + \text{total fluorescence at pole 2})}$$

By definition, pole 1 is the pole with the highest fluorescence. ω varies between zero (bipolar symmetric localization) and one (unipolar localization). The localization patterns were categorized as follows: unipolar ($\omega > 0.9$), bipolar asymmetric ($0.9 > \omega > 0.2$), and bipolar symmetric ($\omega < 0.2$). Diffuse localization was determined when no polar signal was detected, and for these cells, ω was set to zero (Potapova *et al.*, 2020).

11.3.10 Fluorescence recovery after photobleaching and analysis

Fluorescence recovery after photobleaching (FRAP) experiments were performed with a temperature controlled Nikon Ti-E microscope with Perfect Focus System and a CFI PL

APO 100x/1.45 Lambda oil objective at 32°C with a Hamamatsu Orca Flash 4.0 camera using NIS Elements AR 2.30 software (Nikon). For photobleaching, a 651nm or 488 nm laser beam was focused on the central part of the image plane. After the acquisition of an initial pre-bleach picture, cells of interest were bleached using a 0.9 × 0.9 µm circular-shaped region. Photobleaching was performed with 2 laser pulses with 10% laser power and a dwelling time of 250 ms. After imaging, each cell used for FRAP microscopy was outlined using the software oufti (Paintdakhi *et al.*, 2016). The background fluorescence of the image was subtracted and a custom made MATLab script was used to analyze the data further. Cell poles were defined as 10% of cell ends to ensure to include in total polar fluorescence signal, and the fluorescence intensity of the cell poles and the fluorescence of the whole cell was measured. To correct the data for general bleaching of the fluorophore during image acquisition, the fluorescence intensities of the poles were normalized to whole cell fluorescence. The corrected fluorescence intensity before bleaching was set as 1, and the rest of the measurements were normalized to this value. The average normalized relative fluorescence intensities were plotted against the time. Curve fitting was used to estimate the recovery half-time and the mobile fraction. SigmaPlot 14 was used to fit the curve of the bleached pole to the exponential function $y(t) = y_0 + A * (1 - e^{-kt})$ (y_0= relative fluorescence at t=0), A= maximum intensity, k= rate constant) in case of recovery. The resulting rate constant was used to calculate the recovery half-time ($t_{half\ max\ recovery}$) with $t_{\text{half max recovery}} = ln\,(0.5)/-k$ (Kiekebusch *et al.*, 2012).

The mobile fraction was calculated as $M_f = I_\infty + I_0/I_i - I_0$ (I_∞= Intensity plateau, I_0= Intensity after bleaching, I_i= intensity before bleaching). Cells with an R^2 <0.35 and an estimated recovery halftime above the time of measurement were excluded from further analysis. R^2 is the coefficient of determination and used to evaluate curve fitting.

Settings for FRAP microscopy of the different strains was as follows:

Table 8 Setting of Acquisition

Protein	Acquisition	Acquisition after bleaching
PilQ-sfGFP	488nm, 40%, 600 ms, Duration: 1834s	4s (every 2 s), 5 min (every 30 s), 20 min (every 1 min)
PilP-sfGFP	488nm, 40%, 400 ms, Duration: 1834s	4s (every 2 s), 5 min (every 30 s), 20 min (every 1 min)

PilO-sfGFP	488nm, 43%, 1 s, Duration: 1534s	4s (every 2 s), 5 min (every 30 s), 15 min (every 1 min)
TsaP-mCherry	561nm, 30%, 400 ms, Duration: 1834s	4s (every 2 s), 5 min (every 30 s), 20 min (every 1 min)
mCherry-PilM	561nm, 30%,, 400 ms, Duration: 1534s	4s (every 2 s), 5 min (every 30 s), 15 min (every 1 min)
PilB-mCherry	561nm, 40%, 300ms, Duration: 20s	5 sec (every 500 ms), 15 sec (every 1 s)
mCherry-PilT	561nm, 45%, 800ms, Duration: 201s	1.8 s (every 900 ms), 50 s (every 10 s), 2.5 min (every 30 s)

11.3.10.1 Estimation of dwell times

To calculate the dwell times of mCherry-PilM, PilB-mCherry and mCherry-PilT, the average fluorescence intensity at the two poles and in the cytoplasm of the cells before bleaching was used as to calculate the fractions of proteins at the two and in the cytoplasm by using the known amount of proteins in a cell based on quantitative immunoblot analysis (11.5.4.). Then recovery halftimes of the different proteins and the mobile fraction were used to estimate how much protein was exchanged at the reached $t_{1/2}$. Based on that we roughly estimated how much time it would take for one molecule to be exchanged (dwell time) (Milne-Davies *et al.*, 2021).

11.4 Molecular biological methods

11.4.1 Oligonucleotides and plasmids

The names and sequences of all oligonucleotides used in this study are listed Table 9. The restriction sites are indicated in bold. All plasmids used in this study are listed in Table 10.

Table 9 Oligonucleotides used in this study

Name	Sequence	Purpose
Primer for plasmid construction		
pilB-mCA-EcoRI	GCGCGAATTCGATCACCTCGCGTTTGAAG	Replacement of *pilB* by *pilB-mCherry* at native site
pilB-mCC+ overlay	GACGAGCTGTACAAGTAGTCAACCTTCCTCCCAC	
pilB-mCB- overlay	GAGGAAGGTTGACTACTTGTACAGCTCGTCCATG	

PilT fw EcoRI	CGCGAATTCGCTCCTTCCTCC	Replacement of *pilT* by *mCherry-pilT* at native site
PilT rev HindIII	GCGCAAGCTTCTAACGACCAC	
pilO up fw	GCGCGAATTCGGCCTGTTCGCATGATG	Replacement of *pilO* by *pilO-sfGFP* at native site
Pilo up rev pSC106 fusion	TCCAGGTACTTGTCCATGACGGGCAGCCTT GTCAGATGG	
pSC106 fw pilO up fusion	CCATCTGACAAGGCTGCCCGTCATGGACAA GTACCTGG	
sfGFP rev pilO down fusion:	CTTGAGCGGATCAAGTTTTTATTTGTAGAGCTC ATCC	
pilO down fw sfGFP fusion	GGATGAGCTCTACAAATAAAAACTTGATCCGCT CAAG	
pilO down rev Hind III:	GCGCAAGCTTCAGCAGCACCCGGCCAAC	
pilP up fw (EcoR)	GCGCGAATTCCGAGCGCCGCAAGCTGG	Replacement of *pilP* by *pilP-sfGFP* at native site
pilP up rev-pSC102 ovh new	GTAGGGCGACAAGGGGAGTGAGGatgaagacgttcaagg	
psc102fw pilp up ovh new	CCATCTGACAAGGCTGCCCGTCATGGACAAGT ACCTGG	
sfGFP rev pilP down fusion	GAGCGCCTTGGAGGGCGTTATTTGTAGAGCTC ATCCATG	
pilP down fw fusion sfGFP	CATGGATGAGCTCTACAAATAACGCCCTCCAA GGCGCTC	
pilP down rev (HindIII)	GCGCAAGCTTCTGCCTGGGTCTCAACGGC	
tsaP fw EcoRI 2	gcgcgaattcATGCGCTCCCGGATTCTCAC	Replacement of *tsaP* by *tsaP-mCherry* at native site
mch rev down tsap fusion	GCATTTTTCCTGCCGCGCCGCTTACTTGTA	
tsap down fw mch fusion	GCTGTACAAGTAAGCGGCGCGGCAGGAAAA	
tsap down rev Hind III	GCGCAAGCTTAACCGCCGCCTCCCCGTTC	
sgmO up fw EcoRI	GCGCGAATTCGGACCTCTACCTGGACACGG	In-frame deletion of *sgmO*
sgmO up rev	CCTACCCCTGAGTGGTCATGACGCGTGATTC	
sgmO down fw	CATGACCACTCAGGGGTAGGGGCTGGCAGTG	
sgmO down rev Hind III	GCGCGAAGCTTCGGTGCCCCGTCCCTC	

Pnat mxan 4155 fw XbaI	GCGCTCTAGAGGGAGCTCCGGCATCC	Integration of *Pnat-sgmO* at attB site
Pnat mxan4155 rev ovh sgmO	GAGCGGCAGTGGTCAAGTATTCCCCAGGAATTCC	
sgmO fw ovh Pnat mxan4155	CTGGGGAATACTCGATGACCACTGCCGCTCC	
sgmO rev Hind III	CGCGAAGCTTCTACCCCTGCTTCTTCGG	
Pnat mxan 4155 fw XbaI	GCGCTCTAGAGGGAGCTCCGGCATCC	Integration of *Pnat-sgmO-mCherry*
SgmO rev ovh linker	GGAGCCGCCGCCGCCCCCCTGCTTCTTCGGGGC CGTCTTC	
mCherry fw ovh linker	GGCGGCGGCGGCTCCATGGTGAGCAAGGGCGA GGAGGATAAC	
mcherry rev HindIII	CGCGAAGCTTCTACCCCTGCTTCTTCGG	
Pnat mxan 4155 fw XbaI	GCGCTCTAGAGGGAGCTCCGGCATCC	Integration of *Pnat-mCherry-sgmO*
pnat4155 rev ovh mcherry:	CTCGCCCTTGCTCACCATCGAGTATTCCCCAGGAA TTCCGAACGG	
mcherry fw ovh pnat4155	CCTGGGGAATACTCGATGGTGAGCAAGGGCGAG	
mCherry rev ovh linker	GGAGCCGCCGCCGCCCTTGTACAGCTCGTCCATGC	
sgmO rev Hind III	CGCGAAGCTTCTACCCCTGCTTCTTCGG	
pilB fw NdeI	GCGCCCCATATGTCCGGTCGACTCGGTGAA	Overexpression of PilB-His10
pilB rev His 10 Hind III	GCGCAAGCTTCTAGTGATGGTGATGATGGT GGTGATGGTGATGGAAGCGGTCCGGGGCGGTG	
pilB fw NdeI	GGGCGCACATATGTCCGGTCGACTCGGTGAA	Overexpression of $PilB_{(1-182)-His10}$
pilB Nterm rv His10 HindIII	GCGCAAGCTTCTACTAGTGATGGTGATGATGGTG GTGATGGTGATGCAGCTTGA	
pMAT336 fw EcoRI	GCGCGAATTCCCTGAAGTCCTACGCATGG	Replecaement of *pilM* by *pilM-pilN* or *pilM* by *mCherry-pilM-pilN*
PilM rv no stop ovh PilN2	GATGCGAATCATCATGGCCAGCTTGTCGCCC	
pilN fw ovh PilM	GGCGACAAGCTGGCCATGATGATTCGCATCAACCTG	
PilN rev Hind III	GCGCAAGCTTAGTCATCGTGATCTTGAACTCGACC	
Primer for Test PCRs		
pilA E	CGCTTCCGGCCGCAGCACGC	
pilA F	CAGCAGTCCGTAGACCTGGC	

pilA G	CCTGGCCGCCATCGCCATCC	
pilA H	CGATCACCCAGTCATCGAAG	
PilB E	CAGGCAAGGTGCTCCAGCCG	
PilB F	GCGTCGCGTAGCAGATGT	
PilB G	GGCCCAGGAAGAGCAGCAGA	
PilB H	CGGGCGCATCACCTCGTACA	
PilC E	GTGACCTGGAGACGATTG	
PilC F	GGAGAGCTGACGTGAGAG	
PilC G	GCCTCGATATCCTCGCGAG	
PilC H	GATGAGGAAGCCACCGACC	
PilM E	GAGCCTTCATCGCTCGG	
PilM F	TGTTCTTGACCTCGCCG	
PilM G	CAGGACCTGATGTCCGAGCTGAA	
PilM H	GGAGACCACCGTGGTGTAGTCGT	
PilM E2	CCGGAAAATCGGGCCTCCGC	
PilM F2	GACCACCCTCTGGAGACGACGC	
PilO E	GGCGTTGCCAACTACCTCTG	
PilO F	GGGTCCTGCTTCGCATCAGG	
PilP E	CAAATTCGGGGGCCTGGC	
PilP F	CTCATCAGCCTCGGCAGC	
PilP G	GCCTGCAAAGCCCAAGGC	
PilP H	GCATCAGGCTTCAACTGC	
pilT E	CTCCGCCAGGACCCGGACATC	
pilT F	TATCGAGGCACTGCACCA	
pilT G	CTTGAAGACGGCGCCGCTGA	
pilT H	CGCGCTGATTCACGAGGCAG	
PilQ E	CTGCTCGTTCGACTTGGATC	
PilQ F	CACTGTTGACGCTGACC	
PilQ G	GCGCCCGCTCGTTGGTGCGC	
PilQ H	CACCTCCAACGACAGACGCG	
TsaP E	TGGAGCGGGTGGCCCGGT	
TsaP F	ACACGCCCCCTCGGTCCA	
TsaP G	TGAGAGCGCTCCCGGTGA	
TsaP H	TCACCGACTTCGTGGGCA	
aglQ E	TGCTTGGAGGACGGCCTGAC	
aglQ F	GAAGTCGTCTGACTTGTTGC	
aglQ G	GAATGGACACAGGTGGAGGC	
aglQ H	GCCGCGGACACCGACACCTG	
frzE E	GCGGCGGAGATGCGGCGTCT	
frzE F	CGCCCGCCACCATCGCCTGG	
frzE G	GCGTGGAGAGCGACCTCCAC	
frzE H	CCAGCGTGCCG	
frzS E	ACCTCTCCGGGTGCGCTGATT	
frzS F	CACGTTCGACCCGGACGCGAA	
frzS G	AGCGGTGGTGGAAGGCGTGG	
frzS H	TGCTCCAGCTCCAGGCTCTC	
sgmO E	GGACTTCGGCACCGCGAC	
sgmO F	CGCAGCATGAGGCCGAG	

sgmO G	CGTGACGAAGAGGTACAG	
sgmO H	CGCGGAACGAGTTGAG	
att_B_right	GGAATGATCGGACCAGCTGAA	
att_B_left	CGGCACACTGAGGCCACATA	
att_P_right	GCTTTCGCGACATGGAGGA	
att_P_left	GGGAAGCTCTGGGTACGAA	

Table 10 Plasmids used in this study

Plasmid	Description	Resistance	Reference
pBJ114	*galK* containing vector	Kanamycin	(Julien *et al.*, 2000)
pMem38	pET24b+, for overexpression of PilB-His10	Kanamycin	This work
pSL4	pUHE24-2, for overexpression of His6-PilT	Ampicillin	(Jakovljevic *et al.*, 2008)
PSC111	pET45, for overexpression of PilM-PilN(1-16)	Ampicillin	(Bischof *et al.*, 2016)
pMem39	pET24b+, for overexpression of $PilB_{(1-182)-His10}$	Kanamycin	This work
pMem23	pBJ114; for replacement of *pilB* by *pilB-mCherry* at the native site	Kanamycin	This work
pMem33	pBJ114; for replacement of *pilT* by *mCherry-pilT* at the native site	Kanamycin	This work
pMem34	pBJ114; for replacement of *pilO* by *pilO-sfGFP* at the native site	Kanamycin	This work
pMem35	pBJ114; for replacement of *pilP* by *pilP-sfGFP* at the native site	Kanamycin	This work
pMem36	pBJ114; for replacement of *tsaP* by *tsaP-mCherry* at the native site	Kanamycin	This work
pMAT162	pBJ114; for generation of in-frame deletion of *pilA*	Kanamycin	(Szadkowski *et al.*, 2019)
pAP19	pBJ114; for generation of in-frame deletion of *frzE*	Kanamycin	(Potapova *et al.*, 2020)
pBJ∆aglQ	pBJ114; for generation of in-frame deletion of *aglQ*	Kanamycin	(Sun *et al.*, 2011)
pAP37	pBJ114; for replacement of *pilQ* by *pilQ-sfGFP* at the native site	Kanamycin	(Potapova *et al.*, 2020)
pMAT336	pBJ114; for replacement of *pilM* by *mCherry-pilM* at the native site	Kanamycin	(Treuner-Lange *et al.*, 2020)
pMAT163	pBJ114; for generation of in-frame deletion of *pilB*	Kanamycin	(Treuner-Lange *et al.*, 2020)
pMAT353	pBJ114; for generation of in-frame deletion of *pilC*	Kanamycin	(Treuner-Lange *et al.*, 2020)
pIB20	pBJ114; for generation of in-frame deletion of *pilM*	Kanamycin	(Bulyha *et al.*, 2009)
pMAT150	pBJ114; for generation of in-frame deletion of *pilT*	Kanamycin	(Treuner-Lange *et al.*, 2020)

pMAT123	pBJ114; for generation of in-frame deletion of *pilQ*	Kanamycin	(Treuner-Lange *et al.*, 2020)
pIB21	pBJ114; for generation of in-frame deletion of *pilP*	Kanamycin	(Friedrich *et al.*, 2014)
pIMB1	pBJ114; for generation of in-frame deletion of *tsaP*	Kanamycin	(Siewering *et al.*, 2014)
pMAT170	pBJ114; for generation of in-frame deletion of *pilBT*	Kanamycin	Anke Treuner-Lange
pMem44	pBJ114; for generation of in-frame deletion of *sgmO*	Kanamycin	This work
pMem46	pSWU30, for integration of *Pnat-sgmO* in attB site	Tetracycline	This work
pMem48	pSWU30, for integration of *Pnat-sgmO-mCherry* in attB site	Tetracycline	This work
pMem49	pSWU30, for integration of *Pnat-mCherry-sgmO* in attB site	Tetracycline	This work
pMem52	pBJ114; for replacement of *pilM* by *pilM-pilN*	Kanamycin	This work

11.4.2 Construction of plasmids

pMem23: pMem23 (plasmid for replacement of *pilB* by *pilB-mCherry* at the native site) is a plasmid based on pBJ114. It contains a *pilB-mCherry* sequence that was amplified from pAP12 and *M. xanthus* gDNA using the primers pilB-mCA-EcoRI, pilB-mCB-overlay. The primer pair pilBmCC+ overlay, pilB-D-HindIII was used to amplify the downstream fragment of *pilB*. The fragments were used for an overlay PCR with the primers pilB-mCA-EcoRI, pilB-D-HindIII ligated into pBJ114 after restriction digestion with EcoRI and HindIII enzymes.

pMem33: pMem33 (plasmid for replacement of *pilT* by *mCherry-pilT* at the native site) is a plasmid based on pBJ114. It contains a *mCherry-pilT* sequence that was amplified from pAP87 using the primers PilT fw EcoRI (pAP87) and PilT rev HindIII (pAP87). The fragment was ligated into pBJ114 by restriction digestion with EcoRI and HindIII enzymes.

pMem34: pMem34 (plasmid for replacement of *pilO* by *pilO-sfGFP* at the native site) is a plasmid based on pBJ114. The primer pairs pilO up fw, pilO up rev pSC106 and pilP down fw fusion sfGFP, pilO down rev Hind III were used on *M. xanthus* gDNA to amplify up and downstream fragments of *pilO*. The primer pair pSC106 fw pilO up fusion, sfGFP rev pilO

down fusion were used to amplify *pilO-sfGFP* from pSC106 (Friedrich *et al.*, 2014). The primers were designed with respective overhangs. Overlay PCRs were performed to fuse upstream fragment, *pilO-sfGFP* fragment and downstream fragment. Finally, restriction digestion was performed and the DNA fragment was ligated with pBJ114.

pMem35: pMem35 (plasmid for replacement of *pilP* by *pilP-sfGFP* at the native site) is a plasmid based on pBJ114. The primer pairs pilP up fw (EcoR), pilP up rev- pSC102 fusion and p pilP down fw fusion sfGFP, pilP down rev (HindIII) were used on *M. xanthus* gDNA to amplify up and downstream fragments of *pilP*. The primer pair pSC102 fw –pilp up fusion, sfGFP rev pilP down fusion were used to amplify *pilP-sfGFP* from pSC102 (Friedrich *et al.*, 2014). The primers were designed with respective overhangs. Overlay PCRs were performed to fuse upstream fragment, *pilP-sfGFP* fragment and downstream fragment. Finally, restriction digestion was performed and the DNA fragment was ligated with pBJ114.

pMem36: pMem36 (plasmid for replacement of *tsaP* by *tsaP-mCherry* at the native site) is a plasmid based on pBJ114. The primer pair tsaP fw EcoRI, mch rev down tsap fusion was used to amplify *tsaP-mCherry* from pIMB3. Primers tsap down fw mch fusion and tsap down rev Hind III were used on gDNA of *M. xanthus* to amplify a downstream fragment of *tsaP*. A overlay PCR was performed using tsaP fw EcoRI and tsap down rev Hind III. The fragment was used for restriction digestion with EcoRI and HindIII and ligated into pBJ114.

pMem38: pMem38 (plasmid for overexpression of PilB-His10) is a plasmid based on pET24b+. The primer pair pilB fw NdeI, pilB rev His 10 Hind III was used to amplify *pilB-His10* from *M. xanthus* DK1622 gDNA. The fragment was used for restriction digestion with NdeI and Hind III and ligated into pET24b+.

pMem39: pMem39 (plasmid for overexpression of $PilB_{(1\text{-}182)\text{-}His10}$) is a plasmid based on pET24b+. The primer pair pilB fw NdeI, pilB Nterm rv His10 HindIII was used to amplify *pilB(1-182)-His10* from *M. xanthus* DK1622 gDNA. The fragment was used for restrictin digestion with NdeI and HindIII and ligated into pET24b+.

pMem44: pMem44 (plasmid for in-frame deletion of *sgmO*) is based on pBJ114. The primer pairs sgmO up fw EcoRI, sgmO up rev and sgmO down fw, sgmO down rev Hind III were used to ampplyfy upstream and downstream fragments of sgmO from *M. xanthus* DK1622 gDNA. An overlay PCR was performed using sgmO up fw EcoRI and sgmO down rev Hind III and the resulting fragment was used for restriction digestion with EcoRI and HindIII and ligated into pBJ114.

pMem46: pMem46 (plasmid for integration of *Pnat-sgmO* at attB site) is a plasmid based on pSWU30. The primer pairs Pnat mxan 4155 fw XbaI, Pnat mxan4155 rev ovh sgmO and sgmO fw ovh Pnat mxan4155, sgmO rev Hind III were used to amplify *Pnat* and *sgmO* from *M. xanthus* DK1622 gDNA. The resulting fragments were used for an overlay PCR with the primers Pnat mxan 4155 fw Xba, sgmO rev Hind III and restriction digestion with XbaI and HindIII were performed with the resulting fragment. Ligation into pSWU30 followed.

pMem48: pMem48 (plasmid for integration of *Pnat-sgmO-mCherry* at the attB site) is a plasmid based on pSWU30. The primer pairs Pnat mxan 4155 fw XbaI, SgmO rev ovh linker and mCherry fw ovh linker, mcherry rev HindIII were used to amplify *Pnat-sgmO* from pMem46 and *mCherry* from pMAT336. The resulting fragments were used for an overlay PCR with the primers Pnat mxan 4155 fw XbaI and mcherry rev HindIII. The resulting fragment was used for restriction digestion with XbaI and HindIII and ligated into pSWU30.

pMem49: pMem49 (plasmid for integration of Pnat-mCherry-sgmO at the attB site) is a plasmid based on pSWU30. The primer pairs Pnat mxan 4155 fw XbaI, pnat4155 rev ovh mcherry and mcherry fw ovh pnat4155, mCherry rev ovh linker and SgmO fw ovh linker, sgmO rev Hind III were used to amplify *Pnat* and *sgmO* from *M. xanthus* DK1622 gDNA and *mCherry* from pMAT336. The resulting fragments were used for a first overlay PCRs with the primers Pnat mxan 4155 fw XbaI and mCherry rev ovh linker. Then a second overlay PCR with the primers Pnat mxan 4155 fw XbaI and sgmO rev Hind III followed to

fuse all three fragments to one. The resulting fragment was used for restriction digestion with XbaI and HindIII and ligated into pSWU30.

pMem52:

pMem52 (plasmid to fuse *pilM* and *pilN* to each other) is a plasmid based on pBJ114. The primer pairs pMAT336 fw EcoRI, PilM rv no stop ovh PilN2 and pilN fw ovh PilM, PilN rev Hind III were used on *M. xanthus* DK1622 gDNA to amplify fragments of *pilM* and *pilN* and an overlay PCR was performed to fuse the two fragments to each other using the primers pMAT336 fw EcoRI and PilN rev Hind III. The fragment was used for restriction digestion and
ligated into pBJ114.

11.4.3 Generation of in-frame deletions and in-frame insertions

In-frame deletion were generated by two-step homologous recombination as described in (Shi *et al.*, 2008). *M. xanthus* cells were transformed with 1ng plasmid via electroporation and plated on CTT-agar containing kanamycin. The transformed plasmid pBJ114 contains an AB- and CD-fragment (approx. 1000 bp up- and downstream of the gene of interest), which allow homologous recombination into a specific genomic site. Colonies growing on kanamycin were tested for plasmid integration by colony PCR with primer pairs that bind up- or downstream of the AB or CD fragments and M13fw and M13rv primers that bind on the plasmid pBJ114 (e.g. E, M13 fw and F, M13rv). One clone from up and downstream plasmid integration was used for the second step of homologous recombination. Colonies were inoculated in 2 ml CTT media. The second homologous recombination can lead to the wildtype genotype or to the deletion or insertion of the gene of interest. The cells were plated on CTT-agar supplemented with 2,5% galactose. The galactose leads to negative selection pressure on pBJ114 containing cells, because the plasmid contains the gene *galK*, which leads to production of a toxic product (galactose-1-phosphate) for *M. xanthus*. After the second homologous recombination, colonies were streaked on CTT-kanamycin and CTT-gentamycin in the same pattern. Kanamycin-sensitive clones were tested for gene deletion or insertion via colony PCR with EF and GH-primer pairs. The EF pair binds up- and downstream of the gene of interest and the PCR product has a smaller size in case of a deletion or a bigger size in case of an integration. The GH primer pair binds in

the sequence of the gene of interest. A PCR should result in the same size as wildtype in case of a C- or N-terminal insertion or in no PCR product in case of a deletion.

11.4.4 DNA isolation from *E. coli* and *M. xanthus* cells

Plasmid DNA from *E. coli* was isolated using the NucleoSpin Plasmid QuickPure kit (Macherey-Nagel) following the manufacturer's instructions. Genomic DNA from *M. xanthus* cells was isolated using the MasterPure DNA preparation Kit (Epicentre) according to the manufacturer's protocol. The concentration and purity of the DNA was determined with the Nanodrop ND-1000 spectrophotometer. Crude genomic DNA of *M. xanthus* to do colony PCR was prepared by resuspending cells in 30 µl of ddH_2O, boiling for 5 min at 95°C and spinning down the cell debris at 13000 rpm for 1 min. 2 µl from the supernatant was used per PCR reaction.

11.4.5 Polymerase Chain Reaction (PCR)

Specific DNA fragments were amplified using Phusion High-Fidenlity DNA Polymerase (Thermo Scientific™, Darmstadt) or Q5® Hot Start High-Fidelity DNA Polymerase (New England Biolabs, Frankfurt am Main.) in a total reaction volume of 50µl. Colony PCRs were performed using 5 PRIME MasterMix in a total volume of 25µl. Compositions of the corresponding reactions are listed in Table 11.

Table 11 PCR mix

Component	Volume	Final concentration
PCR with Phusion High-Fidelity DNA Polymerase		
Template DNA	1 µl	~50 ng
10 µM primer (each)	2.5 µl	1.25 µM
10 mM dNTPs	1µl	0.2 mM
5x Phsuion GC buffer	10 µl	1x
5x enhancer	10 µl	1x
Phusion DNA polymerase	0.5 µl	1 unit/ 50 µl reaction
ddH_2O	To 50 µl	
PCR with Q5® Hot Start High-Fidelity DNA Polymerase		
Template DNA	1 µl	~50 ng
10 µM primer (each)	2.5 µl	1.25 µM

10 mM dNTPs	1µl	0.2 mM
5x Q5 reaction buffer	10 µl	1x
5x Q5 High GC Enhancer	10 µl	1x
Q5 DNA polymerase	0.5 µl	1 unit/ 50 µl reaction
ddH_2O	to 50 µl	
Colony PCR		
Crude genomic DNA	2µl	~200 ng
10 µM primer (each)	0.5 µl	0.25 µM
5 PRIME Master Mix	12.5 µl	
DMSO	2 µl	8% (v/v)
ddH_2O	to 25µl	

The PCR programs used in this study for DNA amplification are listen in Table 12. Primer annealing temperatures were adjusted depending on the GC content of the primers and the elongation time was chosen depending on the DNA fragment size to be amplified. PCR programs used in this work are listed in Table 12.

Table 12 PCR programs

Step	Temperature	Time	Repeats
Standard/ Colony PCR			
Initial denaturation	95°C	5 min	
Denaturation	95°C	30 s	35x
Primer annealing	5°C below melting temperature	30 s	
Elongation	72°C	1 min / kb – 5 PRIME Master Mix 30 s/kb Phusion/Q5 DNA Polymerase	
Final Elongation	72°C	10 min	
Hold	4°C	∞	
Touch Down PCR			
Initial denaturation	95°C	5 min	
Denaturation	95°C	30 s	10x

Primer annealing	65°C	30 s	
Elongation	72°C	1 min/kb or 30 s/kb	
Denaturation	95°C	30 s	10x
Primer annealing	60°C	30 s	
Elongation	72°C	1 min/kb or 30 s/kb	
Denaturation	95°C	30 s	10x
Primer annealing	55°C	30 s	
Elongation	72°C	1 min/kb or 30 s/kb	
Final Elongation	72°C	10 min	
Hold	4°C	∞	

11.4.6 Agarose gel electrophoresis

Nucleic acid fragments were separated by size via agarose gel electrophoresis. DNA samples were mixed with 6x loading buffer (New England Biolabs, Frankfurt am Main) and separated on 1% (v/v) agarose with 0.01% ethidium bromide or 0.005% gel red (Biotium, USA) in 1 x **T**RIS-**B**orat-**E**DTA (TBE) buffer (Thermo Scientific, Dreieich). Electrophoresis was performed at 100-140 V. As size standard, the 2-log DNA ladder (New England Biolabs, Frankfurt am Main) was used. Agarose gels were documented with the E-BOX VX2 imaging system (PeqLab, Erlangen).

11.4.7 Restriction digestion and ligation of DNA fragments and vector backbones

Vector backbones were digested with restriction enzymes (New England Biolabs, Frankfurt am Main) to make them applicable to ligation. 2–3 µg of plasmid DNA was digested for 3 h at 37°C in a total volume of 50 µl. Subsequently, 6 µl of 10x Antarctic phosphatase buffer, 3 µl of H2O and 1 µl Antarctic Phosphatase (New England Biolabs, Frankfurt am Main) were added to the reaction and incubated another hour at 37°C to perform dephosphorylation reaction. The mixture was applied to an agarose gel electrophoresis and DNA fragments of the correct size were excised from the gel and purified with the NucleoSpin® Gel and PCR Clean-up kit (Macherey & Nagel, Düren) according to the manufacturer´s protocol. PCR fragments were digested with restriction enzymes (New England Biolabs, Frankfurt am Main) according to the manufacturer´s protocol for 3 h at 37°C in a total volume of 50 µl. Afterward, the digested DNA fragments

were purified using NucleoSpin® Gel and PCR Clean-up kit (Macherey & Nagel, Düren). DNA fragments and plasmids were ligated with the T4 DNA Ligase (New England Biolabs, Frankfurt am Main) in a reaction volume of 20 µl according to the manufacturer´s instructions. The reaction was incubated overnight at room temperature. PCR fragments were ligated into vectors in the presence of 3 fold excess of insert DNA. 10µl of the mixture was transformed into *E. coli* NEB Turbo cells.

11.4.8 Preparation and transformation of chemically competent *E. coli* cells

E. coli overnight cultures were used to inoculate 200 ml LB-medium. The cells were grown to an OD_{600} of 0.5-0.7 and harvested at 4700rpm for 10 min at 4°C. The supernatant was discarded and the pellet resuspended in 100 ml ice-cold TFB I buffer (30 mM potassium acetate, 10 mM $CaCl_2$, 50 mM $MnCl_2$, 100 mM RbCl, 15% (v/v) glycerol adjusted to pH=6.5 with acetic acid). As described before, the cells were pelleted once again and resuspended in 4 ml TFB II buffer (10 mm MOPS pH6.5, 75 mM $CaCl_2$, 100 mM RbCl, 15% (v/v) glycerol). The cells were incubated in TFB II for 1 h at 4°C. After incubation, 50 µl aliquots in reaction tubes were frozen in liquid nitrogen and stored at -80°C until used.

For transformation, the aliquots were thawed on ice and 10 µl of ligation mixture or 1µl of plasmid was added to the cells. After 10 minutes of incubation on ice, the cells were treated with a heat shock at 42°C for 90 s and incubated on ice for an additional 3 min. 1 ml of LB-medium was added to the cells and shaken for 1 h at 37°C. Later, the cells were pelleted for 2 min at 13000 rpm. The supernatant was discarded and the cells resuspended in 100µl of LB-medium. The cell suspension was plated on LB-agar plates containing corresponding antibiotics and incubated at 37°C overnight. Colonies were checked for the presence of the plasmid by PCR or plasmid preparation and restriction digestion.

11.4.9 Preparation and transformation of electrocompetent *M. xanthus* cells

2 ml of a *M. xanthus* overnight liquid culture was pelleted for 10 minutes at 4700 rpm and washed with 1 ml of sterile ddH_2O three times. After the final wash, the supernatant was discarded and the cells were resuspended in 50 µl ddH_2O. The cell suspension was transferred into an electroporation-cuvette and mixed with 1 µg plasmid-DNA. The mixture was pulsed with 650 V, 400Ω and 25 µF in a ’GenePulser X-Cell’ (BioRad, München). 1 ml of CTT-medium was added immediately after electroporation. The cell suspension was

transferred to a 25 ml Erlenmeyerflask and 1 ml of CTT was added. After 6 h or 12 h of regeneration the cells were pelleted for 10 min at 4700 rpm, resuspended in 100 µl of CTT and plated onto CTT-agar plates with corresponding antibiotics in concentrations according to Table 5. The plates were incubated at 32°C in the dark for up to 10 days. Colonies were tested for integration of the plasmid by PCR.

11.4.10 Operon mapping

M. xanthus DK1622 RNA was purified and cleaned up with Monarch Total RNA Miniprep and Monarch RNA Cleanup Kits (New England Biolabs (NEB) according to manufacturers protocol. To test if the primer combinations can be used to amplify the intergenic regions, the primers were used for PCRs on gDNA of *M. xanthus* DK1622. To transcribe RNA to cDNA the Applied Biosystems™ High-Capacity cDNA Reverse Transcription Kit (Waltham, USA) was used according to manufacturer's protocol. Then PCRs with Reverse Transcriptase and without (control) were run with the same Master mix as used for the gDNA control. The PCR were run as described in 11.4.511.4.5 with an annealing temperature of 60°C.

For operon mapping of *sgmO* following primer pairs were used:

Table 13 Primer pairs used for operon mapping

intergenic regions of	**Primer 1 (forward)**	**Primer2 (reverse)**
frzS, sgmO	AGCGGTGGTGGAAGGCGTGG	TCATCCGCGAGACGAACAAG
sgmO, brgE	GGGTCGAACGTGAGCATGTA	CATGTCATCGGGCGCAACAC
brgE, birA	GAAGTACCGCTCGCTCATCTT	GGAGGAGTGGTTGGACCTCTA
birA, mxan_4153 (putative lipoprotein)	CTCGAGCGAGGTGAGCC	GGTGAACACGATGACGTTCG
mxan_4153, mxan_4154	GGGCGTCTCACAGGAGTCT	CATCGACCGGCTCAAGGAAG

(conserve domain protein)		
mxan_4154, mxan_4155 (hypothetical protein)	CGCGCCTTTCTGCTCGAAAC	GACGACGTCTTCTGGATTCGT
mxan_4155, mxan_4156 (conserved domain protein)	CTGCTGGATGGACTTCTCGG	CAGCGACAGCCAGACCTC

11.5 Biochemical methods

11.5.1 SDS Polyacrylamide Gel Electrophoresis (SDS-PAGE)

Under denaturing conditions, proteins were separated according to their molecular mass by SDS-PAGE (Laemmli, 1970). To denature proteins, protein samples were prepared as follows:

Cells of a 2ml *M. xanthus* overnight liquid culture were harvested by centrifugation at 13000xg for 2 minutes and the supernatant was removed. The cell pellet was resuspended in 1X SDS-loading buffer (4x concentration= 40% (v/v) glycerin; 200 mM Tris-HCl pH 6,8; 8 mM EDTA, 8% (w/v) SDS, 0,4 M DTT, 0,8% (w/v) bromophenolblue, 8% Tween 20, 40mM 3-(N,N dimethyltetradecylammonio)propanesulfonate). The cells were concentrated to an optical density of OD_{550}=7 and the sample was heated for 10 minutes at 95°C. If required, the sample was stored at -20°C and heated again before usage for SDS-PAGE.

The samples were loaded on precast Any kD™ Mini-PROTEAN® TGX™ Precast Protein Gels (BioRad, München) and gel electrophoresis was performed in Bio-Rad electrophoresis chambers at 130V in 1x Tris/Glycine SDS (TGS) running buffer (BioRad,

München). The PageRuler Pre-stained Ladder from Fermentas was used to determine protein sizes by comparison.

11.5.2 Determination of protein concentration by Bradford

To determine the total amount of protein in samples used for Western-blot analysis, BradfordMX (expedeon, San Diego) was used according to the manufacturer's recommendations. Briefly, 1.5 ml of BradfordMX reagent was mixed with 30 µl of a 1:25 diluted protein sample and incubated 5 min at room temperature. In the same way, a standard curve was created using known concentrations of BSA (bovine serum albumin), showing the protein concentration versus the measured absorbance. The absorbance was measured using an Ultrospec 2100 pro spectrophotometer (GE Healthcare Europe GmbH, Freiburg) at 495 nm. Protein concentrations were determined based on the linear slope of the standard curve.

11.5.3 Immunoblot analysis

Immunoblot analysis was performed to detect proteins of interest with specific antibodies. First, proteins from cell lysates were separated by SDS-PAGE as described in 11.5.1. For this purpose, equal amounts of proteins were loaded per lane. Proteins were transferred to a 0.2 µm thick nitrocellulose membrane using the semi-dry Trans-Blot TurboTM® Transfer System (BioRad, München) with a transfer buffer containing 300 mM glycine, 300 mM Tris and 0.05% SDS with a pH= 9. The transfer was performed using 1.3 A, 25 V for 7 min. Membranes were transferred into a clean plastic container and blocked for 1 h in 5% dried non-fat milk powder (w/v) in 1 x TBS (50 mM Tris-HCl pH 7.5; 150 mM NaCl) shaking at room temperature. After blocking the membrane, the primary antibody was added to the blot in 2% dried non-fat milk powder (w/v) in 1 x TBS at the corresponding dilution (Table 14) and incubated overnight, shaking at 4°C. After washing 3 times with 1x TBST (50 mM Tris-HCl pH 7.5; 150 mM NaCl; 0.1% Tween-20 (v/v)) the secondary antibody was applied. Either anti-rabbit immunoglobulin G peroxidase conjugate (Sigma) in a dilution of 1:15000 or secondary antimouse immunoglobulin G, horseradish peroxidase lined whole antibody (GE Healthcare) in a dilution 1:2000 in 2% dried non-fat milk in 1x TBS.applied for 1h at 4 °C shaking.

Before detecting the signals, the membrane was washed again with 1x TBST. Then, the blot was developed with the Luminata Western HRP Substrate (Millipore Merck, Schwalbach) and visualized with the luminescent image analyzer LAS-4000 (Fujifilm, Düsseldorf).

Table 14 Antibodies used for immunoblotting

Antibody	Dilution
α-PilQ	1:5000
α-TsaP	1:2000
α-PilP	1:2000
α-PilO	1:2000
α-PilM	1:2000
α-PilN	1:3000
α-PilC	1:5000
α-PilB	1:2000
α-PilT	1:2000
α-FrzE	1:2000
α-GFP	1:2000
α-mCherry	1:2500

11.5.4 Quantitative immunoblot analysis

To estimate the number of molecules of mCherry-PilM, PilB-mCherry, mCherry-PilT in M. xanthus cells, quantitative immunoblot analyses were performed as described in (Schumacher *et al.*, 2017). For this, 2 ml *M. xanthus* cultures with the corresponding strains were used to make cell lysates for immunoblot analysis as described above (11.5.3). The cell lysates as well as samples with a known amout of the corresponding proteins were used for SDS-PAGE and immunoblot analysis was performed with the corresponding antibodies as described before (11.5.1; 11.5.3). To determine the number of molecules signal intensities of the bands were measured with Fiji and compared against a standard curve generated from known amounts of proteins on the same immunobot.

11.5.5 PilB-His10 and His6-PilT purification

For overexpression of PilB-His10, *E.coli* Rosetta DE3 cells were transformed with pMem38, for overexpression of His6-PilT *E.coli* Rosetta DE3 cells were transformed with pSL4. Kanamycin-resistant cells were grown in 10ml LB medium supplemented with 1 %

glucose at 37°C overnight. The overnight culture was used to inoculate 2 l LB medium and cells were grown to an OD_{600}=0.5 at 37°C. Protein expression was induced by adding 0.1 M IPTG to the cells, and the culture was incubated at 18°C overnight. Cells were harvested at 4700g for 20 min and resuspended in lysis buffer (50 mM NaH_2PO_4, 300 mM NaCl, 10 mM imidazole, pH 8.0 with cOmplete protease inhibitor (Roche, Basel) and 10 µg/ml DNase I (Thermo Fisher Scientific)). The cell suspension was sonicated for 30 min (30sec on, 30sec off) at (50 W/75%). The cell lysate was centrifuged for 20 min at 20000 g at 4°C and the pellet was resuspended in buffer (100 mM NaH_2PO_4, 10 mM Tris, 8 M Urea, 0.05% Tween-20, pH 6.3 adjusted with NaOH) and incubated at RT for 20 min. The suspension was centrifuged for 20 min at 13000 g at 4 °C. The supernatant was incubated with washed Protino®Ni-NTA agarose for 1 h at 4°C. The suspension was loaded to a gravity flow column and washed with buffer A. Denatured protein was eluted with 8 ml buffer B (100 mM NaH_2PO_4, 10 mM Tris, 8 M Urea, 0.05% Tween-20, pH 5.9 adjusted with NaOH) and 12 ml buffer C (100 mM NaH_2PO_4, 10 mM Tris, 8 M Urea, 0.05% Tween-20, pH 4.5 adjusted with NaOH)

11.5.6 Purification of His6-PilM-PilN(1-16)

For overexpression of His6-PilM-PilN(1-16), *E.coli* Rosetta DE3 cells were transformed with pSC111. Ampicillin resistant cells were grown in 10ml LB medium supplemented with 1% glucose at 37°C overnight. The overnight culture was used to inoculate 2 l LB medium and cells were grown to an OD_{600}=0.5 at 37°C. Protein expression was induced by adding 0.5 mM IPTG to the cells and the culture was incubated at 18°C overnight. Cells were harvested at 4700g for 20 min and resuspended in lysis buffer (50 mM Tris/HCl, pH 7.5, 100 mM NaCl, 10 mM imidazole) containing cOmplete protease inhibitor mixture (Roche Applied Science) and 10 µg/ml DNase I (Thermo Fisher Scientific). The suspension was sonicated for 30 min (30 sec on, 30 sec off) and centrifuged for 30 min at 40000 g at 4°C.

The supernatant was incubated with washed Protino®Ni-NTA agarose for 1 h at 4°C. The suspension was loaded to a gravity flow column and washed with buffer A (50 mM Tris/HCl, pH 7.5, 100 mM NaCl, 10 mM imidazole) according to the manufacturer's protocol. Protein was eluted using buffer B (50 mM Tris/HCl, pH 7.5, 100 mM NaCl, 250 mM imidazole).

12 References

Abendroth, J., Mitchell, D.D., Korotkov, K.V., Johnson, T.L., Kreger, A., Sandkvist, M., and Hol, W.G. (2009) The three-dimensional structure of the cytoplasmic domains of EpsF from the type 2 secretion system of *Vibrio cholerae*. *J Struct Biol* **166**: 303-315.

Aizawa, S.I., and Kubori, T. (1998) Bacterial flagellation and cell division. *Genes Cells* **3**: 625-634.

Arnold, J.W., and Shimkets, L.J. (1988) Cell surface properties correlated with cohesion in *Myxococcus xanthus*. *J Bacteriol* **170**: 5771-5777.

Arts, J., de Groot, A., Ball, G., Durand, E., Khattabi, M.E., Filloux, A., Tommassen, J., and Koster, M. (2007a) Interaction domains in the *Pseudomonas aeruginosa* type II secretory apparatus component XcpS (GspF). *Microbiology (Reading)* **153**: 1582-1592.

Arts, J., van Boxtel, R., Filloux, A., Tommassen, J., and Koster, M. (2007b) Export of the pseudopilin XcpT of the *Pseudomonas aeruginosa* type II secretion system via the signal recognition particle-Sec pathway. *J Bacteriol* **189**: 2069-2076.

Ayers, M., Howell, P.L., and Burrows, L.L. (2010) Architecture of the type II secretion and type IV pilus machineries. *Future microbiology* **5**: 1203-1218.

Ayers, M., Sampaleanu, L., Tammam, S., Koo, J., Harvey, H., Howell, P., and Burrows, L. (2009) PilM/N/O/P proteins form an inner membrane complex that affects the stability of the *Pseudomonas aeruginosa* type IV pilus secretin. *J Mol Biol* **394**: 128-142.

Bai, F., Morimoto, Y.V., Yoshimura, S.D., Hara, N., Kami-Ike, N., Namba, K., and Minamino, T. (2014) Assembly dynamics and the roles of FliI ATPase of the bacterial flagellar export apparatus. *Sci Rep* **4**: 6528.

Balasingham, S.V., Collins, R.F., Assalkhou, R., Homberset, H.v., Frye, S.A., Derrick, J.P., and Tønjum, T. (2007) Interactions between the lipoprotein PilP and the secretin PilQ in *Neisseria meningitidis*. *J Bacteriol* **189**: 5716-5727.

Barker, D.F., and Campbell, A.M. (1981) The birA gene of *Escherichia coli* encodes a biotin holoenzyme synthetase. *J Mol Biol* **146**: 451-467.

Beeby, M. (2019) Evolution of a family of molecular Rube Goldberg contraptions. *PLoS Biology* **17**: e3000405.

Behmlander, R.M., and Dworkin, M. (1994) Biochemical and structural analyses of the extracellular matrix fibrils of *Myxococcus xanthus*. *J Bacteriol* **176**: 6295-6303.

Bellenger, K., Ma, X., Shi, W., and Yang, Z. (2002) A CheW homologue is required for *Myxococcus xanthus* fruiting body development, social gliding motility, and fibril biogenesis. *Journal of Bacteriology* **184**: 5654-5660.

Berg, H.C. (1974) Dynamic properties of bacterial flagellar motors. *Nature* **249**: 77-79.

Berleman, J.E., Chumley, T., Cheung, P., and Kirby, J.R. (2006) Rippling is a predatory behavior in *Myxococcus xanthus*. *J Bacteriol* **188**: 5888-5895.

Berleman, J.E., Vicente, J.J., Davis, A.E., Jiang, S.Y., Seo, Y.-E., and Zusman, D.R. (2011) FrzS regulates social motility in *Myxococcus xanthus* by controlling exopolysaccharide production. *PloS one* **6**: e23920.

Berleman, J.E., Zemla, M., Remis, J.P., Liu, H., Davis, A.E., Worth, A.N., West, Z., Zhang, A., Park, H., Bosneaga, E., van Leer, B., Tsai, W., Zusman, D.R., and Auer, M.

(2016) Exopolysaccharide microchannels direct bacterial motility and organize multicellular behavior. *ISME J* **10**: 2620-2632.

Berry, J.L., and Pelicic, V. (2015) Exceptionally widespread nanomachines composed of type IV pilins: the prokaryotic Swiss Army knives. *FEMS Microbiol Rev* **39**: 134-154.

Berry, J.L., Phelan, M.M., Collins, R.F., Adomavicius, T., Tonjum, T., Frye, S.A., Bird, L., Owens, R., Ford, R.C., Lian, L.Y., and Derrick, J.P. (2012) Structure and assembly of a trans-periplasmic channel for type IV pili in *Neisseria meningitidis*. *PLoS Pathog* **8**: e1002923.

Bischof, L.F., Friedrich, C., Harms, A., Søgaard-Andersen, L., and van der Does, C. (2016) The Type IV Pilus Assembly ATPase PilB of *Myxococcus xanthus* Interacts with the Inner Membrane Platform Protein PilC and the Nucleotide-binding Protein PilM. *J Biol Chem* **291**: 6946-6957.

Black, W., Wang, L., Jing, X., Saldana, R., Li, F., Scharf, B., Schubot, F., and Yang, Z., (2017) The type IV pilus assembly ATPase PilB functions as a signaling protein to regulate exopolysaccharide production in *Myxococcus xanthus*. Sci Rep 7: 7263. In., pp.

Black, W.P., Schubot, F.D., Li, Z., and Yang, Z. (2010) Phosphorylation and dephosphorylation among Dif chemosensory proteins essential for exopolysaccharide regulation in *Myxococcus xanthus*. *Journal of bacteriology* **192**: 4267-4274.

Black, W.P., Wang, L., Davis, M.Y., and Yang, Z. (2015) The orphan response regulator EpsW is a substrate of the DifE kinase and it regulates exopolysaccharide in *Myxococcus xanthus*. *Scientific reports* **5**: 1-9.

Black, W.P., Xu, Q., and Yang, Z. (2006) Type IV pili function upstream of the Dif chemotaxis pathway in *Myxococcus xanthus* EPS regulation. *Mol Microbiol* **61**: 447-456.

Black, W.P., and Yang, Z. (2004) *Myxococcus xanthus* chemotaxis homologs DifD and DifG negatively regulate fibril polysaccharide production. *J Bacteriol* **186**: 1001-1008.

Blackhart, B.D., and Zusman, D.R. (1985) "Frizzy" genes of *Myxococcus xanthus* are involved in control of frequency of reversal of gliding motility. *Proc Natl Acad Sci U S A* **82**: 8767-8770.

Blank, T.E., and Donnenberg, M.S. (2001) Novel topology of BfpE, a cytoplasmic membrane protein required for type IV fimbrial biogenesis in enteropathogenic *Escherichia coli*. *J Bacteriol* **183**: 4435-4450.

Bowden, M.G., and Kaplan, H.B. (1998) The *Myxococcus xanthus* lipopolysaccharide O-antigen is required for social motility and multicellular development. *Mol Microbiol* **30**: 275-284.

Bretl, D.J., Müller, S., Ladd, K.M., Atkinson, S.N., and Kirby, J.R. (2016) Type IV-pili dependent motility is co-regulated by PilSR and PilS2R2 two-component systems via distinct pathways in *Myxococcus xanthus*. *Molecular microbiology* **102**: 37-53.

Buist, G., Steen, A., Kok, J., and Kuipers, O.P. (2008) LysM, a widely distributed protein motif for binding to (peptido)glycans. *Mol Microbiol* **68**: 838-847.

Bulyha, I., Lindow, S., Lin, L., Bolte, K., Wuichet, K., Kahnt, J., van der Does, C., Thanbichler, M., and Søgaard-Andersen, L. (2013) Two small GTPases act in concert with the bactofilin cytoskeleton to regulate dynamic bacterial cell polarity. *Dev Cell* **25**: 119-131.

Bulyha, I., Schmidt, C., Lenz, P., Jakovljevic, V., Hone, A., Maier, B., Hoppert, M., and Sogaard-Andersen, L. (2009a) Regulation of the type IV pili molecular machine by dynamic localization of two motor proteins. *Mol Microbiol* **74**: 691-706.

Burchard, R.P. (1981) Gliding motility of prokaryotes: ultrastructure, physiology, and genetics. *Annu Rev Microbiol* **35**: 497-529.

Burchard, R.P. (1982) Trail following by gliding bacteria. *J Bacteriol* **152**: 495-501.

Burkhardt, J., Vonck, J., and Averhoff, B. (2011) Structure and function of PilQ, a secretin of the DNA transporter from the thermophilic bacterium *Thermus thermophilus* HB27. *J Biol Chem* **286**: 9977-9984.

Bustamante, V.H., Martínez-Flores, I., Vlamakis, H.C., and Zusman, D.R. (2004) Analysis of the Frz signal transduction system of *Myxococcus xanthus* shows the importance of the conserved C-terminal region of the cytoplasmic chemoreceptor FrzCD in sensing signals. *Mol Microbiol* **53**: 1501-1513.

Carballido-Lopez, R. (2006) The bacterial actin-like cytoskeleton. *Microbiol Mol Biol Rev* **70**: 888-909.

Carbonnelle, E., Helaine, S., Nassif, X., and Pelicic, V. (2006) A systematic genetic analysis in *Neisseria meningitidis* defines the Pil proteins required for assembly, functionality, stabilization and export of type IV pili. *Mol Microbiol* **61**: 1510-1522.

Carbonnelle, E., Hélaine, S., Prouvensier, L., Nassif, X., and Pelicic, V. (2005) Type IV pilus biogenesis in *Neisseria meningitidis*: PilW is involved in a step occurring after pilus assembly, essential for fibre stability and function. *Mol Microbiol* **55**: 54-64.

Carreira, L.A.M., Szadkowski, D., Lometto, S., Hochberg, G.K.A., and Søgaard-Andersen, L. (2023) Molecular basis and design principles of switchable front-rear polarity and directional migration in *Myxococcus xanthus*. *Nat Commun* **14**: 4056.

Carreira, L.A.M., Szadkowski, D., Muller, F., and Søgaard-Andersen, L. (2022) Spatiotemporal regulation of switching front-rear cell polarity. *Curr Opin Cell Biol* **76**: 102076.

Carter, T., Buensuceso, R.N., Tammam, S., Lamers, R.P., Harvey, H., Howell, P.L., and Burrows, L.L. (2017) The type IVa pilus machinery is recruited to sites of future cell division. *MBio* **8**: e02103-02116.

Chakravartty, V., and Cronan, J.E. (2013) The wing of a winged helix-turn-helix transcription factor organizes the active site of BirA, a bifunctional repressor/ligase. *J Biol Chem* **288**: 36029-36039.

Chang, Y.W., Rettberg, L.A., Treuner-Lange, A., Iwasa, J., Sogaard-Andersen, L., and Jensen, G.J. (2016) Architecture of the type IVa pilus machine. *Science* **351**: aad2001.

Chernyatina, A.A., and Low, H.H. (2019) Core architecture of a bacterial type II secretion system. *Nat Commun* **10**: 5437.

Chlebek, J.L., Denise, R., Craig, L., and Dalia, A.B. (2021) Motor-independent retraction of type IV pili is governed by an inherent property of the pilus filament. *Proc Natl Acad Sci U S A* **118**: e2102780118.

Clausen, M., Jakovljevic, V., Søgaard-Andersen, L., and Maier, B. (2009a) High-force generation is a conserved property of type IV pilus systems. *J Bacteriol* **191**: 4633-4638.

Clausen, M., Jakovljevic, V., Søgaard-Andersen, L., and Maier, B. (2009b) High-force generation is a conserved property of type IV pilus systems. *J Bacteriol* **191**: 4633-4638.

Collins, R.F., Saleem, M., and Derrick, J.P. (2007) Purification and three-dimensional electron microscopy structure of the *Neisseria meningitidis* type IV pilus biogenesis protein PilG. *J Bacteriol* **189**: 6389-6396.

Cornelis, G.R. (2006) The type III secretion injectisome. *Nat Rev Microbiol* **4**: 811.

Craig, L., Forest, K.T., and Maier, B. (2019) Type IV pili: dynamics, biophysics and functional consequences. *Nat Rev Microbiol* **17**: 429-440.

Craig, L., and Li, J. (2008) Type IV pili: paradoxes in form and function. *Curr Opin Struc Biol* **18**: 267-277.

Craig, L., Taylor, R.K., Pique, M.E., Adair, B.D., Arvai, A.S., Singh, M., Lloyd, S.J., Shin, D.S., Getzoff, E.D., and Yeager, M. (2003) Type IV pilin structure and assembly: X-ray and EM analyses of *Vibrio cholerae* toxin-coregulated pilus and Pseudomonas aeruginosa PAK pilin. *Molecular cell* **11**: 1139-1150.

D'Imprima, E., Salzer, R., Bhaskara, R.M., Sanchez, R., Rose, I., Kirchner, L., Hummer, G., Kuhlbrandt, W., Vonck, J., and Averhoff, B. (2017) Cryo-EM structure of the bifunctional secretin complex of *Thermus thermophilus*. *Elife* **6**.

Daefler, S., Russel, M., and Model, P. (1997) Module swaps between related translocator proteins pIVf1, pIVIke and PulD: identification of a specificity domain. *J Mol Biol* **266**: 978-992.

Dana, J.R., and Shimkets, L.J. (1993) Regulation of cohesion-dependent cell interactions in *Myxococcus xanthus*. *J Bacteriol* **175**: 3636-3647.

Dazzoni, R., Li, Y., Lopez-Castilla, A., Brier, S., Mechaly, A., Cordier, F., Haouz, A., Nilges, M., Francetic, O., Bardiaux, B., and Izadi-Pruneyre, N. (2023) Structure and dynamic association of an assembly platform subcomplex of the bacterial type II secretion system. *Structure* **31**: 152-165 e157.

Delalez, N.J., Berry, R.M., and Armitage, J.P. (2014) Stoichiometry and turnover of the bacterial flagellar switch protein FliN. *mBio* **5**: e01216-01214.

Delalez, N.J., Wadhams, G.H., Rosser, G., Xue, Q., Brown, M.T., Dobbie, I.M., Berry, R.M., Leake, M.C., and Armitage, J.P. (2010) Signal-dependent turnover of the bacterial flagellar switch protein FliM. *Proc Natl Acad Sci U S A* **107**: 11347-11351.

Deng, W., Marshall, N.C., Rowland, J.L., McCoy, J.M., Worrall, L.J., Santos, A.S., Strynadka, N.C.J., and Finlay, B.B. (2017) Assembly, structure, function and regulation of type III secretion systems. *Nat Rev Microbiol* **15**: 323-337.

Denise, R., Abby, S.S., and Rocha, E.P. (2019) Diversification of the type IV filament superfamily into machines for adhesion, protein secretion, DNA uptake, and motility. *PLoS biology* **17**: e3000390.

Denman, A. (1983) Molecular cloning: a laboratory manual. *Immunology* **49**: 411.

Diepold, A., and Armitage, J.P. (2015) Type III secretion systems: the bacterial flagellum and the injectisome. *Philos Trans R Soc Lond B Biol Sci* **370**.

Diepold, A., Kudryashev, M., Delalez, N.J., Berry, R.M., and Armitage, J.P. (2015) Composition, formation, and regulation of the cytosolic c-ring, a dynamic component of the type III secretion injectisome. *PLoS Biol* **13**: e1002039.

Diepold, A., Sezgin, E., Huseyin, M., Mortimer, T., Eggeling, C., and Armitage, J.P. (2017) A dynamic and adaptive network of cytosolic interactions governs protein export by the T3SS injectisome. *Nat Commun* **8**: 15940.

Ducret, A., Fleuchot, B., Bergam, P., and Mignot, T. (2013a) Direct live imaging of cell-cell protein transfer by transient outer membrane fusion in *Myxococcus xanthus*. *Elife* **2**: e00868.

Ducret, A., Théodoly, O., and Mignot, T. (2013b) Single cell microfluidic studies of bacterial motility. *Bacterial Cell Surfaces: Methods and Protocols*: 97-107.

Ducret, A., Valignat, M.P., Mouhamar, F., Mignot, T., and Theodoly, O. (2012) Wet-surface-enhanced ellipsometric contrast microscopy identifies slime as a major adhesion factor during bacterial surface motility. *Proc Natl Acad Sci U S A* **109**: 10036-10041.

Dworkin, M. (1996) Recent advances in the social and developmental biology of the myxobacteria. *Microbiol Rev* **60**: 70-102.

Dye, K.J., Salar, S., Allen, U., Smith, W., and Yang, Z. (2023) *Myxococcus xanthus* PilB interacts with c-di-GMP and modulates motility and biofilm formation. *J Bacteriol*: e0022123.

Dye, K.J., and Yang, Z. (2020) Cyclic-di-GMP and ADP bind to separate domains of PilB as mutual allosteric effectors. *Biochem J* **477**: 213-226.

Ellison, C.K., Dalia, T.N., Vidal Ceballos, A., Wang, J.C., Biais, N., Brun, Y.V., and Dalia, A.B. (2018) Retraction of DNA-bound type IV competence pili initiates DNA uptake during natural transformation in *Vibrio cholerae*. *Nat Microbiol* **3**: 773-780.

Ellison, C.K., Kan, J., Chlebek, J.L., Hummels, K.R., Panis, G., Viollier, P.H., Biais, N., Dalia, A.B., and Brun, Y.V. (2019) A bifunctional ATPase drives tad pilus extension and retraction. *Sci Adv* **5**: eaay2591.

Ellison, C.K., Kan, J., Dillard, R.S., Kysela, D.T., Ducret, A., Berne, C., Hampton, C.M., Ke, Z., Wright, E.R., Biais, N., Dalia, A.B., and Brun, Y.V. (2017) Obstruction of pilus retraction stimulates bacterial surface sensing. *Science* **358**: 535-538.

Francetic, O., Buddelmeijer, N., Lewenza, S., Kumamoto, C.A., and Pugsley, A.P. (2007) Signal recognition particle-dependent inner membrane targeting of the PulG Pseudopilin component of a type II secretion system. *J Bacteriol* **189**: 1783-1793.

Friedrich, C., Bulyha, I., and Sogaard-Andersen, L. (2014) Outside-in assembly pathway of the type IV pilus system in *Myxococcus xanthus*. *J Bacteriol* **196**: 378-390.

Fukuoka, H., Inoue, Y., Terasawa, S., Takahashi, H., and Ishijima, A. (2010) Exchange of rotor components in functioning bacterial flagellar motor. *Biochem Biophys Res Commun* **394**: 130-135.

Galan, J.E., and Collmer, A. (1999) Type III secretion machines: bacterial devices for protein delivery into host cells. *Science* **284**: 1322-1328.

Galan, J.E., and Wolf-Watz, H. (2006) Protein delivery into eukaryotic cells by type III secretion machines. *Nature* **444**: 567-573.

Georgiadou, M., Castagnini, M., Karimova, G., Ladant, D., and Pelicic, V. (2012) Large-scale study of the interactions between proteins involved in type IV pilus biology in *Neisseria meningitidis*: characterization of a subcomplex involved in pilus assembly. *Mol Microbiol* **84**: 857-873.

Giltner, C.L., Habash, M., and Burrows, L.L. (2010) *Pseudomonas aeruginosa* minor pilins are incorporated into type IV pili. *J Mol Biol* **398**: 444-461.

Giltner, C.L., Nguyen, Y., and Burrows, L.L. (2012) Type IV pilin proteins: versatile molecular modules. *Microbiol Mol Biol Rev* **76**: 740-772.

Gloag, E.S., Turnbull, L., Javed, M.A., Wang, H., Gee, M.L., Wade, S.A., and Whitchurch, C.B. (2016) Stigmergy co-ordinates multicellular collective behaviours during *Myxococcus xanthus* surface migration. *Sci Rep* **6**: 26005.

Gloag, E.S., Turnbull, L., and Whitchurch, C.B. (2015) Bacterial stigmergy: an organising principle of multicellular collective behaviours of bacteria. *Scientifica* **2015**.

Gold, V.A., Salzer, R., Averhoff, B., and Kuhlbrandt, W. (2015) Structure of a type IV pilus machinery in the open and closed state. *Elife* **4**.

Golovanov, A.P., Balasingham, S., Tzitzilonis, C., Goult, B.T., Lian, L.Y., Homberset, H., Tonjum, T., and Derrick, J.P. (2006) The solution structure of a domain from the *Neisseria meningitidis* lipoprotein PilP reveals a new beta-sandwich fold. *J Mol Biol* **364**: 186-195.

Greenfield, L.K., and Whitfield, C. (2012) Synthesis of lipopolysaccharide O-antigens by ABC transporter-dependent pathways. *Carbohydr Res* **356**: 12-24.

Guzzo, M., Murray, S., Martineau, E., Lhospice, S., Baronian, G., My, L., Zhang, Y., Espinosa, L., Vincentelli, R., and Bratton, B., (2018a) A gated relaxation oscillator mediated by FrzX controls morphogenetic movements in Myxococcus xanthus. Nat Microbiol 3: 948–959. In., pp.

Hart, B.A., and Zahler, S.A. (1966) Lytic enzyme produced by *Myxococcus xanthus*. *J Bacteriol* **92**: 1632-1637.

Hartung, S., Arvai, A.S., Wood, T., Kolappan, S., Shin, D.S., Craig, L., and Tainer, J.A. (2011) Ultrahigh resolution and full-length pilin structures with insights for filament assembly, pathogenic functions, and vaccine potential. *J Biol Chem* **286**: 44254-44265.

Heiniger, R.W., Winther-Larsen, H.C., Pickles, R.J., Koomey, M., and Wolfgang, M.C. (2010) Infection of human mucosal tissue by Pseudomonas aeruginosa requires sequential and mutually dependent virulence factors and a novel pilus-associated adhesin. *Cellular microbiology* **12**: 1158-1173.

Herfurth, M., Perez-Burgos, M., and Søgaard-Andersen, L. (2023) The mechanism for polar localization of the type IVa pilus machine in *Myxococcus xanthus*. *MBio*: e0159323.

Hoang, H.H., Nickerson, N.N., Lee, V.T., Kazimirova, A., Chami, M., Pugsley, A.P., and Lory, S. (2011) Outer membrane targeting of *Pseudomonas aeruginosa* proteins shows variable dependence on the components of Bam and Lol machineries. *MBio* **2**: e00246-00211.

Hodgkin, J., and Kaiser, D. (1977) Cell-to-cell stimulation of movement in nonmotile mutants of Myxococcus. *Proc Natl Acad Sci U S A* **74**: 2938-2942.

Hodgkin, J., and Kaiser, D. (1979) Genetics of gliding motility in *Myxococcus xanthus* (Myxobacterales): two gene systems control movement. *Mol Gen Genet* **171**: 177-191.

Holkenbrink, C., Hoiczyk, E., Kahnt, J., and Higgs, P.I. (2014) Synthesis and assembly of a novel glycan layer in *Myxococcus xanthus* spores. *J Biol Chem* **289**: 32364-32378.

Hospenthal, M.K., Costa, T.R.D., and Waksman, G. (2017) A comprehensive guide to pilus biogenesis in Gram-negative bacteria. *Nat Rev Microbiol* **15**: 365-379.

Howard, S.P., Estrozi, L.F., Bertrand, Q., Contreras-Martel, C., Strozen, T., Job, V., Martins, A., Fenel, D., Schoehn, G., and Dessen, A. (2019) Structure and assembly of pilotin-dependent and -independent secretins of the type II secretion system. *PLoS Pathog* **15**: e1007731.

Hu, J., Worrall, L.J., Hong, C., Vuckovic, M., Atkinson, C.E., Caveney, N., Yu, Z., and Strynadka, N.C.J. (2018) Cryo-EM analysis of the T3S injectisome reveals the structure of the needle and open secretin. *Nat Commun* **9**: 3840.

Hu, W., Gibiansky, M.L., Wang, J., Wang, C., Lux, R., Li, Y., Wong, G.C., and Shi, W. (2016) Interplay between type IV pili activity and exopolysaccharides secretion controls motility patterns in single cells of *Myxococcus xanthus*. *Scientific reports* **6**: 1-10.

Hu, W., Hossain, M., Lux, R., Wang, J., Yang, Z., Li, Y., and Shi, W. (2011) Exopolysaccharide-independent social motility of *Myxococcus xanthus*. *PLoS One* **6**: e16102.

Hu, W., Lux, R., and Shi, W. (2013) Analysis of exopolysaccharides in *Myxococcus xanthus* using confocal laser scanning microscopy. *Methods Mol Biol* **966**: 121-131.

Hu, W., Yang, Z., Lux, R., Zhao, M., Wang, J., He, X., and Shi, W. (2012) Direct visualization of the interaction between pilin and exopolysaccharides of *Myxococcus xanthus* with eGFP-fused PilA protein. *FEMS microbiology letters* **326**: 23-30.

Hughes, H.Q., Christman, N.D., Dalia, T.N., Ellison, C.K., and Dalia, A.B. (2022) The PilT retraction ATPase promotes both extension and retraction of the MSHA type IVa pilus in *Vibrio cholerae*. *PLoS Genetics* **18**: e1010561.

Inclán, Y.F., Laurent, S., and Zusman, D.R. (2008) The receiver domain of FrzE, a CheA–CheY fusion protein, regulates the CheA histidine kinase activity and downstream signalling to the A-and S-motility systems of *Myxococcus xanthus*. *Mol Microbiol* **68**: 1328-1339.

Inclan, Y.F., Vlamakis, H.C., and Zusman, D.R. (2007) FrzZ, a dual CheY-like response regulator, functions as an output for the Frz chemosensory pathway of *Myxococcus xanthus*. *Mol Microbiol* **65**: 90-102.

Islam, S.T., Vergara Alvarez, I., Saidi, F., Guiseppi, A., Vinogradov, E., Sharma, G., Espinosa, L., Morrone, C., Brasseur, G., Guillemot, J.F., Benarouche, A., Bridot, J.L., Ravicoularamin, G., Cagna, A., Gauthier, C., Singer, M., Fierobe, H.P., Mignot, T., and Mauriello, E.M.F. (2020) Modulation of bacterial multicellularity via spatio-specific polysaccharide secretion. *PLoS Biol* **18**: e3000728.

Jakobczak, B., Keilberg, D., Wuichet, K., and Sogaard-Andersen, L. (2015) Contact- and Protein Transfer-Dependent Stimulation of Assembly of the Gliding Motility Machinery in *Myxococcus xanthus*. *PLoS Genet* **11**: e1005341.

Jakovljevic, V., Leonardy, S., Hoppert, M., and Søgaard-Andersen, L. (2008) PilB and PilT are ATPases acting antagonistically in type IV pilus function in *Myxococcus xanthus*. *J Bacteriol* **190**: 2411-2421.

Julien, B., Kaiser, A.D., and Garza, A. (2000) Spatial control of cell differentiation in *Myxococcus xanthus*. *Proc Natl Acad Sci U S A* **97**: 9098-9103.

Kaimer, C., Berleman, J.E., and Zusman, D.R. (2012) Chemosensory signaling controls motility and subcellular polarity in *Myxococcus xanthus*. *Curr Opin Microbiol* **15**: 751-757.

Kaimer, C., and Zusman, D.R. (2013) Phosphorylation-dependent localization of the response regulator FrzZ signals cell reversals in *Myxococcus xanthus*. *Mol Microbiol* **88**: 740-753.

Kaimer, C., and Zusman, D.R. (2016) Regulation of cell reversal frequency in *Myxococcus xanthus* requires the balanced activity of CheY-like domains in FrzE and FrzZ. *Mol Microbiol* **100**: 379-395.

Kaiser, D. (1979) Social gliding is correlated with the presence of pili in *Myxococcus xanthus*. *Proc Natl Acad Sci U S A* **76**: 5952-5956.

Kanehisa, M., and Goto, S. (2000) KEGG: kyoto encyclopedia of genes and genomes. *Nucleic Acids Res* **28**: 27-30.

Karuppiah, V., Collins, R.F., Thistlethwaite, A., Gao, Y., and Derrick, J.P. (2013) Structure and assembly of an inner membrane platform for initiation of type IV pilus biogenesis. *Proc Natl Acad Sci U S A* **110**: E4638-4647.

Karuppiah, V., and Derrick, J.P. (2011) Structure of the PilM-PilN inner membrane type IV pilus biogenesis complex from *Thermus thermophilus*. *J Biol Chem* **286**: 24434-24442.

Karuppiah, V., Hassan, D., Saleem, M., and Derrick, J.P. (2010) Structure and oligomerization of the PilC type IV pilus biogenesis protein from *Thermus thermophilus*. *Proteins* **78**: 2049-2057.

Kaufenstein, M., van der Laan, M., and Graumann, P.L. (2011) The three-layered DNA uptake machinery at the cell pole in competent *Bacillus subtilis* cells is a stable complex. *J Bacteriol* **193**: 1633-1642.

Kearns, D.B. (2010) A field guide to bacterial swarming motility. *Nat Rev Microbiol* **8**: 634-644.

Kearns, D.B., Campbell, B.D., and Shimkets, L.J. (2000) *Myxococcus xanthus* fibril appendages are essential for excitation by a phospholipid attractant. *Proceedings of the National Academy of Sciences* **97**: 11505-11510.

Keilberg, D., Wuichet, K., Drescher, F., and Sogaard-Andersen, L. (2012a) A response regulator interfaces between the Frz chemosensory system and the MglA/MglB GTPase/GAP module to regulate polarity in *Myxococcus xanthus*. *PLoS Genet* **8**: e1002951.

Keilberg, D., Wuichet, K., Drescher, F., and Søgaard-Andersen, L. (2012b) A response regulator interfaces between the Frz chemosensory system and the MglA/MglB GTPase/GAP module to regulate polarity in *Myxococcus xanthus*. *PLoS Genet* **8**: e1002951.

Kelley, L.A., Mezulis, S., Yates, C.M., Wass, M.N., and Sternberg, M.J. (2015) The Phyre2 web portal for protein modeling, prediction and analysis. *Nat Protoc* **10**: 845-858.

Kiekebusch, D., Michie, K.A., Essen, L.O., Lowe, J., and Thanbichler, M. (2012) Localized dimerization and nucleoid binding drive gradient formation by the bacterial cell division inhibitor MipZ. *Mol Cell* **46**: 245-259.

Knirel, Y.A., and Valvano, M.A., (2013) Bacterial polysaccharides structure and biosynthesis. In: Encyclopedia of biophysics. Springer, pp. 162.

Koch, M.D., Fei, C., Wingreen, N.S., Shaevitz, J.W., and Gitai, Z. (2021) Competitive binding of independent extension and retraction motors explains the quantitative dynamics of type IV pili. *Proc Natl Acad Sci U S A* **118**.

Kolappan, S., Coureuil, M., Yu, X., Nassif, X., Egelman, E., and Craig, L. (2016) Structure of the Neisseria meningitidis type IV pilus. . *Nat Commun* **7**: 13015.

Koo, J., Tammam, S., Ku, S.-Y., Sampaleanu, L.M., Burrows, L.L., and Howell, P.L. (2008) PilF is an outer membrane lipoprotein required for multimerization and localization of the *Pseudomonas aeruginosa* type IV pilus secretin. *J Bacteriol* **190**: 6961-6969.

Korotkov, K.V., Johnson, T.L., Jobling, M.G., Pruneda, J., Pardon, E., Héroux, A., Turley, S., Steyaert, J., Holmes, R.K., and Sandkvist, M. (2011) Structural and functional studies on the interaction of GspC and GspD in the type II secretion system. *PLoS pathogens* **7**: e1002228.

Korotkov, K.V., Sandkvist, M., and Hol, W.G. (2012) The type II secretion system: biogenesis, molecular architecture and mechanism. *Nat Rev Microbiol* **10**: 336-351.

Kowal, J., Chami, M., Ringler, P., Muller, S.A., Kudryashev, M., Castano-Diez, D., Amstutz, M., Cornelis, G.R., Stahlberg, H., and Engel, A. (2013) Structure of the dodecameric *Yersinia enterocolitica* secretin YscC and its trypsin-resistant core. *Structure* **21**: 2152-2161.

Laemmli, U.K. (1970) Cleavage of structural proteins during the assembly of the head of bacteriophage T4. *Nature* **227**: 680-685.

Lancero, H.L., Castaneda, S., Caberoy, N.B., Ma, X., Garza, A.G., and Shi, W. (2005) Analysing protein–protein interactions of the *Myxococcus xanthus* Dif signalling pathway using the yeast two-hybrid system. *Microbiology* **151**: 1535-1541.

Lara-Tejero, M., Kato, J., Wagner, S., Liu, X., and Galan, J.E. (2011) A sorting platform determines the order of protein secretion in bacterial type III systems. *Science* **331**: 1188-1191.

Larsen, S.H., Reader, R.W., Kort, E.N., Tso, W.-W., and Adler, J. (1974) Change in direction of flagellar rotation is the basis of the chemotactic response in *Escherichia coli*. *Nature* **249**: 74-77.

Leake, M.C., Chandler, J.H., Wadhams, G.H., Bai, F., Berry, R.M., and Armitage, J.P. (2006) Stoichiometry and turnover in single, functioning membrane protein complexes. *Nature* **443**: 355-358.

Leeuwenhoek, A.V. (1676) Observations, communicated to the publisher by Mr. Antony van Leewenhoeck, in a dutch letter of the 9th Octob. 1676. here English'd: concerning little animals by him observed in rain-well-sea-and snow water; as also

in water wherein pepper had lain infused. *Philosophical Transactions of the Royal Society of London* **12**: 821-831.

Leighton, T.L., Buensuceso, R.N., Howell, P.L., and Burrows, L.L. (2015) Biogenesis of *Pseudomonas aeruginosa* type IV pili and regulation of their function. *Environmental microbiology* **17**: 4148-4163.

Leighton, T.L., Yong, D.H., Howell, P.L., and Burrows, L.L. (2016) Type IV Pilus Alignment Subcomplex Proteins PilN and PilO Form Homo- and Heterodimers in Vivo. *J Biol Chem* **291**: 19923-19938.

Lemkul, J.A., and Bevan, D.R. (2011) Characterization of interactions between PilA from *Pseudomonas aeruginosa* strain K and a model membrane. *The Journal of Physical Chemistry B* **115**: 8004-8008.

Leonardy, S., Freymark, G., Hebener, S., Ellehauge, E., and Sogaard-Andersen, L. (2007) Coupling of protein localization and cell movements by a dynamically localized response regulator in *Myxococcus xanthus*. *EMBO J* **26**: 4433-4444.

Leonardy, S., Miertzschke, M., Bulyha, I., Sperling, E., Wittinghofer, A., and Sogaard-Andersen, L. (2010a) Regulation of dynamic polarity switching in bacteria by a Ras-like G-protein and its cognate GAP. *EMBO J* **29**: 2276-2289.

Leonardy, S., Miertzschke, M., Bulyha, I., Sperling, E., Wittinghofer, A., and Søgaard-Andersen, L. (2010b) Regulation of dynamic polarity switching in bacteria by a Ras-like G-protein and its cognate GAP. *EMBO J* **29**: 2276-2289.

Letunic, I., and Bork, P. (2018) 20 years of the SMART protein domain annotation resource. *Nucleic Acids Res* **46**: D493-D496.

Letunic, I., Khedkar, S., and Bork, P. (2021) SMART: recent updates, new developments and status in 2020. *Nucleic Acids Res* **49**: D458-D460.

Li, H., and Sourjik, V. (2011) Assembly and stability of flagellar motor in *Escherichia coli*. *Mol Microbiol* **80**: 886-899.

Li, Y., Sun, H., Ma, X., Lu, A., Lux, R., Zusman, D., and Shi, W. (2003) Extracellular polysaccharides mediate pilus retraction during social motility of *Myxococcus xanthus*. *Proc Natl Acad Sci U S A* **100**: 5443-5448.

Lu, A., Cho, K., Black, W.P., Duan, X.Y., Lux, R., Yang, Z., Kaplan, H.B., Zusman, D.R., and Shi, W. (2005) Exopolysaccharide biosynthesis genes required for social motility in *Myxococcus xanthus*. *Mol Microbiol* **55**: 206-220.

Luciano, J., Agrebi, R., Le Gall, A.V., Wartel, M., Fiegna, F., Ducret, A., Brochier-Armanet, C., and Mignot, T. (2011) Emergence and modular evolution of a novel motility machinery in bacteria. *PLoS Genet* **7**: e1002268.

Lukose, V., Walvoort, M.T.C., and Imperiali, B. (2017) Bacterial phosphoglycosyl transferases: initiators of glycan biosynthesis at the membrane interface. *Glycobiology* **27**: 820-833.

Maier, B., Potter, L., So, M., Long, C.D., Seifert, H.S., and Sheetz, M.P. (2002) Single pilus motor forces exceed 100 pN. *Proc Natl Acad Sci U S A* **99**: 16012-16017.

Majewski, D.D., Worrall, L.J., and Strynadka, N.C. (2018) Secretins revealed: structural insights into the giant gated outer membrane portals of bacteria. *Curr Opin Struc Biol* **51**: 61-72.

Marciano, D.K., Russel, M., and Simon, S.M. (2001) Assembling filamentous phage occlude pIV channels. *Proc Natl Acad Sci U S A* **98**: 9359-9364.

Mauriello, E.M., Mouhamar, F., Nan, B., Ducret, A., Dai, D., Zusman, D.R., and Mignot, T. (2010) Bacterial motility complexes require the actin-like protein, MreB and the Ras homologue, MglA. *EMBO J* **29**: 315-326.

Mauriello, E.M., and Zusman, D.R. (2007) Polarity of motility systems in Myxococcus xanthus. *Curr Opin Microbiol* **10**: 624-629.

McBride, M.J., and Nakane, D. (2015) *Flavobacterium* gliding motility and the type IX secretion system. *Curr Opin Microbiol* **28**: 72-77.

McCallum, M., Tammam, S., Khan, A., Burrows, L.L., and Howell, P.L. (2017) The molecular mechanism of the type IVa pilus motors. *Nat Commun* **8**: 15091.

McCallum, M., Tammam, S., Little, D.J., Robinson, H., Koo, J., Shah, M., Calmettes, C., Moraes, T.F., Burrows, L.L., and Howell, P.L. (2016) PilN Binding Modulates the Structure and Binding Partners of the *Pseudomonas aeruginosa* Type IVa Pilus Protein PilM. *J Biol Chem* **291**: 11003-11015.

McCallum, M., Tammam, S., Rubinstein, J.L., Burrows, L.L., and Howell, P.L. (2021) CryoEM map of *Pseudomonas aeruginosa* PilQ enables structural characterization of TsaP. *Structure* **29**: 457-466 e454.

Mercier, R., Bautista, S., Delannoy, M., Gibert, M., Guiseppi, A., Herrou, J., Mauriello, E.M.F., and Mignot, T. (2020) The polar Ras-like GTPase MglA activates type IV pilus via SgmX to enable twitching motility in Myxococcus xanthus. *Proc Natl Acad Sci U S A* **117**: 28366-28373.

Mercier, R., and Mignot, T. (2016) Regulations governing the multicellular lifestyle of *Myxococcus xanthus*. *Curr Opin Microbiol* **34**: 104-110.

Merz, A.J., So, M., and Sheetz, M.P. (2000) Pilus retraction powers bacterial twitching motility. *Nature* **407**: 98-102.

Miertzschke, M., Koerner, C., Vetter, I.R., Keilberg, D., Hot, E., Leonardy, S., Søgaard-Andersen, L., and Wittinghofer, A. (2011) Structural analysis of the Ras-like G protein MglA and its cognate GAP MglB and implications for bacterial polarity. *EMBO J* **30**: 4185-4197.

Mignot, T., Merlie, J.P., Jr., and Zusman, D.R. (2005) Regulated pole-to-pole oscillations of a bacterial gliding motility protein. *Science* **310**: 855-857.

Mignot, T., and Nöllmann, M. (2017) New insights into the function of a versatile class of membrane molecular motors from studies of *Myxococcus xanthus* surface (gliding) motility. *Microbial Cell* **4**: 98.

Mignot, T., Shaevitz, J.W., Hartzell, P.L., and Zusman, D.R. (2007) Evidence that focal adhesion complexes power bacterial gliding motility. *Science* **315**: 853-856.

Milne-Davies, B., Wimmi, S., and Diepold, A. (2021) Adaptivity and dynamics in type III secretion systems. *Mol Microbiol* **115**: 395-411.

Misic, A.M., Satyshur, K.A., and Forest, K.T. (2010) P. aeruginosa PilT structures with and without nucleotide reveal a dynamic type IV pilus retraction motor. *J Mol Biol* **400**: 1011-1021.

Mistry, J., Chuguransky, S., Williams, L., Qureshi, M., Salazar, G.A., Sonnhammer, E.L.L., Tosatto, S.C.E., Paladin, L., Raj, S., Richardson, L.J., Finn, R.D., and Bateman, A. (2021) Pfam: The protein families database in 2021. *Nucleic Acids Res* **49**: D412-D419.

Miyata, M., and Hamaguchi, T. (2016) Prospects for the gliding mechanism of *Mycoplasma mobile*. *Curr Opin Microbiol* **29**: 15-21.

Moak, P.L., Black, W.P., Wallace, R.A., Li, Z., and Yang, Z. (2015) The Hsp70-like StkA functions between T4P and Dif signaling proteins as a negative regulator of exopolysaccharide in *Myxococcus xanthus*. *PeerJ* **3**: e747.

Müller, F.D., Schink, C.W., Hoiczyk, E., Cserti, E., and Higgs, P.I. (2012) Spore formation in *Myxococcus xanthus* is tied to cytoskeleton functions and polysaccharide spore coat deposition. *Molecular microbiology* **83**: 486-505.

Munoz-Dorado, J., Marcos-Torres, F.J., Garcia-Bravo, E., Moraleda-Munoz, A., and Perez, J. (2016) Myxobacteria: Moving, Killing, Feeding, and Surviving Together. *Front Microbiol* **7**: 781.

Muñoz-Dorado, J., Marcos-Torres, F.J., Garcia-Bravo, E., Moraleda-Muñoz, A., and Perez, J. (2016) Myxobacteria: Moving, Killing, Feeding, and Surviving Together. *Front Microbiol* **7**: 781.

Nan, B., Chen, J., Neu, J.C., Berry, R.M., Oster, G., and Zusman, D.R. (2011) Myxobacteria gliding motility requires cytoskeleton rotation powered by proton motive force. *Proc Natl Acad Sci U S A* **108**: 2498-2503.

Nan, B., McBride, M.J., Chen, J., Zusman, D.R., and Oster, G. (2014) Bacteria that glide with helical tracks. *Current Biology* **24**: R169-R173.

Ng, D., Harn, T., Altindal, T., Kolappan, S., Marles, J.M., Lala, R., Spielman, I., Gao, Y., Hauke, C.A., and Kovacikova, G. (2016) The *Vibrio cholerae* minor pilin TcpB initiates assembly and retraction of the toxin-coregulated pilus. *PLoS pathogens* **12**: e1006109.

Nguyen, Y., Sugiman-Marangos, S., Harvey, H., Bell, S.D., Charlton, C.L., Junop, M.S., and Burrows, L.L. (2015) *Pseudomonas aeruginosa* minor pilins prime type IVa pilus assembly and promote surface display of the PilY1 adhesin. *J Biol Chem* **290**: 601-611.

Nouwen, N., Ranson, N., Saibil, H., Wolpensinger, B., Engel, A., Ghazi, A., and Pugsley, A.P. (1999) Secretin PulD: association with pilot PulS, structure, and ion-conducting channel formation. *Proc Natl Acad Sci U S A* **96**: 8173-8177.

Nudleman, E., Wall, D., and Kaiser, D. (2006) Polar assembly of the type IV pilus secretin in *Myxococcus xanthus*. *Mol Microbiol* **60**: 16-29.

Nunn, D.N., and Lory, S. (1991) Product of the *Pseudomonas aeruginosa* gene pilD is a prepilin leader peptidase. *Proc Natl Acad Sci U S A* **88**: 3281-3285.

Nwodo, U.U., Green, E., and Okoh, A.I. (2012) Bacterial exopolysaccharides: functionality and prospects. *Int J Mol Sci* **13**: 14002-14015.

O'Toole, G.A., and Kolter, R. (1998) Flagellar and twitching motility are necessary for *Pseudomonas aeruginosa* biofilm development. *Mol Microbiol* **30**: 295-304.

Opalka, N., Beckmann, R., Boisset, N., Simon, M.N., Russel, M., and Darst, S.A. (2003) Structure of the filamentous phage pIV multimer by cryo-electron microscopy. *J Mol Biol* **325**: 461-470.

Overgaard, M., Wegener-Feldbrügge, S., and Søgaard-Andersen, L. (2006) The orphan response regulator DigR is required for synthesis of extracellular matrix fibrils in *Myxococcus xanthus*. *Journal of bacteriology* **188**: 4384-4394.

Paintdakhi, A., Parry, B., Campos, M., Irnov, I., Elf, J., Surovtsev, I., and Jacobs-Wagner, C. (2016) Oufti: an integrated software package for high-accuracy, high-throughput quantitative microscopy analysis. *Mol Microbiol* **99**: 767-777.

Parge, H.E., Forest, K.T., Hickey, M.J., Christensen, D.A., Getzoff, E.D., and Tainer, J.A. (1995) Structure of the fibre-forming protein pilin at 2.6 Å resolution. *Nature* **378**: 32-38.

Park, D., Lara-Tejero, M., Waxham, M.N., Li, W., Hu, B., Galán, J.E., and Liu, J. (2018) Visualization of the type III secretion mediated *Salmonella*–host cell interface using cryo-electron tomography. *Elife* **7**: e39514.

Paul, K., Gonzalez-Bonet, G., Bilwes, A.M., Crane, B.R., and Blair, D. (2011) Architecture of the flagellar rotor. *EMBO J* **30**: 2962-2971.

Peabody, C.R., Chung, Y.J., Yen, M.R., Vidal-Ingigliardi, D., Pugsley, A.P., and Saier, M.H. (2003) Type II protein secretion and its relationship to bacterial type IV pili and archaeal flagella. *Microbiology (Reading)* **149**: 3051-3072.

Pelicic, V. (2008) Type IV pili: e pluribus unum? *Mol Microbiol* **68**: 827-837.

Pelicic, V. (2023) Mechanism of assembly of type 4 filaments: everything you always wanted to know (but were afraid to ask). *Microbiology* **169**: 001311.

Perez-Burgos, M., Garcia-Romero, I., Jung, J., Schander, E., Valvano, M.A., and Søgaard-Andersen, L. (2020a) Characterization of the Exopolysaccharide Biosynthesis Pathway in *Myxococcus xanthus*. *J Bacteriol* **202**.

Perez-Burgos, M., Garcia-Romero, I., Jung, J., Valvano, M.A., and Søgaard-Andersen, L. (2019) Identification of the lipopolysaccharide O-antigen biosynthesis priming enzyme and the O-antigen ligase in *Myxococcus xanthus*: critical role of LPS O-antigen in motility and development. *Mol Microbiol* **112**: 1178-1198.

Perez-Burgos, M., Garcia-Romero, I., Valvano, M.A., and Søgaard Andersen, L. (2020b) Identification of the Wzx flippase, Wzy polymerase and sugar-modifying enzymes for spore coat polysaccharide biosynthesis in *Myxococcus xanthus*. *Mol Microbiol* **113**: 1189-1208.

Perez-Burgos, M., and Søgaard-Andersen, L. (2020) Biosynthesis and function of cell-surface polysaccharides in the social bacterium *Myxococcus xanthus*. *Biol Chem* **401**: 1375-1387.

Pham, V.D., Shebelut, C.W., Mukherjee, B., and Singer, M. (2005a) RasA is required for *Myxococcus xanthus* development and social motility. *J Bacteriol* **187**: 6845-6848.

Pham, V.D., Shebelut, C.W., Zumstein, E.J., and Singer, M. (2005b) BrgE is a regulator of *Myxococcus xanthus* development. *Molecular microbiology* **57**: 762-773.

Planet, P.J., Kachlany, S.C., DeSalle, R., and Figurski, D.H. (2001) Phylogeny of genes for secretion NTPases: identification of the widespread tadA subfamily and development of a diagnostic key for gene classification. *Proc Natl Acad Sci U S A* **98**: 2503-2508.

Poggio, S., Takacs, C.N., Vollmer, W., and Jacobs-Wagner, C. (2010) A protein critical for cell constriction in the Gram-negative bacterium *Caulobacter crescentus* localizes at the division site through its peptidoglycan-binding LysM domains. *Mol Microbiol* **77**: 74-89.

Porter, S.L., Wadhams, G.H., and Armitage, J.P. (2011) Signal processing in complex chemotaxis pathways. *Nat Rev Microbiol* **9**: 153-165.

Potapova, A., Carreira, L.A.M., and Søgaard-Andersen, L. (2020) The small GTPase MglA together with the TPR domain protein SgmX stimulates type IV pili formation in *M. xanthus*. *Proc Natl Acad Sci U S A* **117**: 23859-23868.

Roca, C., Alves, V.D., Freitas, F., and Reis, M.A. (2015) Exopolysaccharides enriched in rare sugars: bacterial sources, production, and applications. *Front Microbiol* **6**: 288.

Rocha, J.M., Richardson, C.J., Zhang, M., Darch, C.M., Cai, E., Diepold, A., and Gahlmann, A. (2018) Single-molecule tracking in live *Yersinia enterocolitica* reveals distinct cytosolic complexes of injectisome subunits. *Integr Biol (Camb)* **10**: 502-515.

Rodriguez-Soto, J.P., and Kaiser, D. (1997) Identification and localization of the Tgl protein, which is required for *Myxococcus xanthus* social motility. *J Bacteriol* **179**: 4372-4381.

Ryll, R.R., Rudel, T., Scheuerpflug, I., Barten, R., and Meyer, T.F. (1997) PilC of *Neisseria meningitidis* is involved in class II pilus formation and restores pilus assembly, natural transformation competence and adherence to epithelial cells in PilC-deficient gonococci. *Mol Microbiol* **23**: 879-892.

Sampaleanu, L.M., Bonanno, J.B., Ayers, M., Koo, J., Tammam, S., Burley, S.K., Almo, S.C., Burrows, L.L., and Howell, P.L. (2009) Periplasmic domains of *Pseudomonas aeruginosa* PilN and PilO form a stable heterodimeric complex. *J Mol Biol* **394**: 143-159.

Satyshur, K.A., Worzalla, G.A., Meyer, L.S., Heiniger, E.K., Aukema, K.G., Misic, A.M., and Forest, K.T. (2007) Crystal structures of the pilus retraction motor PilT suggest

large domain movements and subunit cooperation drive motility. *Structure* **15**: 363-376.

Schumacher, D., Bergeler, S., Harms, A., Vonck, J., Huneke-Vogt, S., Frey, E., and Sogaard-Andersen, L. (2017) The PomXYZ Proteins Self-Organize on the Bacterial Nucleoid to Stimulate Cell Division. *Dev Cell* **41**: 299-314 e213.

Schumacher, D., and Sogaard-Andersen, L. (2017) Regulation of Cell Polarity in Motility and Cell Division in *Myxococcus xanthus*. *Annu Rev Microbiol* **71**: 61-78.

Schwabe, J., Perez-Burgos, M., Herfurth, M., Glatter, T., and Søgaard-Andersen, L. (2022) Evidence for a Widespread Third System for Bacterial Polysaccharide Export across the Outer Membrane Comprising a Composite OPX/beta-Barrel Translocon. *MBio* **13**: e0203222.

Seef, S., Herrou, J., de Boissier, P., My, L., Brasseur, G., Robert, D., Jain, R., Mercier, R., Cascales, E., and Habermann, B.H. (2021) A Tad-like apparatus is required for contact-dependent prey killing in predatory social bacteria. *Elife* **10**: e72409.

Shi, W., Yang, Z., Sun, H., Lancero, H., and Tong, L. (2000) Phenotypic analyses of frz and dif double mutants of *Myxococcus xanthus*. *FEMS Microbiol Lett* **192**: 211-215.

Shi, W., and Zusman, D.R. (1993) The two motility systems of *Myxococcus xanthus* show different selective advantages on various surfaces. *Proc Natl Acad Sci U S A* **90**: 3378-3382.

Shi, X., Wegener-Feldbrugge, S., Huntley, S., Hamann, N., Hedderich, R., and Søgaard-Andersen, L. (2008) Bioinformatics and experimental analysis of proteins of two-component systems in *Myxococcus xanthus*. *J Bacteriol* **190**: 613-624.

Shimkets, L.J. (1986) Role of cell cohesion in *Myxococcus xanthus* fruiting body formation. *J Bacteriol* **166**: 842-848.

Siewering, K., Jain, S., Friedrich, C., Webber-Birungi, M.T., Semchonok, D.A., Binzen, I., Wagner, A., Huntley, S., Kahnt, J., Klingl, A., Boekema, E.J., Sogaard-Andersen, L., and van der Does, C. (2014) Peptidoglycan-binding protein TsaP functions in surface assembly of type IV pili. *Proc Natl Acad Sci U S A* **111**: E953-961.

Silhavy, T.J., Kahne, D., and Walker, S. (2010) The bacterial cell envelope. *Cold Spring Harb Perspect Biol* **2**: a000414.

Silva, A.K., Letourneur, D., and Chauvierre, C. (2014) Polysaccharide nanosystems for future progress in cardiovascular pathologies. *Theranostics* **4**: 579-591.

Silva, Y.R.O., Contreras-Martel, C., Macheboeuf, P., and Dessen, A. (2020) Bacterial secretins: Mechanisms of assembly and membrane targeting. *Protein Sci* **29**: 893-904.

Silverman, M., and Simon, M. (1974) Flagellar rotation and the mechanism of bacterial motility. *Nature* **249**: 73-74.

Simsek, A.N., Koch, M.D., Sanfilippo, J., Gitai, Z., Gompper, G., and Sabass, B. (2023) Type-IV pili tune an adhesion-migration trade-off during surface colonization of *Pseudomonas aeruginosa*. *bioRxiv*: 2023.2005. 2009.538458.

Skerker, J.M., and Berg, H.C. (2001) Direct observation of extension and retraction of type IV pili. *Proc Natl Acad Sci U S A* **98**: 6901-6904.

Skotnicka, D., Petters, T., Heering, J., Hoppert, M., Kaever, V., and Søgaard-Andersen, L. (2016a) Cyclic di-GMP regulates type IV pilus-dependent motility in *Myxococcus xanthus*. *J Bacteriol* **198**: 77-90.

Skotnicka, D., Petters, T., Heering, J., Hoppert, M., Kaever, V., and Søgaard-Andersen, L. (2016b) Cyclic di-GMP regulates type IV pilus-dependent motility in *Myxococcus xanthus*. *Journal of bacteriology* **198**: 77-90.

Skotnicka, D., Smaldone, G.T., Petters, T., Trampari, E., Liang, J., Kaever, V., Malone, J.G., Singer, M., and Søgaard-Andersen, L. (2016c) A Minimal Threshold of c-di-

GMP Is Essential for Fruiting Body Formation and Sporulation in *Myxococcus xanthus*. *PLoS Genet* **12**: e1006080.

Spormann, A.M. (1999) Gliding Motility in Bacteria: Insights from Studies of *Myxococcus xanthus*. *Microbiol Mol Biol Rev* **63**: 621-641.

Spormann, A.M., and Kaiser, A.D. (1995) Gliding movements in *Myxococcus xanthus*. *J Bacteriol* **177**: 5846-5852.

Strom, M.S., Nunn, D.N., and Lory, S. (1993) A single bifunctional enzyme, PilD, catalyzes cleavage and N-methylation of proteins belonging to the type IV pilin family. *Proc Natl Acad Sci U S A* **90**: 2404-2408.

Sudo, S.Z., and Dworkin, M. (1969) Resistance of vegetative cells and microcysts of *Myxococcus xanthus*. *J Bacteriol* **98**: 883-887.

Sun, M., Wartel, M., Cascales, E., Shaevitz, J.W., and Mignot, T. (2011) Motor-driven intracellular transport powers bacterial gliding motility. *Proc Natl Acad Sci U S A* **108**: 7559-7564.

Szabo, Z., Stahl, A.O., Albers, S.V., Kissinger, J.C., Driessen, A.J., and Pohlschroder, M. (2007) Identification of diverse archaeal proteins with class III signal peptides cleaved by distinct archaeal prepilin peptidases. *J Bacteriol* **189**: 772-778.

Szadkowski, D., Carreira, L.A.M., and Søgaard-Andersen, L. (2022) A bipartite, low-affinity roadblock domain-containing GAP complex regulates bacterial front-rear polarity. *PLoS Genet* **18**: e1010384.

Szadkowski, D., Harms, A., Carreira, L.A.M., Wigbers, M., Potapova, A., Wuichet, K., Keilberg, D., Gerland, U., and Sogaard-Andersen, L. (2019) Spatial control of the GTPase MglA by localized RomR-RomX GEF and MglB GAP activities enables *Myxococcus xanthus* motility. *Nat Microbiol* **4**: 1344-1355.

Takhar, H.K., Kemp, K., Kim, M., Howell, P.L., and Burrows, L.L. (2013) The platform protein is essential for type IV pilus biogenesis. *J Biol Chem* **288**: 9721-9728.

Tammam, S., Sampaleanu, L.M., Koo, J., Manoharan, K., Daubaras, M., Burrows, L.L., and Howell, P.L. (2013) PilMNOPQ from the *Pseudomonas aeruginosa* type IV pilus system form a transenvelope protein interaction network that interacts with PilA. *J Bacteriol* **195**: 2126-2135.

Tammam, S., Sampaleanu, L.M., Koo, J., Sundaram, P., Ayers, M., Chong, P.A., Forman-Kay, J.D., Burrows, L.L., and Howell, P.L. (2011) Characterization of the PilN, PilO and PilP type IVa pilus subcomplex. *Mol Microbiol* **82**: 1496-1514.

Terashima, H., Li, N., Sakuma, M., Koike, M., Kojima, S., Homma, M., and Imada, K. (2013) Insight into the assembly mechanism in the supramolecular rings of the sodium-driven *Vibrio* flagellar motor from the structure of FlgT. *Proc Natl Acad Sci U S A* **110**: 6133-6138.

Thiery, S., Turowski, P., Berleman, J.E., and Kaimer, C. (2022) The predatory soil bacterium *Myxococcus xanthus* combines a Tad- and an atypical type 3-like protein secretion system to kill bacterial cells. *Cell Rep* **40**: 111340.

Thomas, D.R., Francis, N.R., Xu, C., and DeRosier, D.J. (2006) The three-dimensional structure of the flagellar rotor from a clockwise-locked mutant of *Salmonella enterica* serovar Typhimurium. *J Bacteriol* **188**: 7039-7048.

Thomas, J.D., Reeves, P.J., and Salmond, G.P. (1997) The general secretion pathway of *Erwinia carotovora* subsp. carotovora: analysis of the membrane topology of OutC and OutF. *Microbiology* **143**: 713-720.

Thomassin, J.L., Santos Moreno, J., Guilvout, I., Tran Van Nhieu, G., and Francetic, O. (2017) The trans-envelope architecture and function of the type 2 secretion system: New insights raising new questions. *Mol Microbiol* **105**: 211-226.

Treuner-Lange, A., Chang, Y.W., Glatter, T., Herfurth, M., Lindow, S., Chreifi, G., Jensen, G.J., and Søgaard-Andersen, L. (2020) PilY1 and minor pilins form a complex priming the type IVa pilus in *Myxococcus xanthus*. *Nat Commun* **11**: 5054.

Treuner-Lange, A., Macia, E., Guzzo, M., Hot, E., Faure, L.M., Jakobczak, B., Espinosa, L., Alcor, D., Ducret, A., and Keilberg, D. (2015a) The small G-protein MglA connects to the MreB actin cytoskeleton at bacterial focal adhesions. *Journal of Cell Biology* **210**: 243-256.

Treuner-Lange, A., Zheng, W., Viljoen, A., Lindow, S., Herfurth, M., Dufrene, Y.F., Søgaard-Andersen, L., and Egelman, E.H. (2023) Large pilin subunits provide distinct structural and mechanical properties for the *Myxococcus xanthus* type IV pilus. *bioRxiv*.

Turner, L.R., Lara, J.C., Nunn, D.N., and Lory, S. (1993) Mutations in the consensus ATP-binding sites of XcpR and PilB eliminate extracellular protein secretion and pilus biogenesis in *Pseudomonas aeruginosa*. *J Bacteriol* **175**: 4962-4969.

Tusk, S.E., Delalez, N.J., and Berry, R.M. (2018) Subunit Exchange in Protein Complexes. *J Mol Biol* **430**: 4557-4579.

Tytgat, H.L., and Lebeer, S. (2014) The sweet tooth of bacteria: common themes in bacterial glycoconjugates. *Microbiol Mol Biol Rev* **78**: 372-417.

Valvano, M.A. (2011) Common Themes in Glycoconjugate Assembly Using the Biogenesis of O-Antigen Lipopolysaccharide as a Model System. *Biochemistry-Moscow+* **76**: 729-735.

Voulhoux, R., Bos, M.P., Geurtsen, J., Mols, M., and Tommassen, J. (2003) Role of a highly conserved bacterial protein in outer membrane protein assembly. *Science* **299**: 262-265.

Wadhwa, N., and Berg, H.C. (2022) Bacterial motility: machinery and mechanisms. *Nat Rev Microbiol* **20**: 161-173.

Waite, D.W., Chuvochina, M., Pelikan, C., Parks, D.H., Yilmaz, P., Wagner, M., Loy, A., Naganuma, T., Nakai, R., and Whitman, W.B. (2020) Proposal to reclassify the proteobacterial classes Deltaproteobacteria and Oligoflexia, and the phylum *Thermodesulfobacteria* into four phyla reflecting major functional capabilities. *International Journal of Systematic and Evolutionary Microbiology* **70**: 5972-6016.

Wall, D., Kolenbrander, P.E., and Kaiser, D. (1999) The *Myxococcus xanthus pilQ* (*sglA*) gene encodes a secretin homolog required for type IV pilus biogenesis, social motility, and development. *J Bacteriol* **181**: 24-33.

Wang, F., Coureuil, M., Osinski, T., Orlova, A., Altindal, T., Gesbert, G., Nassif, X., Egelman, E.H., and Craig, L. (2017) Cryoelectron Microscopy Reconstructions of the *Pseudomonas aeruginosa* and *Neisseria gonorrhoeae* Type IV Pili at Sub-nanometer Resolution. *Structure* **25**: 1423-1435 e1424.

Wang, J., Hu, S., Nie, S., Yu, Q., and Xie, M. (2016a) Reviews on Mechanisms of In Vitro Antioxidant Activity of Polysaccharides. *Oxid Med Cell Longev* **2016**: 5692852.

Wang, Y.C., Chin, K.H., Tu, Z.L., He, J., Jones, C.J., Sanchez, D.Z., Yildiz, F.H., Galperin, M.Y., and Chou, S.H. (2016b) Nucleotide binding by the widespread high-affinity cyclic di-GMP receptor MshEN domain. *Nat Commun* **7**: 12481.

Ward, M.J., Lew, H., and Zusman, D.R. (2000) Social motility in *Myxococcus xanthus* requires FrzS, a protein with an extensive coiled-coil domain. *Molecular microbiology* **37**: 1357-1371.

Weaver, S.J., Ortega, D.R., Sazinsky, M.H., Dalia, T.N., Dalia, A.B., and Jensen, G.J. (2020) CryoEM structure of the type IVa pilus secretin required for natural competence in *Vibrio cholerae*. *Nature communications* **11**: 5080.

Whitfield, C., and Trent, M.S. (2014) Biosynthesis and export of bacterial lipopolysaccharides. *Annu Rev Biochem* **83**: 99-128.

Whitfield, C., Wear, S.S., and Sande, C. (2020) Assembly of Bacterial Capsular Polysaccharides and Exopolysaccharides. *Annu Rev Microbiol* **74**: 521-543.

Wilson, K.P., Shewchuk, L.M., Brennan, R.G., Otsuka, A.J., and Matthews, B.W. (1992) *Escherichia coli* biotin holoenzyme synthetase/bio repressor crystal structure delineates the biotin- and DNA-binding domains. *Proc Natl Acad Sci U S A* **89**: 9257-9261.

Wimmi, S., Fleck, M., Helbig, C., Brianceau, C., Langenfeld, K., Szymanski, W., Angelidou, G., Glatter, T., and Diepold, A. (2022) Pilotins are mobile T3SS components involved in assembly and substrate specificity of the bacterial type III secretion system. *bioRxiv*.

Winther-Larsen, H.C., Wolfgang, M., Dunham, S., van Putten, J.P., Dorward, D., Lovold, C., Aas, F.E., and Koomey, M. (2005) A conserved set of pilin-like molecules controls type IV pilus dynamics and organelle-associated functions in Neisseria gonorrhoeae. *Mol Microbiol* **56**: 903-917.

Wolfaardt, G.M., Lawrence, J.R., and Korber, D.R., (1999) Function of EPS. In: Microbial extracellular polymeric substances. Springer, pp. 171-200.

Wolfgang, M., Park, H.-S., Hayes, S.F., Van Putten, J.P., and Koomey, M. (1998) Suppression of an absolute defect in type IV pilus biogenesis by loss-of-function mutations in pilT, a twitching motility gene in *Neisseria gonorrhoeae*. *Proc Natl Acad Sci U S A* **95**: 14973-14978.

Wolgemuth, C., Hoiczyk, E., Kaiser, D., and Oster, G. (2002) How myxobacteria glide. *Current Biology* **12**: 369-377.

Worrall, L., Hong, C., Vuckovic, M., Deng, W., Bergeron, J., Majewski, D., Huang, R., Spreter, T., Finlay, B., and Yu, Z. (2016) Near-atomic-resolution cryo-EM analysis of the Salmonella T3S injectisome basal body. *Nature* **540**: 597-601.

Wu, S.S., and Kaiser, D. (1995) Genetic and functional evidence that type IV pili are required for social gliding motility in *Myxococcus xanthus*. *Mol Microbiol* **18**: 547-558.

Wu, S.S., and Kaiser, D. (1997) Regulation of expression of the *pilA* gene in *Myxococcus xanthus*. *J Bacteriol* **179**: 7748-7758.

Xue, S., Mercier, R., Guiseppi, A., Kosta, A., De Cegli, R., Gagnot, S., Mignot, T., and Mauriello, E.M.F. (2022) The differential expression of PilY1 proteins by the HsfBA phosphorelay allows twitching motility in the absence of exopolysaccharides. *PLoS Genet* **18**: e1010188.

Yamagata, A., and Tainer, J.A. (2007) Hexameric structures of the archaeal secretion ATPase GspE and implications for a universal secretion mechanism. *EMBO J* **26**: 878-890.

Yamaguchi, T., Makino, F., Miyata, T., Minamino, T., Kato, T., and Namba, K. (2021) Structure of the molecular bushing of the bacterial flagellar motor. *Nat Commun* **12**: 4469.

Yan, Z., Yin, M., Xu, D., Zhu, Y., and Li, X. (2017) Structural insights into the secretin translocation channel in the type II secretion system. *Nature structural & molecular biology* **24**: 177-183.

Yang, R., Bartle, S., Otto, R., Stassinopoulos, A., Rogers, M., Plamann, L., and Hartzell, P. (2004) AglZ is a filament-forming coiled-coil protein required for adventurous gliding motility of *Myxococcus xanthus*. *J Bacteriol* **186**: 6168-6178.

Yang, Z., Geng, Y., Xu, D., Kaplan, H.B., and Shi, W. (1998) A new set of chemotaxis homologues is essential for *Myxococcus xanthus* social motility. *Molecular microbiology* **30**: 1123-1130.

Yang, Z., and Li, Z. (2005) Demonstration of interactions among *Myxococcus xanthus* Dif chemotaxis-like proteins by the yeast two-hybrid system. *Archives of microbiology* **183**: 243-252.

Yang, Z., Ma, X., Tong, L., Kaplan, H.B., Shimkets, L.J., and Shi, W. (2000) *Myxococcus xanthus* dif genes are required for biogenesis of cell surface fibrils essential for social gliding motility. *J Bacteriol* **182**: 5793-5798.

Youderian, P., and Hartzell, P.L. (2006) Transposon insertions of magellan-4 that impair social gliding motility in *Myxococcus xanthus*. *Genetics* **172**: 1397-1410.

Zhang, Y., Ducret, A., Shaevitz, J., and Mignot, T. (2012a) From individual cell motility to collective behaviors: insights from a prokaryote, *Myxococcus xanthus*. *FEMS microbiology reviews* **36**: 149-164.

Zhang, Y., Franco, M., Ducret, A., and Mignot, T. (2010) A bacterial Ras-like small GTP-binding protein and its cognate GAP establish a dynamic spatial polarity axis to control directed motility. *PLoS Biol* **8**: e1000430.

Zhang, Y., Guzzo, M., Ducret, A., Li, Y.-Z., and Mignot, T. (2012b) A dynamic response regulator protein modulates G-protein–dependent polarity in the bacterium *Myxococcus xanthus*. *PLoS Genet*.

Zhou, T., and Nan, B. (2017) Exopolysaccharides promote *Myxococcus xanthus* social motility by inhibiting cellular reversals. *Mol Microbiol* **103**: 729-743.

Zimmermann, L., Stephens, A., Nam, S.-Z., Rau, D., Kübler, J., Lozajic, M., Gabler, F., Söding, J., Lupas, A.N., and Alva, V. (2018) A completely reimplemented MPI bioinformatics toolkit with a new HHpred server at its core. *J Mol Biol* **430**: 2237-2243.

13 Supplement

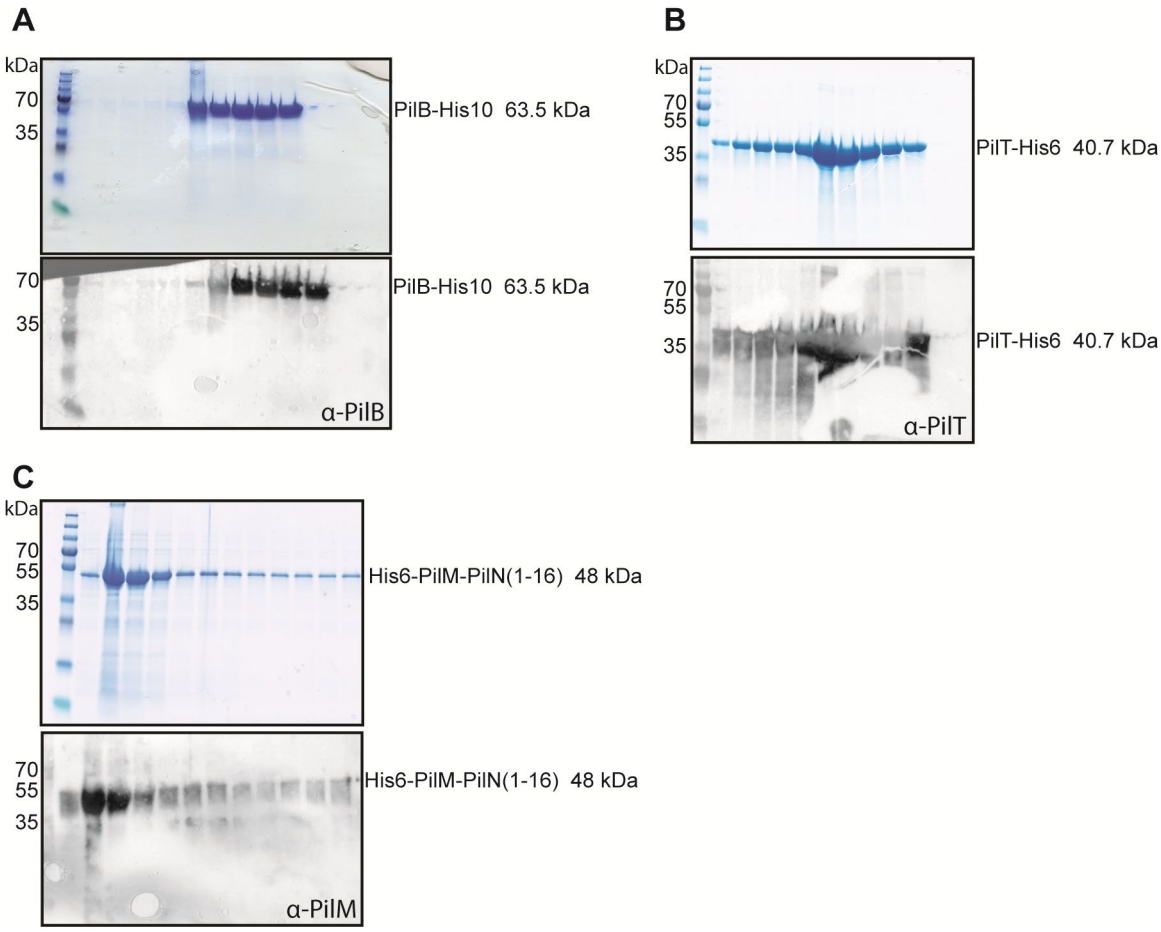

Supplementary Figure 1 Purification of PilB-His10, PilT-His6 and His6-PilM-PilN(1-1) A. 10 µl samples of 2ml elution fraction for PilB-His10 purification were loaded on a SDS-Gel and SDS-PAGE and immunoblot analysis with α-PilB was performed as described in 11.5.5. **B.** 10 µl samples of 2 ml elution fraction for PilT-His6 purification were loaded on a SDS-Gel and SDS-PAGE and immunoblot analysis with α-PilB was performed as described in 11.5.5. **C.** 10 µl samples of 2 ml elution fraction for His6-PilM-N(1-16) purification were loaded on a SDS-Gel and SDS-PAGE and immunoblot analysis with α-PilB was performed as described in 11.5.5. Exact description of Protein purifications can be found in 11.5.5 and 11.5.6.

14 Danksagung/ Teşekkürler/ Acknowledgment

Zuallererst möchte ich mich bei Prof. Dr. Søgaard-Andersen für die Betreuung meiner Doktorarbeit und auch für das Ermöglichen meiner Bachelor-, Masterarbeit in Ihrer Arbeitsgruppe danken. Ich konnte in diesen Jahren sehr viel lernen und persönlich wachsen.

Ein weiterer Dank gilt Prof. Dr. Thanbichler, der mich mit seinen spannenden Mikrobiologie-Vorlesungen begeistern konnte. Ich möchte mich auch das Feedback in den TAC-Meetings und auch die Übernahme des Zweitgutachtens bedanken.

Ich möchte mich auch bei den weiteren Mitgliedern meiner Prüfungskommission Prof. Dr. Sourjik und Prof. Dr. Randau bedanken.

Bei Dr. Andreas Diepold möchte ich mich dafür bedanken, dass er in meinen TAC-Meetings, aber auch sonst, jederzeit ein offenes Ohr hatte und mir geholfen hat, insbesondere, wenn ich Fragen zum Thema FRAP hatte.

Bei Dr. Dominik Schumacher möchte ich mich dafür bedanken, dass er mir zum einen beigebracht hat, wie ich überhaupt FRAP durchführe, aber vor allem dafür, dass er mir zur Seite stand, wenn es mal wieder Probleme mit dem Mikroskop gab und ich total am Verzweifeln war. Auch danke für die vielen lustigen Gespräche in den Kaffeepausen!

I would also like to thank Dr. Luis Carreíra for his help with the FRAP analysis and for his support, creative ideas, thoughts, and discussions about my results.

Bei Dr. Anke Treuner-Lange möchte ich mich für Ihre allgemeine Unterstützung bedanken, insbesondere wenn es um T4P, Stämme oder Plasmide ging, für Ihre Korrekturen und auch Ihre Betreuung während meiner Bachelor- und Masterarbeit. In dieser Zeit habe ich unheimlich viel lernen können.

Bei Dr. María Pérez Burgos möchte ich mich für all die Zeit bedanken, die wir im Labor 1 und im zweiten Stock verbracht haben. Sie stand mir damals immer mit Rat und Tat zur Seite. Und ich möchte mich für all die Zeit bedanken, die du dir genommen hast, um mir zu helfen, sei es bei Motility Assays oder anderen Experimenten, Berichten, die geschrieben werden mussten, oder Präsentationen, die vorbereitet werden mussten. Ich möchte mich auch für die vielen Unternehmungen und schönen Momente außerhalb der Arbeit bedanken.

Nun möchte ich mich ganz besonders bei den Leuten bedanken, ohne die ein Laboralltag und meine Arbeit nicht möglich gewesen wäre. Vielen Dank an Yvonne Ried, Steffi Lindow, Andrea Harms und Susanne Kneip.

Yvonne möchte ich auch für die vielen lustigen Gespräche danken und dafür, dass sie mir einiges über hessische Traditionen beigebracht hat.

Andrea Harms danke ich auch für die witzigen Kaffeepausen und dafür, dass Sie mir stets geholfen hat, wenn es um Aufreinigung von Proteinen ging.

Einen ganz besonderen Dank möchte ich für Steffi Lindow aussprechen. Liebe Steffi, du hast mir seit meiner Bachelor-Zeit unheimlich viel beigebracht und hast mir immer mit Rat und Tat zur Seite gestanden, sei es eine Transformation, eine Klonierung oder Tipps und Tricks zur Protein-Aufreinigung. Ich konnte mich mit jedem Problem an dich wenden und habe stets Hilfe bekommen.

Ich möchte mich bei Jana Jung, Michel Oklitscheck und Franziska Müller bedanken, dafür, dass wir diesen sehr langen Weg gemeinsam gegangen sind! Michel und Jana, ich danke euch für die

lustige Zeit im Labor eins (das war noch ganz am Anfang). Jana, ich erinnere mich noch daran, wie wir einige Aufgaben zusammen erledigt haben, weil Autoklaven und Stickstoff am Anfang auch sehr gefährlich wirken. Ich konnte einiges von dir lernen, da du eine innere Ruhe und Stärke hast, die ich stets bewundert habe!

Michel, du hattest immer einen guten Spruch auf Lager, immer ein offenes Ohr und es hat mir immer geholfen, mich mit dir auszutauschen. Ich bin dir sehr dankbar für deine klare Sicht und deine direkte und ehrliche Art.

Liebe Franzi, wir haben die Promotion gleichzeitig gestartet und beenden sie nun auch gleichzeitig. Danke, für die lustigen, aber auch ernsten Momente, die wir hatten. Ich konnte mich besonders auf deine Unterstützung und dich als Freundin verlassen. Ich habe stets deine Stärke und Entschlossenheit bewundert. Danke, dass du in dieser Zeit für mich da warst. Und auch für die vielen schönen Erinnerungen.

Bei Dr. Michael Seidel möchte ich mich auch herzlich bedanken. Michael, wir haben viel zusammen gelacht! Und auch im Labor habe ich einiges von dir lernen können. Vielen Dank für all die schöne Zeit, die wir auch außerhalb des Labors hatten.

Sevgili Ozan, sıra sende. Bana bu doktoranın en zor zamanlarında, yani son iki senede, belki de bazen hiç fark etmeden çok büyük bir destek oldun. Seninle bütün düşüncelerimi paylaşabildim. Beni her zaman dinlediğin için ve her zaman anlayış gösterdiğin için, çok teşekkür ederim.

Lieber Marco, bei dir möchte ich mich auch für deine Hilfe bedanken, besonders wenn es um Protein-Aufreinigung oder Skripte ging oder auch den guten Schlicker, den du stets mit mir geteilt hast! Ich habe dich als eine sehr hilfreiche Person kennengelernt und habe dies sehr bewundert. Vielen Dank auch für die vielen lustigen Momente und deine Empfehlungen für gute Dokus!

Bei Johannes Schwabe möchte ich mich für unsere gemeinsame Reise zur Konferenz nach Boston und die tollen Momente unterwegs bedanken.

Philipp Klos danke ich für die lustigen Momente in den Pausen, Digger!

Ich möchte mich auch bei all meinen Freunden bedanken, die mir in dieser Zeit immer den Rücken gestärkt haben!

Son olarak, aileme özellikle anneme, Zeynebe ve Zehraya teşekkür etmek istiyorum. Canım annem, benim her zaman arkamda oldun ve beni her zaman destekledin. Benim için yaptığın fedakarlıkları asla unutmam. Sana minnettarım ve senin gibi sevgi dolu bir anneye sahip olduğum için asla yeterince teşekkür edemem. Zeyneb ve Zehra, bunları anlamak için belki daha küçüksünüz. Kendimce zor zamanlar geçirirken, sizinle zaman geçirmek, sizinle oynamak ve size ablalık etmek bana hayatta asıl nelerin önemli olduğunu hatırlattı. İyiki varsınız, kardeşlerim.

16 Eigenständigkeitserklärung

Ich versichere, dass ich meine Dissertation mit dem Titel „Mapping of the differential exchange & dynamics of type IVa pilus machine components: Implications for function''

Implications for function“ selbstständig ohne unerlaubte Hilfe angefertigt und mich dabei keiner anderen als der von mir ausdrücklich bezeichneten Quellen und Hilfsmittel bedient habe.

Diese Dissertation wurde in der jetzigen oder einer ähnlichen Form noch bei keiner anderen Hochschule eingereicht und hat noch keinen sonstigen Prüfungszwecken gedient.

Ort, Datum	Memduha Muratoğlu

17 Einverständniserklärung

Ich erkläre mich damit einverstanden, dass die vorliegende Arbeit:

- in Bibliotheken allgemein zugänglich gemacht wird. Dazu gehört, dass sie von der Bibliothek der Einrichtung, in der ich meine Arbeit angefertigt habe, zur Benutzung in ihren Räumen bereitgehalten wird;
- in konventionellen und maschinenlesbaren Katalogen, Verzeichnissen und Datenbanken verzeichnet wird;
- der UB für die lokale Nutzung und für Fernleihzwecke zur Verfügung steht;
- im Rahmen der urheberrechtlichen Bestimmungen für Kopierzwecke genutzt werden kann.

_____

Marburg, den

_____

Unterschrift des Autors